UNIVERSIDADE ESTADUAL PAULISTA
«Júlio de Mesquita Filho»

Estudos sobre Defeitos em Semicondutores

Luis Vicente de Andrade Scalvi

BAURU
2002

unesp

abrcas : ... abril / 2006

Luis Vicente de Andrade Scalvi

Física
CAPES: 10500006

ESTUDOS SOBRE DEFEITOS EM SEMICONDUTORES

Tese de Livre-Docência apresentada à Faculdade de Ciências da Universidade Estadual Paulista – UNESP, Câmpus de Bauru, como requisito para obtenção do Título de Livre-Docente na Disciplina "Física Geral", junto ao Departamento de Física.

Prof. Titular Adalberto Fazzio – IF-USP

Professor Livre-Docente Renato de Figueiredo Jardim – IF-USP

Professor Livre-Docente João Carlos Silos de Moraes – UNESP/ Ilha Solteira

Professor Livre-Docente José Antonio Eiras – UFSCar

Professor Livre-Docente Rogério Pinto Mota – UNESP/ Guaratinguetá

Data de Aprovação: 18 de outubro de 2002.

Número de chamada
Clas. T/UNESP
PHA. 5293e
Tombo nº 1.362

Luís Vicente de Andrade Scalvi

Estudos sobre Defeitos em Semicondutores

BIBLIOTECA UNESP CAMPUS BAURU

Trabalho apresentado ao Departamento de Física da Faculdade de Ciências de Bauru da UNESP, para obtenção do título de Livre-Docente.

Bauru

2002

Ficha catalográfica elaborada por
DIVISÃO TÉCNICA DE BIBLIOTECA E DOCUMENTAÇÃO
UNESP - Bauru

Scalvi, Luís Vicente de Andrade
Estudos sobre defeitos em semicondutores / Luís Vicente de Andrade Scalvi - - Bauru : [s.n.], 2002.
140 f.

Trabalho (Livre - Docência) – Universidade Estadual Paulista. Faculdade de Ciências.

1. Semicondutores – defeitos – arseneto de gálio e alumínio. 2. Semicondutores – defeitos – dióxido de estanho. 3. Semicondutores – transporte elétrico. I – Título. II – Universidade Estadual Paulista. Faculdade de Ciências.

AGRADECIMENTOS

O trabalho apresentado aqui corresponde a várias etapas e em cada uma delas diversas pessoas estiveram envolvidas, pois este texto só pode ser montado graças à enorme colaboração e apoio de muita gente. Assim não seria justo mencionar alguns nomes e esquecer muito deles, pois afinal são vários anos de minha vida. Portanto meu agradecimento vai para todos aqueles que direta ou indiretamente têm participado de meu trabalho: estudantes, colegas, colaboradores, funcionários e outros, tanto de Bauru, como de São Carlos e Araraquara.

Naturalmente não poderia deixar de agradecer às agências de fomento: à FAPESP, que tem financiado minha pesquisa, dado bolsas a meus estudantes e me ajudado a participar de conferências no exterior; ao CNPq, que me deu apoio no começo da carreira e atualmente me concede uma bolsa de pesquisa; à CAPES que me deu um grande impulso na carreira ao me conceder uma bolsa para estágio na Oregon State University (ainda no doutorado) e recentemente me apoia no convênio CAPES-COFECUB, Brasil-França; e ao M.C.T.-PRONEX – Núcleo de Óptica Básica e Aplicada de São Carlos, que tem nos socorrido em várias oportunidades.

Um agradecimento muito especial vai para minha família, que tem me aguentado nesses anos todos, o que eu sei que não é tarefa fácil.

cm 1 2 3 4 5 6 7 unesp 11 12 13 14 15 16 17 18

RESUMO

Este trabalho corresponde ao que fiz de mais relevante em termos científicos desde 1993 (2 anos após a conclusão de meu doutorado). De modo geral trabalho se refere à investigação de defeitos em semicondutores, particularmente $Al_xGa_{1-x}As$ (arseneto de gálioe alumínio) e SnO_2 (dióxido de estanho). Em cada capítulo é feita uma breve discussão do tema proposto, seguido dos artigos científicos mais importantes publicados neste período, cujas cópias foram anexadas.

ABSTRACT

This work is related to the author scientific production since 1993 (2 years after his Ph. D. defense). Generally speaking the work concerns defect investigation in semiconductors, particularly $Al_xGa_{1-x}As$ (aluminum gallium arsenide) and SnO_2 (tin dioxide). In each chapter, there is a short explanation on the issue, followed by the most important papers published in this period, which are attached.

SUMÁRIO

Pag.

Introdução.....5

Capítulo I Investigação de defeitos em $Al_xGa_{1-x}As$.....7

I.1 Corrente de despolarização termicamente estimulada em $Al_xGa_{1-x}As$ de gap direto e indireto.....8

I.2 Relaxação de dipolos induzida por luz em $Al_xGa_{1-x}As$.....10

I.3 Captura de elétrons fotoinduzida. em $Al_xGa_{1-x}As$, a baixa temperatura 12

I.4 Artigos selecionados publicados sobre o assunto.....14

Capítulo II Caracterização de SnO_2 depositado via sol-gel.....65

II. 1 A Resistividade de SnO_2.....66

II.2 Fotocondutividade de SnO_2.....67

III. 3 Espalhamento de Elétrons no contorno de grão.....68

II.4 Artigos publicados sobre o assunto.....71

Capítulo III Pesquisas atuais e proposta de continuidade.....102

III.1 SnO_2 dopado com Sb.....103

III.2 SnO_2 dopado com Er.....108

III.3 Fotocondutividade persistente em SnO_2.....109

Capítulo IV Outras contribuições.....112

I.4 Artigos selecionados publicados 112

Conclusão.....140

INTRODUÇÃO

Em agosto de 1991 defendi minha tese de doutoramento junto ao Instituto de Física e Química de São Carlos. Esta tese era um estudo sobre um defeito conhecido como centro DX, que está presente em ligas de Arseneto de Gálio e Alumínio ($Al_xGa_{1-x}As$). Em minha banca estava presente o Prof. Dr. Máximo Siu Li que me perguntou se aquele defeito podia formar algum tipo de dipolo elétrico neste material. Aquela pergunta aparentemente nada tinha a ver com meu trabalho e eu não soube responde-la, simplesmente porque não havia até então me preocupado com esta possibilidade. Em meados de 1992, já contratado pelo Departamento de Física – Faculdade de Ciências - UNESP campus Bauru, eu e o Prof. Máximo retomamos àquela questão e iniciamos um trabalho de colaboração que viria a dar muitos frutos nos anos seguintes. Uma síntese deste trabalho está no capítulo I.

Em dezembro de 1995 estava apresentando resultados deste trabalho em um congresso (CBECIMAT) em Águas de São Pedro, e encontrei o Prof. Dr. Celso Valentim Santilli do Instituto de Química de Araraquara UNESP. O Prof. Santilli , um antigo colega dos tempos de graduação, ficou interessado no tema de meu trabalho, sobre semicondutores, e disse que também trabalhava com este tipo de material. Ele propôs me enviar algumas amostras de SnO_2 depositadas através do processo sol-gel, e eu me propus a realizar algumas medidas similares às que vinha realizando em $Al_xGa_{1-x}As$. A partir daí eu comecei a aprender sobre um tipo de semicondutor completamente diferente do que vinha estudando. A começar da alta concentração de impurezas, que deveria levar a um semicondutor completamente degenerado, até os efeitos de adsorção de oxigênio no contorno de grão, responsáveis pela modulação da condutividade elétrica. Este tem sido um trabalho bastante enriquecedor e que também tem gerado bons frutos, principalmente com relação à formação de estudantes. Uma síntese deste trabalho está no capítulo II.

Estes trabalhos de pesquisa propiciaram a construção de um pequeno laboratório em Bauru, o Laboratório de Experimentos Eletro-Óticos em Semicondutores, que contou com financiamento da FAPESP (Proc. 94/3465-1) e do CNPq (Proc. 530127/93-8), e cuja construção foi um projeto pioneiro em Bauru. Diversos alunos de Iniciação Científica e Mestrado já se formaram trabalhando neste laboratório e também no laboratório do grupo de Defeitos em Semicondutores e Dielétricos (cadastrado no CNPq sob minha coordenação), localizado na Central de Laboratórios da Faculdade de Ciências. Com relação à pesquisa com SnO_2 (dióxido de estanho) tenho um projeto em andamento na

FAPESP (proc. 99/04205-7) e além disso, este trabalho permitiu a entrada de nosso grupo no projeto REDE SOL ("smart oxide layers"), convênio CAPES-COFECUB (Brasil-França) para intercâmbio de pesquisadores (Proc. CAPES 290/99-2). Como parte deste convênio tive a oportunidade de fazer um pequeno estágio no L.U.R.E., Universidade Paris-Sud, Orsay-França (10 a 24/09/2000), além de visitar outros centros de pesquisa em Limoges e Montpellier. Este convênio deverá permitirá a meus estudantes realizarem pesquisas em laboratórios franceses.

Capítulo I

Investigação de Defeitos em $Al_xGa_{1-x}As$

A pergunta do Prof. Maximo sobre a formação de dipolos está relacionada ao estado de carga do centro DX, no nível de energia mais baixa. Segundo o modelo mais aceito pelos pesquisadores naquela época, o centro DX nada mais era do que o próprio doador – Si, que capturava dois elétrons e se alojava num sítio intersticial, usando-se a notação DX^-. Este modelo ficou conhecido como devido a Chadi e Chang [1]. Um simples balanço de carga mostra que para cada DX^- formado deveríamos ter um centro d^+, que seria o próprio átomo doador em sua posição substitucional carregado positivamente, ou seja, ionizado. Esta existência de impurezas carregadas com cargas opostas no material sugere a possível existência de dipolos e aguçou a curiosidade do Prof. Máximo, que propôs que realizássemos o experimento conhecido como Corrente de Despolarização Termicamente Estimulada (CDTE) para verificar a possível existência destes dipolos. CDTE é um experimento que é usado com sucesso desde os anos 60 para a caracterização de dielétricos e polímeros. No entanto para a caracterização de semicondutores ainda não havia sido usado. No final de 1992 iniciamos então a tentativa de se medir bandas de CDTE em $Al_xGa_{1-x}As$, o que contou também com a participação da Profa. Dra. Ligia de Oliveira Ruggiero, então uma aluna de doutorado do Prof. Maximo.

O experimento de CDTE consiste em se polarizar a amostra à temperatura ambiente (usamos 2,5V), cuja temperatura é abaixada até 10K, no escuro. A polarização é removida e a temperatura é aumentada à taxa fixa (0,081 K/s em nosso caso), situação na qual a corrente é medida com auxílio de um eletrômetro, usando os mesmos eletrodos onde foi

cm 1 2 3 4 5 6 7 unesp 11 12 13 14 15 16 17 18

aplicada a tensão. As amostras utilizadas foram crescidas por Epitaxia de Feixe Molecular (M.B.E.) na Oregon Sttate University (E.U.A) e sua estrutura está descrita detalhadamente em alguns dos artigos anexados.

I.1 CORRENTE DE DESPOLARIZAÇÃO TERMICAMENTE ESTIMULADA EM $Al_xGa_{1-x}As$ DE GAP DIRETO E INDIRETO

No modelo de Chadi e Chang [1] o centro DX é apenas um outro estado do átomo doador que captura 2 elétrons e se move ao longo da direção <111>, se alojando num sítio intersticial. Embora a hipótese de deslocamento havia sido proposta por Morgan [2], a característica que distingue o modelo de Chadi e Chang é o defeito se tornar carregado negativamente, ou seja, DX^-. Neste quadro, o centro DX teria uma interação de U-negativo com forte acoplamento elétron-fonon. À baixa temperatura a concentração de impurezas neutras seria desprezível, desde que este estado carregado seria muito mais estável [1,3]. Assim o número de impurezas ionizadas seria essencialmente constante desde que o doador existiria ou na forma d^+ ou DX^-. Cabe ressaltar que em todo o texto deste trabalho, assim como nos artigos anexos a notação d^+ e d^0 significa o átomo doador numa posição substitucional com carga positiva ou neutra respectivamente; já a notação DX^-, DX^0 ou DX^+, significa o átomo doador numa posição intersticial (de acordo com o modelo de Chadi e Chang), com carga negativa, neutra ou positiva, respectivamente.

Segundo O'Reilly [4] há um outro ponto que deveria ser levado em conta : centros d^+ e DX^- seriam fortemente correlacionados e efeitos dipolares envolvendo d^+-DX^- deveriam ser usados para descrever corretamente o espalhamento de elétrons por impurezas ionizadas neste material. Se as impurezas estivessem distribuídas aleatoriamente na amostra de $Al_xGa_{1-x}As$, a probabilidade de um centro d^+ ser primeiro vizinho de um centro DX^- é bastante baixa. Porém a energia eletrostática ganha ao se colocar um centro d^+ próximo de um centro DX^- possui magnitude significativa para uma fração razoável de sítios nas proximidades do defeito. Então existe uma tendência para o elétron ser capturado num doador de Si próximo de outro átomo de Si.

O experimento de corrente de despolarização termicamente estimulada (CDTE) feito numa amostra de gap direto (x=0,32) mostrou uma banda com pico a 39K. O melhor ajuste numérico para estes dados foi uma distribuição assimétrica de tempos de relaxação, similar à proposta por Havriliak e Negami [5]. A energia de ativação média é cerca de

cm 1 2 3 4 5 6 7 unesp 11 12 13 14 15 16 17 18

0,108eV e a constante do tempo de relaxação é de $9x10^{-13}$s. A banda de CDTE obtida é uma forte evidência que a captura de elétrons que ocorre quando a temperatura é abaixada, leva a estados localizados carregados, pois impurezas neutras não seriam responsáveis por uma corrente de relaxação dipolar. É importante mencionar que a magnitude da corrente medida, da ordem de 10^{-12}A, assegura que não há corrente eletrônica. A dúvida que surgiu é se d^+-DX^- são próximos o suficiente para ser considerado um dipolo. Nossa conclusão, baseada nos dados de CDTE, é que existe uma fração não desprezível de centros d^+ localizados perto o suficiente de centros DX^- para que possam ser considerados uma perturbação no potencial do centro DX^-.

Um outro aspecto fundamental que dá suporte à esta hipótese é o fato que somente uma distribuição de tempos de relaxação fornece bom ajuste numérico para a banda de CDTE. Isto pois está ligado a pelo menos dois pontos principais:

a) A distribuição randômica de centros d^+ em torno da impureza DX^- (distribuição de dipolos com diversos comprimentos)
b) A distribuição de átomos de Al em torno dos estados carregados, que contribuiria para o potencial local. Devemos lembrar que o centro DX possui diferentes níveis de energia dependendo de quantos átomos de Al são primeiros vizinhos [6,7].

O aspecto mais surpreendente do ajuste de dados de CDTE é a energia de relaxação média obtida, de 0,108eV. Este é exatamente o mesmo valor da energia de ligação do nível dominante do átomo doador, que para esta composição ($x \cong 0,32$) é exatamente o centro DX [8].

Todos estes resultados nos levaram a concluir que o centro DX é realmente carregado negativamente, como propunha o modelo de Chadi e Chang e que havia efeitos dipolares na liga $Al_xGa_{1-x}As$, como previra O'Reilly e que portanto, a banda de CDTE obtida estava relacionada a efeitos de correlação entre d^+ e DX^-.

O mesmo experimento de CDTE realizado para uma amostra de $Al_xGa_{1-x}As$ ($x \cong 0,50$) de gap indireto mostrou uma banda com pico em torno de $\cong$50K. A simulação das curvas de acordo com o modelo de distribuição de tempos de relaxação forneceu uma energia de ativação média de 0,124eV e uma constante de tempo de relaxação de $9,7x10^{-13}$s. Embora a fotocondutividade persistente (PPC) fosse constatada experimentalmente no intervalo 80-100K [9], a ordem de magnitude da corrente fotoinduzida era menor que no material de gap direto. A literatura trazia que para amostras de $Al_xGa_{1-x}As$ dopados com Te [10,11], abaixo de 60K PPC deveria desaparecer, devido ao estado hidrogênico associado

cm 1 2 3 4 5 6 7 unesp 11 12 13 14 15 16 17 18

com o vale X, que capturaria elétrons metaestavelmente, não havendo barreira para esta captura. Então o sinal de CDTE obtido seria aparentemente contraditório com a hipótese da formação de dipolos do tipo d^+-DX^-, pois a não existência de PPC abaixo de 60K significaria a destruição dos centros DX^-. No entanto, se levarmos em conta o modo como CDTE é realizado, ou seja, totalmente no escuro, concluiremos que os centros DX continuariam a existir a baixa temperatura, pois não há excitação por luz para promover elétrons dos centros DX para o estado de massa efetiva do vale X.

No espectro de CDTE para $Al_{0,5}Ga_{0,5}As$ havia também uma banda menor com pico a 62K e energia de ativação de 0,165eV. Devido à existência de uma grande quantidade de vacâncias de As em $Al_xGa_{1-x}As$ [12], nós esperaríamos que elas também capturassem elétrons e se tornassem V_{As}^-. O nível desocupado de V_{As} é ressonante com a banda de condução, enquanto que o nível ocupado relaxa para um estado ligado no gap [13]. Numa vacância de As existem três elétrons pendentes [14], dois deles populam o estado do tipo s (a_s) e o terceiro ocupa o estado triplamente degenerado t_2. O elétron extra da vacância carregada (V_{As}^-) também pertenceria a este estado, que teria simetria t_2 e seria um candidato para uma distorção de Jahn-Teller [2,15]. Esta distorção na posição do íon V_{As}^- poderia ser responsável pelo sistema dipolar que se relaxa durante a medida de CDTE, gerando a segunda banda do espectro de CDTE em $Al_{0,5}Ga_{0,5}As$.

I.2 RELAXAÇÃO DE DIPOLOS INDUZIDA POR LUZ EM $Al_xGa_{1-x}As$

A possibilidade de captura de elétrons pelo estado de massa efetiva do vale X fez de nosso material de gap indireto totalmente apropriado para testar a origem das bandas de CDTE, ou seja, pudemos combinar fotoexcitação a baixa temperatura com o procedimento convencional de CDTE. A idéia consistia em se iluminar a amostra a baixa temperatura, juntamente com a remoção da polarização. Esta iluminação, com energia superior ao valor limitante para excitação do centro DX, de $\cong$0,8eV [15], deveria então excitar os elétrons do centro DX para o estado hidrogênico ligado ao vale X, o que eliminaria as bandas de CDTE.

O procedimento foi o seguinte: a amostra era polarizada à temperatura ambiente com um campo elétrico de 15,7V/cm (o mesmo usado no experimento de CDTE "convencional"). Então a temperatura foi abaixada a 10K, iluminado-se a amostra por 5

cm 1 2 3 4 5 6 7 unesp 11 12 13 14 15 16 17 18

min. Então a amostra é deixada no escuro novamente e remove-se o campo elétrico. Daí a temperatura é aumentada à taxa fixa. Para a iluminação foi usado λ =488nm de um laser de Ar^+ e λ=647nm de um laser de Kr^+. Ambas linhas destroem completamente as bandas de CDTE. Este efeito tornou-se uma indicação excelente de que a principal relaxação dipolar obtida das bandas de CDTE em $Al_{0.5}Ga_{0.5}As$ está relacionada ao centro DX, e que o estado fundamental era carregado negativamente como propunham Chadi e Chang [11], desde que nenhum estado neutro poderia ser responsável pela corrente de relaxação dipolar obtidas anteriormente com o procedimento convencional.

Para se compreender completamente a influência da fotoionização nas bandas de CDTE, amostra foi iluminada com energia mínima de ativação do centro DX, que corresponde a um comprimento de onda de 1,55 μm. Esta luz monocromática não destrói a banda a banda de CDTE, mas induz um deslocamento do pico principal para 39 K, correspondendo a uma energia de ativação de 0,121 eV. Ainda continua a existir uma pequena banda na posição original. Iluminando a amostra com 1,55 μm por tempos mais longos, o pico principal é deslocado para temperaturas cada vez mais baixas, e além disso, existe sempre um pico secundário numa posição muito próxima a banda de CDTE obtida no escuro, o que significa que uma parte do sistema dipolar original não foi completamente destruída, mesmo após 15 min de iluminação. Mooney et. Al [15] mostraram que embora 0,8eV seja o valor limitante (mínimo) para fotoexcitação do centro DX, existe variação de diversas ordens de magnitude quando a energia vai de 0,8 a 2,0 eV, o que também depende da composição da liga. Então nós não esperaríamos que a banda de CDTE fosse destruída com iluminação de 1,55 μm. No entanto o deslocamento do pico de corrente foi um tanto inesperado e sugeriu que a influência de luz monocromática deste comprimento de onda não foi somente depletar elétrons dos centros DX^-. Existem algumas possibilidades para explicar este efeito e nós acreditamos que a presença de vacâncias no material é muito importante para se entender o processo de recombinação que ocorre neste experimento de CDTE modificado. Nossas hipóteses estão explicadas em detalhes no principal artigo que publicamos a este respeito [Scalvi et. al. Phys Rev. B 51, 13864 (1995)], cuja cópia está anexada a este texto.

cm 1 2 3 4 5 6 7 unesp 11 12 13 14 15 16 17 18

I.3 - CAPTURA DE ELÉTRONS FOTINDUZIDA EM $Al_xGa_{1-x}As$, A BAIXA TEMPERATURA

Experimentos de variação da fotocondutividade com o comprimento de onda da luz incidente, para amostras de gap indireto foram feitos para um amplo intervalo de temperatura, indicando quais as melhores regiões para se medir a transição de energia proibida ('bandgap') e as regiões onde existe maior influência do centro DX. Mostraram resultados surpreendentes para temperaturas menores que 34 K. Para um intervalo de temperatura de 34 K até aproximadamente 120K, as propriedades de transporte são dominadas pelo centro DX. Neste intervalo não é possível avaliar o bandgap, desde que o começo e o final da transição não são claramente observados neste intervalo. No começo da varredura no espectro de fotocondutividade, a luz monocromática tem energia suficiente para excitar elétrons dos centros DX e esta excitação depende do tempo de exposição à luz e não depende do valor absoluto de energia, desde que esta seja muito maior que o valor limitante da fotoionização do centro DX, 0,8 eV [115]. Conforme o valor da energia da transição do gap é aproximado, a taxa de fotoionização é aumentada pois agora teremos dois processos: excitação de elétrons dos centros DX e geração de pares elétron-buraco, devido à transição do gap. Conforme o comprimento de onda se torna mais curto (maior energia) a geração de pares elétron-buraco é inibida, mas a fotocondutividade não diminui, pois os elétrons advindos dos centros DX, responsáveis pela maior parte do transporte, estão sob influência da fotocondutividade persistente (PPC). Acima de ≅120K, a taxa de excitação do bandgap é observada muito mais facilmente pois PPC é bastante reduzido.

Abaixo de 34 K, o comportamento é diferente do observado em outras regiões. Por exemplo a 13 K, existe um pico de fotocondutividade a 566 nm e uma diminuição até cerca de 561 nm, onde existe um mínimo local, e então existe um novo aumento com pico em torno de 550 nm, começando novamente a decair. O primeiro pico e o decaimento final são comportamentos esperados, pois correspondem ao espectro comum de fotocondutividade, consistente com outras regiões de temperatura em $Al_xGa_{1-x}As$, mas o mínimo local é um tanto inesperado. Este comportamento continua a ocorrer até a temperatura de 34K, aproximadamente. A variação da fotocondutividade com o comprimento de onda da luz incidente sob a amostra mantida abaixo de 34K deve ser entendido como segue: luz de 600nm tem energia suficiente para excitar elétrons dos centros DX, de modo lento, pois a taxa de fotoionização é baixa. Conforme a energia aumenta a transição do bandgap é

cm 1 2 3 4 5 6 7 unesp 11 12 13 14 15 16 17 18

atingida e aa ionização torna-se maior. Quanto menor a temperatura, menor o sinal da fotocondutividade, o que significa que os elétrons excitados dos centros DX, são recapturados por outro nível, provavelmente o estado de massa efetiva dos vale X. A profundidade do nível do vale X de Si deve ser de ordem de magnitude similar ao nível do vale-X de Te, ≅40 meV [10]. O pico a 566 nm não deve ser associado com o valor exato da transição do gap, pois sua energia depende da velocidade de varredura e da taxa de ionização do centro DX. O que podemos dizer é que nesta posição existe um máximo na geração de portadores, fruto da combinação entre geração de pares elétron-buraco e elétrons advindos dos centros DX^-. A captura de elétrons que ocorre na sequência, ou seja a 561 nm deve ter outra explicação. Nossa hipótese é que numa temperatura tão baixa quanto 13K, a baixa energia térmica não permite a relaxação imediata do centro DX. O centro DX^+ é altamente instável e está localizado ≅20meV acima do mínimo da banda de condução. Então ele é capaz de recapturar um elétron daqueles gerados pela transição de gap e torna-se DX^o de acordo com a reação:

$$DX^+ + 1e^- \rightarrow DX^o \qquad (I.1)$$

Iluminando-se com energias mais altas que a do centro DX^+, a condutividade volta a crescer pois voltamos a ter transição de gap e excitação de centros DX^- e DX^o. Quando a temperatura é aumentada, o tempo de vida de DX^+ torna-se mais curto e esta diminuição na condutividade em torno de 561 nm não é mais observada. Um estado DX^o já havia sido proposto por diversos autores [10,16-18]. No intervalo 13-34K, a energia térmica é bastante baixa e um estado intermediário DX^o tem um tempo de vida longo o suficiente para ser responsável pelo mínimo local na curva de fotocondutividade.

REFERÊNCIAS DESTE CAPÍTULO

[1] – Chadi, D. J. e Chang,, K. J. , Phys. Rev. Lett. **61** (21), p. 2187-2190, 1988

[2] – Morgan, T.N., Phys. Rev. B **34** (4), p. 2664-2669, 1986

[3] – Zhang, S. B. e Chadi, D. J., Phys. Rev. B **42** (11), p.7174-7117, 1990

[4] – O'Reilly, E P. Appl. Phys. Lett. **55** (14), p.1409-141, 1989

[5] – Havriliak, S. e Negami, S., Polymer **8** (4), p.161-224, 1967

[6] –Baba, T.; Mizuta, M.; Fujisawa, T.; Yoshino, J. e Kukimoto, H. Jpn. J. Appl. Phys **28** (6), p. L891-L894, 1989

[7] –Brunthaler, G e Kohler, K., Appl. Phys. Lett. **57** (21), p. 2225-2227, 1990

[8] – Chand, N.; Henderson, T.; Klem, J.; Ted Masselink, W. T.; Fischer, R.; Chang, Y-C e Morkoç, H., Phys. Rev. B **30** (8), p. 4481-4492, 1984

[9] – Scalvi, L.V. A e Minami, E., phys. stat. solidi (a) **239**, p. 145-152, 1993

[10] – Dmochowski, J. E.; Dobaczewiski, L.; Langer, J. M. e Jantsch, J., Phys. Rev. B **40** (14), p. 9671-9682, 1989

[11] – Dobaczewiski, L. e Kaczor, P Phys. Rev. B **44** (16), p. 8621-8632, 1991

[12] – Van Vechten, J. A, J. Phys.:Condens. Matter **1**, p. 5171-5177, 1989

[13] – Lang, D. V.; Logan, R. A e Jaros, M., Phys. Rev. B **19** (2), p. 1015-1030, 1979

[14] – Jaros, M. e Brand, S., Phys. Rev. B **14**(10), p.4494-4505, 1976

[15] – Mooney, P.M.; G A Northrop, G. A; Morgan, T.N. e Grimmeis, H. G., Phys. Rev. B **37**(14), p. 8298-8307, 1998

[16] – Theis, T.N. e Mooney, P. M., Mat. Res. Soc. Symp. Proc. **163**, p. 729-735, 1990

[17] – Sampaio, J. F.; Chaves, A S.; Ribeiro, G.M.; P. Guimarães, P. S. S.; Carvalho R. P. e Oliveira, A. G., Phys. Rev. B **44**(19), p.10933-10936, 1991

[18] – Ghosh, S. e Kumar, V., Solid State Commun. **104**(12), p. 781-785, 1997

I.4 – ARTIGOS SELECIONADOS PUBLICADOS SOBRE O ASSUNTO (anexados na sequência)

I.4.1. –**Scalvi, L. V A;** Oliveira, L.; Minami, E. e Siu Li, M.; *Dipole Relaxation Current in n-type $Al_xGa_{1-x}As$*, Appl. Phys. Lett. **63** (19), p. 2658-2660, 1993

I.4.2 – **Scalvi L. V A** e Minami, E. *The Energy Barrier for Electron trapping in $Al_xGa_{1-x}As$, phys.* stat. solidi (a) **139**, p.145-152, 1993

I.4.3 - **Scalvi, L. V A**; Oliveira, L. e Siu Li, M. *Dipole Relaxation Current in n-type $Al_xGa_{1-x}As$*, Mat. Res. Soc. Symp. Proc. **325**, p. 285-290, 1994

I.4.4 - **Scalvi, L. V A**; Oliveira, L. e Siu Li, M.; *Light Induced Relaxing Dipoles in n-type $Al_xGa_{1-x}As$*, Phys. Rev. B **51** (19), p. 13864-13867, 1995

I.4.5 - **Scalvi, L. V A**; Oliveira, L. e Siu Li, M; *Light and Thermal Excitation of Depolarization Current in Indirect Bandgap* $Al_xGa_{1-x}As$, Braz. J. Phys. **26** (1), p. 239-244, 1996

I.4.6 – Taquecita, M.H.; **Scalvi, L. V A;** Oliveira, L; Siu Li, M. e Parreira, S.B.; *Investigation of Temperature Influence on Photo-Induced Conductivity in n-type $Al_xGa_{1-x}As$*, Rad. Eff. & Def. Solids **146**, p. 175-186, 1998

I.4.7 – **Scalvi, L. V A**; Taquecita, M.H. e Vega, B. A V.; *Photo-Induced Electron trapping in Indirect Bandgap $Al_xGa_{1-x}As$ at Low Temperature*, J. Phys.: Condens. Matter **11**, p. 425-433, 1999

Dipole relaxation current in n-type $Al_xGa_{1-x}As$

L. V. A. Scalvi
Departamento de Física, Universidade Estadual Paulista Júlio de Mesquita Filho-Bauru, Caixa Postal 473, Bauru-SP 17033, Brazil

L. de Oliveira, E. Minami, and M. Siu-Li
Departamento de Física e Ciência dos Materiais, Instituto de Física e Química de São Carlos, Universidade de São Paulo, Caixa Postal 369, São Carlos-SP 13560, Brazil

(Received 14 June 1993; accepted for publication 31 August 1993)

We report for the first time the thermally stimulated depolarization current (TSDC) spectrum for a direct band-gap AlGaAs sample, where the presence of DX centers is clearly observed by photoconductivity measurements. A TSDC band is obtained, revealing the presence of dipoles, which could be attributed to DX^--d^+ pairs as indeed predicted by O'Reilly [Appl. Phys. Lett. 55, 1409 (1989)]. The data are fitted by relaxation time distribution approach yielding an average activation energy of 0.108 eV. This is the most striking feature of our data, since this energy has approximately the same value of the DX center binding energy.

Self-consistent total energy calculations were performed by Chadi and Chang[1] to show that the DX center is just another state of the substitutional donor itself which traps two electrons and moves along a ⟨111⟩ direction towards an interstitial site. Although the hypothesis of migration was first proposed by Morgan,[2] the striking feature of Chadi and Chang's model is the trapping of two electrons by the same center becoming negatively charged. At low temperatures the concentration of neutral impurities is negligible since the DX center state of the substitutional impurity is much more stable.[1,3] Charge balance assures that the creation of a certain number of DX^- centers generates the same amount of d^+ centers. DX and d represent threefold (interstitial) and fourfold (substitutional) coordinated states of the same atom, respectively. In such a picture DX has a negative-U effective interaction with strong electron-phonon coupling. Although Chadi and Chang's model has been accepted by most DX center researchers, Maude *et al.*[4,5] have used mobility data to support a positive-U model. These data show increasing mobility as the free carrier density decreases with pressure in highly doped GaAs. In a positive-U model trapout occurs as impurity donors become neutral, so the number of ionized scattering centers decreases with decreasing free carrier concentration. In the negative-U Chadi and Chang's model, the number of ionized impurity is essentially unchanged since the donor exists either in a d^+ state or DX^- state. In both models, scattering centers are isolated ionized impurities since the donors are uniformly distributed throughout the sample.

O'Reilly[6] has argued that there is another important point which should be taken care of: d^+ and DX^- centers will be strongly correlated and a dipole-like picture should be used to describe scattering by DX^--d^+ pairs. In order for the DX^--d^+ be considered as a dipole, the d^+ center should be located close enough to the DX^- center such that it may be a perturbation in the DX potential. If impurity donors are randomly distributed in the GaAs sample, the probability that d^+ and DX^- are first neighbors is negligibly low. However, the extra electrostatic energy gained by placing a d^+ center close to a DX^- center is of significant magnitude at a large fraction of sites.[6] Then it is energetically very favorable to a DX^- center be created close to a d^+ center. This behavior is quite different from conventional samples, where charged defects are introduced during growth, usually at high temperatures.

DX centers are present in n-type $Al_xGa_{1-x}As$ with x higher than approximately 0.22 with no need of applying pressure. Our measurements are carried out in a Si-doped ($\cong 1\times10^{18}$ cm^{-3}) molecular beam epitaxy (MBE) grown $Al_xGa_{1-x}As$ sample 2 μm thick. Care was taken to avoid the formation of a two-dimensional electron gas (2DEG) using the following sample structure: a 0.25 μm undoped GaAs buffer layer was grown on the semi-insulating substrate followed by a 0.25 μm of undoped $Al_xGa_{1-x}As$ that is compositionally graded from $x=0$ to $x\cong0.32$, a 0.25 μm layer of undoped $Al_{0.32}Ga_{0.68}As$ and the 2 μm active layer. The photoconductivity spectrum at 10 K is shown in Fig. 1. The wavelength is scanned from higher to lower value. The wavelength scanning speed is 50 nm/min. At about 640 nm there is a sharp increase in the conductance which ends at about 620 nm. Using the equations given by Adachi

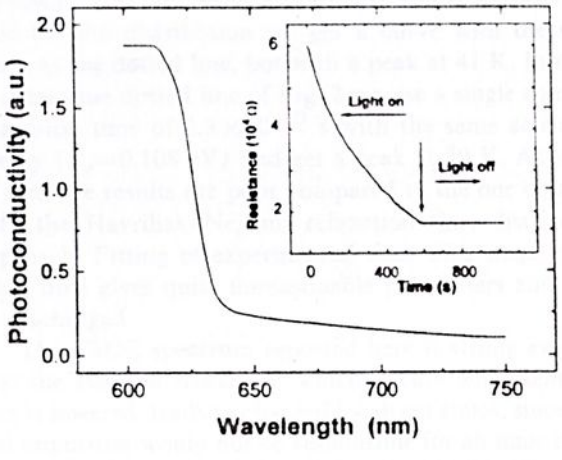


FIG. 1. Photoconductivity spectrum for the $Al_xGa_{1-x}As$ sample at about 10 K. Inset—illumination of this sample proceeds until 600 s with a 560 nm monochromatic light, then light is turned off and the conductance remains steady ($T\cong10$ K).

 0003-6951/93/63(19)/2658/3/$6.00 © 1993 American Institute of Physics

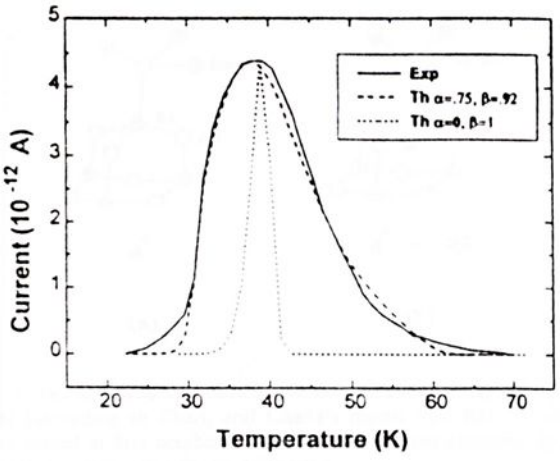


FIG. 2. Thermally stimulated dipole current for the $Al_xGa_{1-x}As$ sample. Solid line—experimental data. Dashed line—Havriliak–Negami fit (see Ref. 10). Dotted line—single relaxation time approach.

and an average wavelength (630 nm) the band gap is estimated, considering the temperature corrections for the Γ valley:[7]

$$E_g^{\Gamma}(10\ \mathrm{K}) = E_g^{\Gamma}(300\ \mathrm{K}) + (-3.95 - 1.15x)10^{-4}\Delta T, \quad (1)$$

where

$$E_g^{\Gamma}(300\ \mathrm{K}) = 1.424 + 1.247x, \quad (2)$$

resolving Eqs. (1) and (2) for 630 nm, it is found that $x \cong 0.32$. In this composition, it is expected that *DX* center dominates the transport properties, since *DX* energy level is located below the conduction band. There are two features in Fig. 1 which confirm this behavior: When the monochromatic light energy is around the forbidden gap transition, there is a slow increase in the photoconductivity which is a *DX* center characteristic. Above this transition the electrons do not return to the nonconductive state, trapped at *DX* centers. Besides, the inset in Fig. 1 shows that after illuminating the sample with a monochromatic light of 560 nm the resistance decreases slowly to a steady value, close to its value at room temperature ($\cong 1\ \mathrm{k}\Omega$). In this figure we have measured the current with 50 mV of applied voltage. Then the illumination is removed and the resistance remains unchanged for an unmeasurable time. This is a well-known property related to *DX* centers and called persistent photoconductivity (PPC). So we can deduce from Fig. 1 that the $Al_xGa_{1-x}As$ sample has a direct forbidden band-gap transition ($x \cong 0.32$) and shows PPC, a property related to *DX* center in bulk AlGaAs and furthermore, it shows no 2DEG conduction since the resistance does not reach a value lower than at room temperature.

Figure 2 shows the experimental TSDC spectrum (solid line). In this measurement the sample is biased at room temperature (2.5 V). Then the temperature is lowered down to liquid He temperature in the dark. The applied bias is removed and the temperature is allowed to increase at fixed rate (0.081 K/s), always in the dark, when the depolarization current is measured with an electrometer and recorded. In other words, no illumination is done on the sample during the whole measurement. As the temperature goes down in the dark an electron freezeout at the *DX* centers occurs. Considering that there is no light on the sample, no electron is photoexcited to the conduction band and, moreover, the electron thermal energy is not enough to overcome the emission barrier. The only way to explain the current peak seen in Fig. 2 is by a dipole reorientation current. The dipoles, originally randomly distributed throughout the sample, are biased with the applied voltage at room temperature. When the applied bias is removed at liquid-helium temperature, the oriented dipoles are frozen at a metastable state. Then, the temperature is allowed to increase at a fixed rate and the dipoles relax to their equilibrium positions generating a depolarization current shown in Fig. 2, with a peak at 39 K. A strong evidence that it is indeed, a dipole reorientation current is the order of magnitude of the experimental curve. Comparing the values calculated from Fig. 1 (inset) using 50 mV of applied voltage, and values from Fig. 2 it is clearly seen that the electronic photoinduced current is about five orders of magnitude higher than the TSDC spectrum current. There is no known process which could be responsible for releasing a few electrons and trapping them back at 39 K in the dark, under such experimental conditions, since there is not enough thermal energy to overcome the *DX* center thermal emission barrier.

The TSDC curve is usually fitted by a single curve, showing Debye behavior[8,9] with a single relaxation time and activation energy. However, our data are better fitted by an asymmetric relaxation time distribution, the type of distribution first proposed by Havriliak and Negami.[10]

By using their equations, where the dimensionless parameters α and β evaluate the shape of distribution, the best fit to the TSDC experimental curve is obtained with a continuous distribution of activation energies. The average activation energy is about 0.108 eV and the constant relaxation time is 9×10^{-13} s, with a peak at 37 K. It is shown in Fig. 2 by a dashed line. The other curve (dotted line) in Fig. 2 is another attempt to fit the experimental data with similar parameters, but by using a single relaxation time approach. With the same parameters as the average ones used for the distribution we get a curve with the same shape as the dotted line, but with a peak at 41 K. In order to obtain the dotted line of Fig. 2 we use a single constant relaxation time of 2.3×10^{-13} s with the same activation energy ($E_a = 0.108$ eV) and get a peak at 39 K. As it can be seen the results are poor compared to the one obtained with the Havriliak–Negami relaxation time distribution approach. Fitting of experimental data with single relaxation time gives quite unreasonable parameters and must be discharged.

The TSDC spectrum reported here is strong evidence that the electron freezeout, which occurs when temperature is lowered, leads to charged localized states, since neutral impurities would not be responsible for an ionic dipole current. Such a current takes place when the biased dipoles are relaxing to more stable states, returning to their random distribution throughout the sample. It is very important to notice the dipole current magnitude because it as-

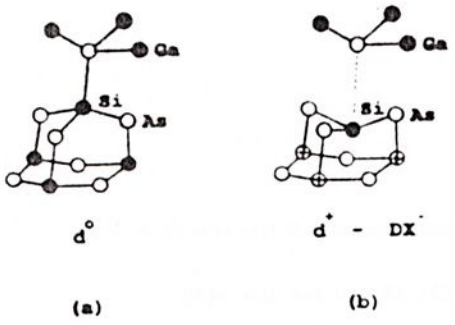


FIG. 3. (a) Si placed at a normal substitutional site in GaAs. (b) DX^- center [according to Chadi and Chang's model (see Ref. 1)] and d^+ center placed at first neighbor sites. The ⊕ symbols represent the three equivalent positions for dipole relaxation.

sures that there is no electronic current, which means the strongly localized DX^- center does not release electrons to the conduction band. The question which arises from these data is whether or not d^+-DX^- is close enough to be considered a dipole. In Chadi and Chang's model, shown in Fig. 3, there are three equivalent first neighbor positions for the d^+ state, which could be responsible for dipole reorientation. Although it is energetically very favorable to a d^+ center to be formed close to a DX^- center, the randomly distributed impurities are placed at their sites during growth and the probability that two impurities are first neighbors is negligibly small. However, the reported data shows that if the measured current comes indeed from the d^+-DX^- pair there is a non-negligible fraction of d^+ centers located as close to the DX^- center as to be considered a perturbation in the DX^- screening potential.

Another strong point to support his hypothesis is the fact that no single relaxation time approach can be used to fit satisfactorily the experimental data. Good fit is only obtained with activation energy distribution. This is quite consistent with at least two major points.

(1) The random distribution of d^+ center around the DX^- impurity (generation of a dipole length distribution).

(2) The random distribution of Al atoms around both charge states should also contribute to the local field potential. The DX center has different energy levels depending on how many Al atoms are first neighbors.[11,12]

Another striking feature of our results is that the average activation energy obtained is $E_a \cong 0.108$ eV which is the same value of the dominant donor level binding energy,[13] which coincides with the DX center binding energy in this Al composition. It suggests another possibility for the dipole relaxation: The extra electron trapped at the DX center could be donated to a d^+ center and the interstitial donor atom migrates back to its normal substitutional site. This migration is responsible for the TSDC signal as recorded.

If the extra electrostatic energy gained by placing a d^+ center close to a DX^- center is of significant magnitude,[6] there is a tendency for the electrons to be trapped at a Si donor located close to another Si donor. Moreover, the way the TSDC measurement itself is carried out adds an external factor to this picture: The temperature is decreased with an applied voltage to the sample. As the temperature gets lower, more electrons are trapped at DX centers. So the most stable situation corresponds to the creation of oriented dipole states. Even with such a favorable picture it is still hard to believe that all the measured dipole currents of Fig. 2 come from first neighbors relaxation alone, but a similar picture can be drawn for atoms located at farther apart sites. The idea will remain essentially as the one shown in Fig. 3.

Our conclusion is that a dipole relaxation current occurs in a Si-doped $Al_xGa_{1-x}As$ sample where the presence of DX centers is clearly evident. We interpret such a dipole current using the Chadi and Chang's DX model, and mainly the dipole scattering effects present in this alloy as predicted by O'Reilly. The most interesting data obtained from our calculation is that the activation energy for dipole relaxation is about 0.108 eV, approximately the same value as the binding energy of the dominant impurity state in $Al_xGa_{1-x}As$ (DX center). Further work is needed to clearly determine whether this dipole is the d^+-DX^- pair or some other kind of dipole is present in this sample.

This sample was grown at the Advanced Materials Laboratory of Oregon State University. Luis V. A. Scalvi thanks Professor John R. Arthur for the hospitality during his stay at O.S.U. We also acknowledge the partial financial support from Fundação de Amparo a Pesquisa do Estado de São Paulo(Fapesp), Conselho Nacional de Desenvolvimento Científico e Tecnológico(CNPq), Financiadora de Estudos e Projetos(Finep) and Coordenação de Aperfeiçoamento de Pessoal de Nível Superior (Capes).

[1] D. J. Chadi and K. J. Chang, Phys. Rev. Lett. **61**, 873 (1988); Phys. Rev. B **39**, 10063 (1989).
[2] T. N. Morgan, Phys. Rev. B **34**, 2664 (1986).
[3] S. B. Zhang and D. J. Chadi, Phys. Rev. B **42**, 7174 (1990).
[4] D. K. Maude, L. Eaves, T. J. Foster, and J. C. Portal, Phys. Rev. Lett. **62**, 1922 (1989).
[5] D. K. Maude, J. C. Portal, L. Dmowski, T. J. Foster, L. Eaves, M. Nathan, M. Heiblum, J. J. Harris, and R. B. Beall, Phys. Rev. Lett. **55**, 815 (1987).
[6] E. P. O'Reilly, Appl. Phys. Lett. **55**, 1409 (1989).
[7] S. Adachi, J. Appl. Phys. **58**, R1 (1985).
[8] L. Oliveira, P. Magna, H. J. H. Gallo, E. C. Domenicucci, and M. S. Li, Phys. Status Solidi B **171**, 141 (1992).
[9] W. van Weperen and H. W. den Hartog, Phys. Rev. B **18**, 2857 (1978).
[10] S. Havriliak and S. Negami, Polymer **8**, 161 (1967).
[11] T. Baba, M. Mizuta, T. Fujisawa, J. Yoshino, and H. Kukimoto, Jpn. J. Appl. Phys. **28**, L891 (1989).
[12] G. Brunthaler and K. Köhler, Appl. Phys. Lett. **57**, 2225 (1990).
[13] N. Chand, T. Hendersen, J. Klem, W. T. Masselink, R. Fischer, Y. C. Chang, and H. Morko, Phys. Rev. B **30**, 4481 (1984).

phys. stat. sol. (a) **139**, 145 (1993)

Subject classification: 71.55 and 72.40; S7.15

Departamento de Fisica, UNESP, Bauru [1]) *(a) and*
Instituto de Fisica e Quimica de São Carlos, Universidade de São Paulo[2]) *(b)*

The Energy Barrier for Electron Trapping in $Al_xGa_{1-x}As$

By

L. V. A. SCALVI (a) and E. MINAMI (b)

Transient decay of persistent photoconductivity measurements are carried out in samples of different compositions. The capture barrier for electron trapping by DX centers is obtained using a method which employs the Brooks-Herring equation for the electronic mobility. The effect of polarization of the screening cloud is analysed using Takimoto's potential and specifies the limits of applicability of the Brooks-Herring equation in $Al_xGa_{1-x}As$.

1. Introduction

The so-called persistent photoconductivity (PPC) is a metastable property of $Al_xGa_{1-x}As$ alloys doped with group IV or VI impurity atoms. A few years ago Chadi and Chang [1, 2] stated that every donor atom from these two chemical groups would become a DX center and, thus, give rise to the PPC effect. The striking feature of Chadi and Chang's model is that the DX center captures two electrons concomitant with a lattice distortion along a ⟨111⟩ direction, becoming located at a interstitial site. The electron–phonon interaction stabilizes the Coulomb repulsion due to the presence of a second electron. In this model the interaction energy (U) is negative and the PPC is associated with large lattice relaxation originated from the placement of the donor atom in the interstitial position.

Although most experiments have confirmed this model [3], contradiction among some experiments [4, 5] makes possible for the defenders of small lattice relaxation (SLR) [6] models still believe that the DX center is just a metastable electronic state of the donor linked to the L valley. There have been several alternative models [7] proposed to explain the DX center behavior. Either models which invoke SLR or models which claim LLR propose a neutral ground state for the DX center, the only exceptions being Chadi and Chang's and Van Vechten's [8, 9]. One should note that the idea of a donor impurity placed at an interstitial position, i.e. a Jahn-Teller dislocation, was first proposed by Morgan [10]. However, in Morgan's proposal the DX center would have a neutral ground state (positive U), whereas in Chadi and Chang's model trapping of two electrons implies that the DX center has a negatively charged ground state.

Independent which model we choose to explain the defect, the presence of PPC is a proof for the existence of an energy barrier separating different charge states of the DX center. In this paper we investigate this capture barrier for Si-doped $Al_xGa_{1-x}As$ for various aluminium compositions using the transient decay of persistent photoconductivity (TDPPC) technique at different temperatures. The TDPPC technique has already been described

[1]) C.P. 473, 17033 Bauru (SP), Brasil.
[2]) C.P. 369, CEP 13560 São Carlos (SP), Brasil.

elsewhere [11]. Experimental conductivity data are used to obtain this capture energy through a method which employs the Brooks-Herring equation for the mobility. Limitations of this method are discussed based in the ionized impurity scattering.

2. The Energy Barrier for DX Capture

When below-band-gap light irradiates a sample, electrons are excited from the DX center to the conduction band. When the light is turned off, electron capture by DX centers can only take place if the electrons have sufficient thermal energy to overcome an energy barrier which exists between the trapped and free-carrier states. The aluminium composition in Al_xGa_xAs sample has an important role in establishing the magnitude of this capture barrier. Independent of which model is employed to explain the DX center behavior, the donor atom neighborhood will influence either the position of the effective mass states or the activation energy for the donor atom migration.

The capture barrier is evaluated monitoring TDPPC at different temperatures. Decay in the conductance resulting from electron capture is shown in Fig. 1 for two different aluminium compositions. The capture energy is then obtained as follows. The electron capture rate is given by

$$\frac{dn}{dt} = -\sigma_n V_{th} n^2 , \tag{1}$$

V_{th} is the electron thermal velocity and σ_n is the capture cross section, given by

$$\sigma_n = \sigma_\infty \exp\left(-\frac{E_{cap}}{k_B T}\right), \tag{2}$$

where σ_∞ is the capture cross section at infinite temperature, k_B Boltzmann's constant, and T the absolute temperature.

By solving (1) analytically and assuming that the dominating scattering process is by ionized impurities, which could be described by the Brooks-Herring equation, the inverse of the conductance (G) is given by

$$\frac{1}{G(t)} = \frac{N_{ii} T^{-3/2}}{k_1 n(0)} (1 + C_n n(0)\, t) \ln\left(\frac{1 + C_n n(0)\, t}{C_t}\right). \tag{3}$$

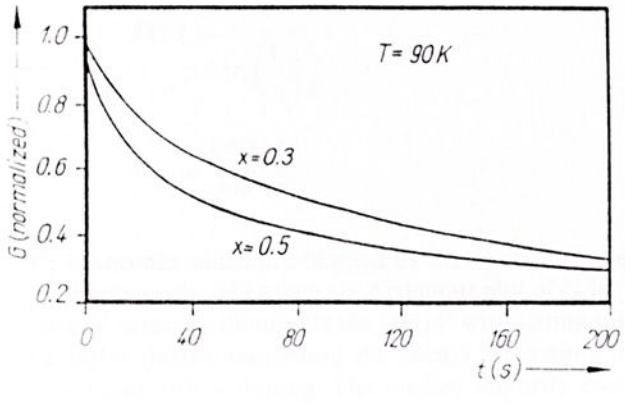


Fig. 1. Transient decay of persistent photoconductivity of $Al_xGa_{1-x}As$ for two different aluminium compositions. The measured conductance is normalized

where N_{ii} is the ionized impurity concentration, k_1 and C_T are constants obtained by manipulating several constants coming from the Brooks-Herring and decay equations. When t goes to infinity, $1/G(t)$ becomes linear in time. Therefore we could choose this straight part of the $1/G(t)$ curve at each temperature to obtain E_{cap} [11]. However, this time may be too long and the thermal emission processes may become important. In this case (1) is no longer valid, since the free carrier concentration has to be evaluated considering other processes besides the electron capture by DX centers, as assumed in (1). Moreover, if the time is too long, the conductance signal may be too low and it becomes very hard to avoid noise. Then we have to find another way to relate the decay at some time range with temperature and E_{cap}. The expression should be general and provide the desired value of E_{cap}. If we choose j and k such that

$$t_1 = \frac{j-1}{C_n n(0)}, \tag{4}$$

$$t_2 = \frac{k-1}{C_n n(0)}, \tag{5}$$

where for convenience, j and k are integers and $j < k$, we have a way to relate the time range at different temperatures [12].

The linear regression of the experimental data located between t_1 and t_2 is a straight line whose slope is, within a good approximation, the same slope of the straight line which links $1/G(t_1)$ and $1/G(t_2)$. (This approximation is even better as j gets closer to k or t_1 and t_2 are far from the origin) If S_{l0} is the value obtained for the slope obtained by the linear regression, then using (3), (4), and (5), we obtain

$$S_{l0} \approx \frac{\Delta(1/G)}{\Delta t} = \frac{N_{ii} T^{-3/2} C_n}{k_1 (k-j)} \left[k \ln\left(\frac{k}{C_T}\right) - j \ln\left(\frac{j}{C_T}\right) \right]. \tag{6}$$

With a few simplifications, we get a general expression valid for any temperature:

$$k_B \ln [f(T)\, S_{l0}] = C_F - \frac{E_{cap}}{T}, \tag{7}$$

where

$$f(T) = \frac{T}{\ln\left(\dfrac{C_{jk}}{C_T}\right)}, \tag{8}$$

$$C_{jk} = \frac{k^{(k/(k-j))}}{j^{(j/(k-j))}} \tag{9}$$

C_F is another constant obtained by manipulating several constants coming from equations used previously. Therefore, an Arrhenius plot of $k_B \ln [f(T)\, S_{l0}]$ versus $1/T$ gives the capture barrier. Since we illuminate the sample with strong sub-bandgap light until the conductance saturates (before measuring the decay), we assume that all the impurities are ionized at $t = 0$ and $n(0) =$ doping. The ionized impurity concentration (N_{ii}) is also assumed as a

Table 1
Obtained values of E_{cap} according to the developed method

Al composition	doping (cm^{-3})	j, k	R^2	E_{cap}
0.3	1×10^{18}	2, 3	0.9956	0.248
		3, 4	0.9966	0.247
0.4	1×10^{18}	2, 3	0.9977	0.207
		3, 4	0.9997	0.216
0.5	5×10^{17}	2, 3	0.9996	0.195
		3, 4	0.9986	0.195

constant. This is particularly true if Chadi and Chang's model is correct, for the dopant would be either in a d^+ state or in a DX^- state (in the kinetics of Van Vechten's model, this is also valid). If DX has positive U, then $N_{ii}(t) = n(t)$ since the impurities will be ionized only when the electrons are excited to the conduction band. $n(t)$ would be canceled in (3) and then, when t goes to infinity, $1/G(t)$ becomes constant. With such a theoretical expression no fit to the experimental data is possible, as we observed in a previous paper [11]. Table 1 shows results from this method applied to samples of different compositions, using various values of k and j. Some of these calculations are shown in Fig. 2 with the calculated points from experimental data. The values obtained for R^2 are very close to unity, which shows the precision of the method just developed. Only with $x = 0.4$ there is a slightly significant difference. The $x = 0.4$ sample had the poorest signal among all the tested samples (but it was the only one available with such a composition). As the decay goes, there is increasing noise and possibly we may have competing charge state transitions, as emission from the DX center or capture by shallower levels. In this case (1) is no longer valid, as already discussed. Thus, the obtained value for $j = 2$ and $k = 3$ should be more reliable. The values obtained for E_{cap} are in good agreement with the literature [3, 13].

This method is applied to a sample of unknown composition, and yields $E_{cap} = 0.232$ eV. Values obtained for E_{cap} at $x = 0.3$ and 0.4 (we do not use the value at 0.5 for there is a change in the dependence around the bandgap direct–indirect crossover [13]) and also from the literature [3, 13] suggest the aluminum composition to be around 0.35. The photoconductivity spectrum of this sample at 77 K (Fig. 3) confirms that the unknown composition is approximately 0.34.

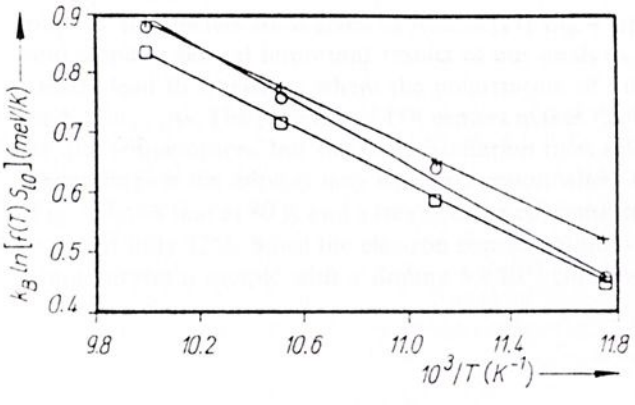


Fig. 2. Arrhenius plot to obtain the capture energy according to the developed method. + $x = 0.4$, $j = 2$, $k = 3$. □ $x = 0.4$, $j = 3$, $k = 4$. ○ $x = 0.3$, $j = 2$, $k = 3$

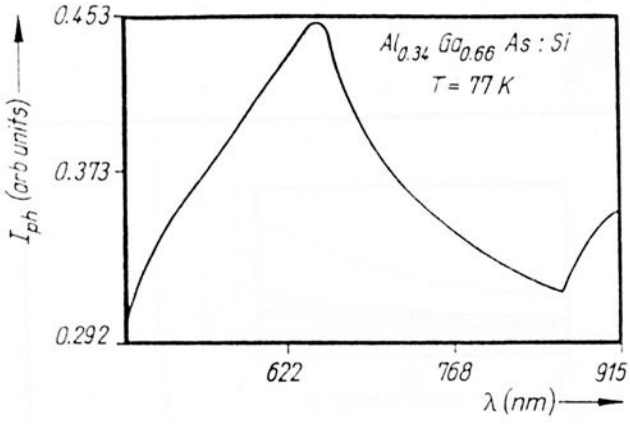


Fig. 3. Photoconductivity for a sample of $Al_{0.34}Ga_{0.66}As$ at 77 K

3. Ionized Impurity Scattering in $Al_xGa_{1-x}As$

In the range of temperature where TDPPC is carried out (80 to 100 K), the dominant scattering is by ionized impurities. Although the Brooks-Herring equation is widely used to calculate such scattering, there are some issues that should be considered. This is particularly important for the DX center case, for the samples usually employed have very high concentrations and the measurement temperatures are very low. In the Brooks-Herring analysis, the electrons around the positively charged nucleus diminish the Coulomb repulsion and this screening effect is taken into account to evaluate the electronic mobility. However, as the free electron concentration increases, the screening cloud is increasingly deformed by the field generated by colliding electrons. Takimoto [14] treated this problem and gave the following expression for the mobility, when the polarization of the screening cloud is accounted for [15]:

$$\mu_T = \frac{64\sqrt{2\pi}\,\varepsilon^2(k_B T)^{3/2}}{3m_e^{1/2}N_{ii}e^3Z^2}\int_0^{\gamma}\frac{x_0^3\exp(-x_0)\,dx_0}{J_\gamma(\sqrt{x_0})} \tag{10}$$

Using the suitable form for $J_\gamma(\sqrt{x_0})$ given by Hall [16] numerical evaluation of Takimoto's mobility is straightforward.

In order to evaluate the range of validity of the method developed in Section 2, we compare the Takimoto and Brooks-Herring mobilities for $Al_xGa_{1-x}As$ using different variables such as carrier concentration, temperature, and aluminum composition. The physical parameters are as given by Adachi [17]. Fig. 4 represents examples of this comparison and displays several important results of our analysis. High doping and low temperature clearly lead to situations where the polarization of the screening cloud is very important in $Al_xGa_{1-x}As$. The presence of DX centers makes the free carrier concentration very small at low temperatures, but the photoexcitation frees electrons to the conduction band and depending on the doping, may lead to a region where the BH equation cannot be applied. Fig. 4 shows that at 80 K and a free electron concentration of 3×10^{17} cm^{-3} the discrepancy is about only 12%. Since the electron concentration is very high (in our TDPPC range of temperature) a sample with a doping 5×10^{17} cm^{-3} will not have measurable differences

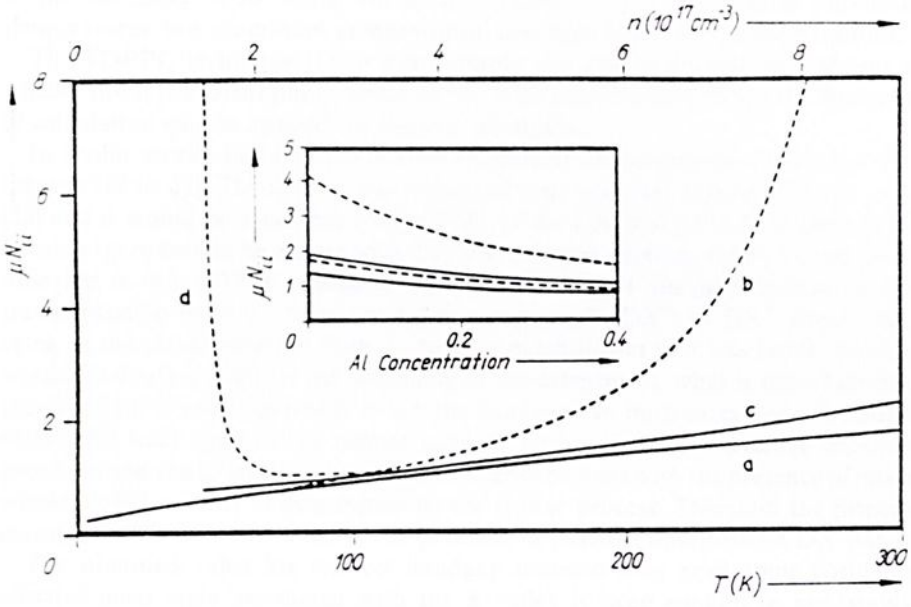


Fig. 4. Mobility (μ) times ionized impurity concentration (N_{ii}) for $Al_xGa_{1-x}As$ calculated according to Brooks-Herring equation (broken line) and Takimoto (full line). (a) and (b) refer to the top scale ($T = 80$ K). (c) and (d) refer to the bottom scale ($n = 3 \times 10^{17}$ cm^{-3}). Inset: Mobility times N_{ii} for different aluminum compositions at 80 K upper curves — free carrier concentration $n = 5 \times 10^{17}$, lower curves 3×10^{17} cm^{-3}

in these two approaches. However, in a sample with doping greater than $\approx 1 \times 10^{18}$ one should be concerned with this problem. Besides samples with such a high doping become completely degenerate and other scattering mechanisms may play a more important role in the mobility [18]. The inset in Fig. 4 shows that there are significant differences when the aluminum composition is low and the electron concentration high. The indirect band gap material is not shown in the figure for there are no meaningful discrepancies between these two approaches (since all the electrons are in the X valley, with heavier effective mass).

In our case of Si doping in the range 5×10^{17} to 1×10^{18} cm^{-3}, the magnitudes of the experimentally deduced capture barriers imply that the capture is rather fast (in this range of Al composition and temperature) and the BH equation can be used with no further complications. However, in samples with higher capture barrier, where the photoexcited electrons remain in the conduction band, the range of temperature in the TDPPC measurement must be increased and then other scattering mechanisms could be important. Otherwise the same range of temperature could be used but Takimoto's correction must be included in the analysis and the final Arrhenius plot may differ from that found from conventional BH analysis. When the capture barrier is lower, the range of temperature should be decreased and then, depending on the free carrier concentration, again the use of the Brooks-Herring equation is a problem, recalling once more Fig. 4.

4. Conclusion

The capture energy barrier of the DX center has been evaluated for $Al_xGa_{1-x}As$ of different compositions using a method based on the Brooks-Herring potential for ionized impurity

scattering. Limitations of this method of analysis are discussed in terms of the polarization of the screening cloud, using Takimoto's theory. This is particularly important at low temperatures, low aluminum compositions, and high free carrier concentrations.

The TDPPC technique [11] is quite simple and can be applied for different structures which exhibit persistent photoconductivity. With some modifications, the discussed method of calculation can be applied for distinct situations.

In recent works there is a tendency to include an intermediate state for the electron capture [19 to 21]. The idea of this transition state was first argued by Theis and Mooney [22] and it would be a natural consequence of the DX ground state to have two electrons because there should be a state with only one trapped electron. However, the smooth decay observed in our TDPPC measurements suggests that, if this intermediate state exists, the transformation from d^+ to d^0 (or DX^0) and from d^0 (DX^0) to DX^- should have similar rates, or the transformation from d^+ to d^0 is much slower (if it was faster, the conductance would go down quickly at the beginning of the experiment, what is not observed since the incident light is kept rigorously below the bandgap). In both cases our calculation remains essentially valid since in the former case the global rate is the average between the two processes and the latter case characterizes a series process with the presence of intermediates, whose global velocity is determined by the slower process. Therefore the principle of our calculation will be valid, even in the presence of possible intermediate DX states.

The obtained value for indirect bandgap material may need some corrections if the effective mass state associated with the X valley is deep enough to metastably capture photogenerated electrons, instead of being captured by the relaxed DX center [20, 23, 24]. However, in this range of temperature (80 to 100 K), these corrections are small since the DX center dominates the transport properties.

Acknowledgements

The sample growth and most of the measurements were carried out at Advanced Materials Laboratory of Oregon State University (USA). One of us (L. V. A. Scalvi) would like to thank Prof. J. R. Arthur for letting him use all the facilities and for very fruitful discussions, L. Ungier for the help with the MBE sample growth and Seung-Bae Kim for all the help with the TDPPC setup. We mainly thank Prof. J. F. Wager without whom this work would never be done. We finally thank C.N.Pq. and CAPES for financial support.

References

[1] D. J. Chadi and K. J. Chang, Phys. Rev. Letters **61**, 873 (1988).
[2] D. J. Chadi and K. J. Chang, Phys. Rev. B **39**, 10063 (1989).
[3] P. M. Mooney, J. appl. Phys. **67**, R1 (1990).
[4] K. A. Kachaturyan, D. D. Awschalon, J. R. Rozen, and E. R. Weber, Phys. Rev. Letters **63**, 1311 (1989).
[5] S. Katsumoto, N. Matsunaga, Y. Yoshida, K. Sugiyama, and S. Kobayashi, Proc. 20th Internat. Conf. Phys. Semicond., Thessaloniki (Greece) 1990 (p. 481).
[6] J. C. Bourgoin and A. Maude, Appl. Phys. Letters **53**, 749 (1988).
[7] M. Lanoo, in: Physics of DX Centers in GaAs Alloys, Ed. J. C. Bourgoin, Sci.-Tech. Publ., Brookfield 1990 (p. 209).
[8] J. A. Van Vechten, Mater. Res. Soc. Symp. Proc. **46**, 83 (1985).
[9] J. A. Van Vechten, J. Phys.: Condensed Matter **1**, 5171 (1989).
[10] T. N. Morgan, Phys. Rev. B **34**, 2664 (1986).
[11] T. W. Dobson, L. V. A. Scalvi, and J. F. Wager, J. appl. Phys. **68**, 601 (1990).

[12] L. V. A. SCALVI and E. MINAMI, unpublished.
[13] P. M. MOONEY, N. S. CASWELL, and S. L. WRIGHT, J. appl. Phys. **62**, 4786 (1987).
[14] N. TAKIMOTO, J. Phys. Soc. Japan **14**, 1142 (1959).
[15] D. CHATTOPADHYAY and H. J. QUEISSER, Rev. mod. Phys. **53**, 745 (1981).
[16] G. L. HALL, J. Phys. Chem. Solids **23**, 1147 (1962).
[17] S. ADACHI, J. appl. Phys. **58**, R1 (1985).
[18] A. BARALDI, C. GUEZZI, A. PARISINI, A. BOSACCHI, and S. FRANCHI, Phys. Rev. B **44**, 8713 (1991).
[19] T. N. THEIS, P. M. MOONEY, and B. D. PARKER, J. electronic Mater. **20**, 35 (1991).
[20] L. DOBACZEWSKI and P. KACZOR, Phys. Rev. B **44**, 8621 (1991).
[21] V. MOSSER, S. CONTRERAS, J. L. ROBERT, R. PIOTRZKOWSKI, and J. F. ROCHETTE, Phys. Rev. Letters **66**, 1737 (1991).
[22] T. N. THEIS and P. M. MOONEY, Mater. Res. Soc. Symp. Proc. **163**, 729 (1990).
[23] J. E. DMOCHOWSKI, L. DOBACZEWSKI, J. M. LANGER, and W. JANTSCH, Phys. Rev. B **40**, 9671 (1989).
[24] P. SÉGUY, M. ZIGONE, and G. MARTINEZ, Phys. Rev. Letters **68**, 518 (1992).

(Received January 19, 1993)

MATERIALS RESEARCH SOCIETY SYMPOSIUM PROCEEDINGS VOLUME 325

Physics and Applications of Defects in Advanced Semiconductors

Symposium held November 29-December 1, 1993, Boston, Massachusetts, U.S.A.

EDITORS:

M.O. Manasreh
Wright Laboratory
Wright-Patterson Air Force Base, Ohio, U.S.A.

H.J. von Bardeleben
University of Paris VII/CNRS
Paris, France

G.S. Pomrenke
Air Force Office of Scientific Research
Bolling Air Force Base, D.C., U.S.A.

M. Lannoo
Institut Supériure d'Electronique du Nord
Lille, France

D.N. Talwar
Indiana University of Pennsylvania
Indiana, Pennsylvania, U.S.A.

MRS
MATERIALS RESEARCH SOCIETY
Pittsburgh, Pennsylvania

DIPOLE RELAXATION CURRENT IN N-TYPE $Al_xGa_{1-x}As$

LUIS V.A. SCALVI*, L. OLIVEIRA** AND M. SIU LI**

*Departamento de Fisica, UNESP - Bauru, Cx. Postal 473, 17033 Bauru - SP, Brazil

**Departamento de Fisica e Ciência dos Materiais, Instituto de Fisica e Quimica de São Carlos - USP, Cx. Postal 369, 13560 São Carlos - SP, Brazil

ABSTRACT

Thermally stimulated depolarization current (TSDC) spectra are reported for $Al_xGa_{1-x}As$ alloys with direct and indirect bandgap for the first time. The experimental data reveal the presence of electric dipoles in both samples which are interpreted by using the negative-U DX center model. These data are fitted by a relaxation time distribution approach yielding average activation energies in close coincidence with the DX center binding energy value.

INTRODUCTION

In the Chadi and Chang's negative-U model for the DX center [1], the substitutional impurity traps two electrons concomitant with lattice distortion along the <111> direction becoming located at an interstitial site. Then, the DX center ground state is negatively charged (DX^- state) and charge balance assures that the same amount of d^+ centers (substitutional sites) are generated in the $Al_xGa_{1-x}As$ sample, suggesting the formation of electric dipoles. Although Chadi and Chang's model has been accepted by most DX center researchers, Maude et al [2,3] have used mobility data to support a positive-U model. O'Reilly[4] has argued that mobility can be better fitted by a negative-U model where d^+ and DX^- center are strongly correlated and a dipole-like picture is used to describe scattering by $DX^- - d^+$ pairs. If impurity donors are randomly distributed in the AlGaAs sample, the probability that d^+ and DX^- to be first neighbors is negligibly low. However, the extra electrostatic energy gained by placing a d^+ center close to a DX^- center is of significant magnitude at a large fraction of sites [4]. Then, trapout occurs such that formation of DX^- centers close to d^+ centers is energetically very favorable.

In this paper we report experimental evidence for the existence of electric dipoles in n-type $Al_xGa_{1-x}As$ of direct and indirect bandgap, which are fitted by a Havriliak-Negami relaxation time distribution approach [5]. The average activation energy for dipoles

Mat. Res. Soc. Symp. Proc. Vol. 325. ©1994 Materials Research Society

reorientation has approximately the same value of the DX center binding energy, which represents the most striking feature of our data

EXPERIMENTAL PROCEDURE

We have used Si-doped molecular beam epitaxy (MBE) grown $Al_xGa_{1-x}As$ samples, 2 μm thick with the same structure as proposed by Chand et al [6], which has been published elsewhere [7]. The direct bandgap sample used is doped with $\equiv 1x10^{18}$ cm^{-3} (sample I) and the indirect bandgap sample is doped with $\equiv 5x10^{17}$ cm^{-3} (sample II). Aluminum composition of sample I is $x \equiv 0.32$ and sample II, $x \equiv 0.50$.

Thermally stimulated depolarization current (TSDC) is carried out as follows [7]: the sample is biased at room temperature (2.5 V) in darkness and cooled down to liquid He temperature, where the applied bias is removed. Subsequently the temperature is increased at a fixed rate, always in darkness, and the current is measured with the help of an electrometer and a recorder. No voltage is applied on the sample during the increase of temperature and no light is irradiated on the sample during the whole measurement.

TSDC RESULTS AND SIMULATION

Figure 1 shows the experimental TSDC spectrum for sample I. The temperature is increased at a rate of 0.081 K/sec and the measured thermally stimulated current presents a peak at 39 K. Considering that there is no light on the sample, no electron is photoexcited to the conduction band. The current seen in figure 1 can not be associated to an electronic current, which is evident by its order of magnitude, since the photoinduced current obtained for this sample is about 5 orders of magnitude higher than the TSDC current [7]. There is no known process which could be responsible for releasing few electrons and trapping them back at 39 K in the dark, since there is not enough thermal energy to overcome the DX center thermal emission barrier. We believe that the current peak seen in figure 1 is due to dipole reorientation. When the sample is biased at room temperature, the dipoles are oriented according to the electric field direction. Then the applied bias is removed at the lowest temperature. Increasing the temperature the oriented dipoles are allowed to reorient to their original positions, randomly distributed throughout the sample. Then an ionic dipole current is observed as shown in figure 1

cm 1 2 3 4 5 6 7 unesp 11 12 13 14 15 16 17

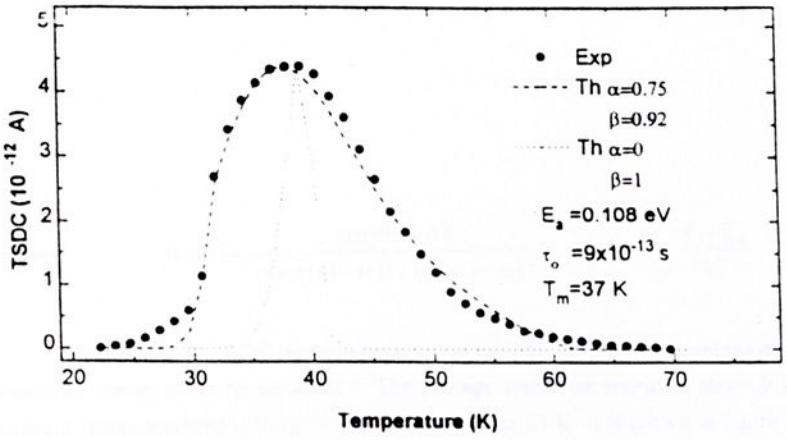


Figure 1. Thermally stimulated depolarization current of Si doped $Al_{0.32}Ga_{0.68}As$

TSDC experimental curve is usually fitted by a single curve, showing Debye behavior [8,9], with a single relaxation time and activation energy. However our data are better fitted by an asymmetric relaxation time distribution, the type of distribution first proposed by Havriliak and Negami [5]. In this case TSDC current density is given by:

$$J(T) = \frac{Q_p}{\tau_o} \int_{-\infty}^{\infty} f(u) \exp\left\{-\left[\left(u + \frac{E_a}{kT}\right) + \frac{kT^2}{\tau_o b E_a} \exp\left[-\left(u + \frac{E_a}{kT}\right)\right]\right]\right\} \qquad (1)$$

Where Q_p is the polarization charge (area under the experimental curve), τ_o is the relaxation constant time from Arrhenius formula, k is the Boltzmann constant, b is the heating rate and E_a is the activation energy. The distribution function is given by:

$$f(u) = \frac{1}{\pi} \operatorname{sen}\beta\theta \left\{1 + 2\cos(1-\alpha)\exp\left[-u(1-\alpha) + \exp\left[-2u(1-\alpha)\right]\right]\right\}^{-\frac{\beta}{2}} \qquad (2)$$

where $\tan(\theta) = \dfrac{\operatorname{sen}\pi(1-\alpha)}{\{\exp[u(1-\alpha)] + \cos\pi(1-\alpha)\}}$ and $u = \dfrac{E - E_a}{kT}$ (3)

The best fit to TSDC experimental curve is obtained with the continuous distribution of activation energy given by equation 2. The average activation energy is about 0.108 eV and the constant relaxation time is $9x10^{-13}$ sec, with a peak at 37 K. It is shown in figure 1 - dashed line. Debye single relaxation time ($\alpha = 0$, $\beta = 1$) gives a curve similar to the dotted line, using the same parameters as the average ones used for the distribution we get a curve with the same shape as the dotted line, but with a peak a 41 K. In order to obtain the dotted line of figure 1 we use a single constant relaxation time of $2.3x10^{-13}$ sec with the same activation energy (E_a = 0.108 eV) and get a peak at 39 K. As it can be seen the results are poor compared to the one obtained with Havriliak-Negami relaxation time distribution approach. Experimental data can also be fitted with single relaxation time approach. However it yields quite unreasonable parameters and must be disregarded. The obtained activation energy has the same value of the DX center binding energy what is the most striking feature of our data, suggesting a mechanism of electron transfer involving the DX center, which needs further investigation to confirm it.

TSDC spectrum is also reported for indirect bandgap material (sample II) as shown in figure 2 (solid circle). The heating rate is 0.076 K/sec and the current peak is at 46 K. Simulating the curves according to the relaxation time distribution approach (dashed line) yields an average activation energy of 0.124 eV and constant relaxation time of $9.7x10^{-13}$ sec.

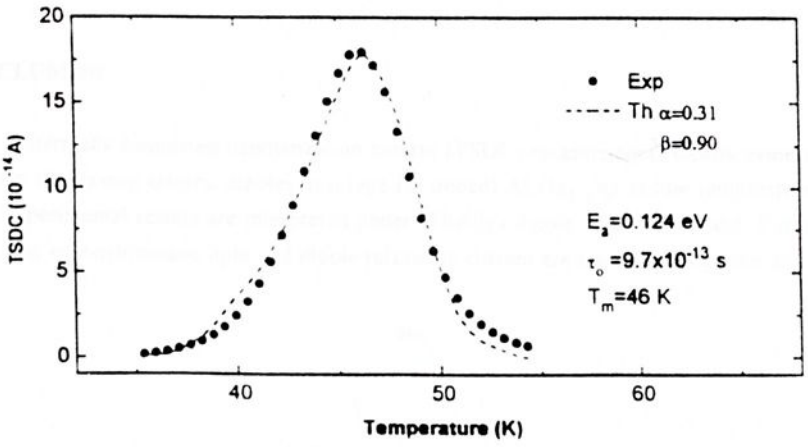


Figure 2. Thermally stimulated depolarization current of Si doped $Al_{0.5}Ga_{0.5}As$

The data reported here are strong evidences that the electron freezeout at DX centers, which occurs when temperature is lowered down, leads to charged localized states, since neutral impurities would not be responsible for ionic dipole current. In Chadi and Chang's model there are three first neighbors equivalent positions for a d^+ center close to a DX^- center. Although the probability that a d^+ and a DX^- centers to be first neighbors is negligibly small, O'Reilly [4] has argued that for a large fraction of sites the d^+ center can be considered as a perturbation in the DX screening potential and then, the $DX^- - d^+$ pair has to be treated as a dipole-like picture. A strong point to support the hypothesis that the observed current comes from the relaxation of $DX^- - d^+$ pairs is the fact that no single relaxation time approach can be used to fit satisfactorily the experimental data. This is consistent with other points such as the random distribution of d^+ center around the DX^- charged impurity (generation of a dipole length distribution) and the random distribution of Al atoms around both charge states which should contribute to the local field potential.

Although there is persistent photoconductivity (PPC) in indirect bandgap $Al_xGa_{1-x}As$ in the range 80-100 K [10], the order of magnitude of the photoinduced current is lower than in direct bandgap material. Below approximately 60 K the PPC vanishes, because the hydrogenic state associated with the X valley is deep and capture electrons metastably [11,12]. There is no reason to believe that there is a barrier for electron capture by this X valley effective mass state, since there is no lattice relaxation involved. Then, the obtained TSDC current shown in figure 2 is apparently contradictory with our $DX^- - d^+$ dipole hypothesis since vanishing of PPC in indirect bandgap AlGaAs should rule out this possibility, because the negatively charged DX ground state would be destroyed. However the way TSDC is carried out, support O'Reilly hypothesis because there is no light irradiated on the sample during the whole measurement. Thus, when the temperature is lowered, DX^- state is generated in the range 100 -80 K, and at lower temperature the electrons remain trapped at this negatively charged state since there is no light to excite electrons from the DX center to the effective mass X valley state. The lower magnitude of TSDC signal for sample II compared to sample I is also consistent with this hypothesis, since the number of generated DX^- state above 60 K is lower in indirect bandgap material. The obtained average activation energy is also in fair agreement with the DX center binding energy [6].

CONCLUSION

Thermally stimulated depolarization current (TSDC) measurements clearly evidenced the presence of relaxing electric dipoles in n-type (Si doped) $Al_xGa_{1-x}As$ at low temperature in the dark. Experimental results are interpreted under O'Reilly's dipole scattering model. Experiments combining monochromatic light and dipole relaxation current are under investigation and will be

fundamental to clearly determine whether observed currents come from DX^{-} - d^{+} pairs or any other kind of dipole. The most striking feature of our data is that the obtained activation energy has a very close value to the DX center binding energy. A model to explain these features has also been worked out and shall be published opportunely.

ACKNOWLEDGMENTS

These samples were grown at Advanced Materials Laboratory of Oregon State University. One of us (Luis V. A. Scalvi) thanks Prof. John R. Arthur for the hospitality during his stay at O.S.U. We also acknowledge the partial financial support from brazilian agencies Fapesp, CNPq, Finep and Capes.

REFERENCES

[1] D.J. Chadi and K.J. Chang, Phys. Rev. Lett. **61**, 873 (1988), Phys Rev. B **39**, 10063 (1989)

[2] D.K. Maude, L. Eaves, T.J. Foster and J.C. Portal, Phys Rev. Lett. **62**, 1922 (1989)

[3] D.K. Maude, J.C. Portal, L. Dmowski, T.J. Foster, L. Eaves, M. Nathan, M. Heiblum, J.J. Havris and R.B. Beal, Phys. Rev. Lett. **55**, 815 (1987)

[4] E.P. O'Reilly, Appl. Phys. Lett. **55**, 1409 (1989)

[5] S. Havriliak and Negami, Polymer **8**, 161 (1967)

[6] N. Chand, T. Hendersen, J. Klem, W. T. Masselink, R. Fisch, Y.C. Chang and H. Morkoç, Phys. Rev. B **30**, 4481 (1984)

[7] L.V.A. Scalvi, L. Oliveira, E. Minami and M. Siu Li, Appl. Phys. Lett. **63**, (in press)

[8] L. Oliveira, P. Magna, H.J.H. Gallo, E.C. Domenicucci and M. Siu Li, phys. stat. solidi (b) **171**, 141 (1992)

[9] W. van Weperen and H.W. den Hartog, Phys. Rev. B **18**, 2857 (1978)

[10] L.V.A. Scalvi and E. Minami, phys. stat. solidi (a) **139**, 145 (1993)

[11] J.E. Dmochowski , L. Dobackewski, J.M. Langer and W. Jantsch, Phys. Rev. B **40**, 9671 (1989)

[12] L. Dobaczewski and P. Kaczor, Phys. Rev. B **44**, 8621 (1991)

Light-induced relaxing dipoles in n-type $Al_xGa_{1-x}As$

Luis V. A. Scalvi
Departamento de Física UNESP Bauru, Caixa Postal 473, Bauru, São Paulo 17033-360, Brazil

Ligia de Oliveira
Departamento de Física Universidade Estadual Paulista Bauru, Caixa Postal 473, Bauru, São Paulo 17033-360, Brazil and Departamento de Física e Ciência dos Materias, Instituto de Física de São Carlos, Universidade de São Paulo, Caixa Postal 369, São Carlos, São Paulo 13560-970, Brazil

M. Siu Li
Departamento de Física e Ciência dos Materias, Instituto de Física de São Carlos, Universidade de São Paulo, Caixa Postal 369, São Carlos, São Paulo 13560-970, Brazil

(Received 6 January 1995; revised manuscript received 10 March 1995)

Thermally stimulated depolarization-current measurements with monochromatic light excitation are applied to $Al_xGa_{1-x}As$. We obtain conclusive evidence that electric-dipole relaxation occurs in this alloy. Light-induced relaxation of depolarization-current measurements show that relaxing dipoles have characteristics that are influenced by the wavelength of the monochromatic light. We associate these dipoles with a negatively charged DX-center ground state, since charge-relaxation currents are destroyed by photoionization of $Al_{0.50}Ga_{0.50}As$ using either 647-nm Kr^+ or 488-nm Ar^+ laser lines. Correlation may exist among charged donor states, DX^--d^+. Ionization at the DX-center threshold photoionization energy, $\cong$0.8 eV, leads to a striking current-peak shift, which can be explained using a model that involves As vacancies.

It is well known that the DX center is the dominant deep level in $Al_xGa_{1-x}As$ and the cause of persistent photoconductivity (PPC) observed in this alloy at low temperatures. In Chadi and Chang's negative-U model,[1] the substitutional impurity traps two electrons concomitant with lattice distortion, generating an interstitial negatively charged impurity (DX^-). Since electrons come from the dopant, when DX^- are generated, charge balance assures that the same amount of d^+ centers (substitutional donor after releasing one electron) are created in the $Al_xGa_{1-x}As$ sample. A few years ago O'Reilly[2] stated that mobility data in GaAs under hydrostatic pressure can only be explained with dipole scattering by DX^--d^+ pairs, since the extra electrostatic energy gained by placing a d^+ center close to a DX^- center is significant. Although, under regular doping concentrations, the probability that a d^+ center is the nearest neighbor to a DX^- center is negligibly small, correlation among DX^--d^+ charged donors has provided an explanation for some phenomena in $Al_xGa_{1-x}As$-based structures.[3,4]

Thermally stimulated depolarization-current (TSDC) measurements have given us conclusive evidence of the presence of the electric dipoles in both direct[5] and indirect[6] band-gap $Al_xGa_{1-x}As$. The results are modeled under O'Reilly's DX^--d^+ picture. In this paper we present results of a modified TSDC experiment, to verify the DX^- participation in the TSDC bands observed. In this procedure, an indirect band-gap sample is illuminated with monochromatic light at low temperature in order to remove electrons from DX centers. Such a treatment does not produce PPC in this material. Then, monochromatic light will not photoinduce an electronic current, due to the absence of PPC, and there is no depolarization current as well, because DX-center-related dipoles are destroyed by such a procedure.

Lang, Logan, and Jaros[7] proposed a DX model in which the defect is a complex involving a donor and an As vacancy (V_{As}). The attractive donor potential would lower the symmetry of V_{As} and split the triply degenerate t_2 state, but the overall properties would be determined by the vacancy potential itself.[8] Although it is claimed by Van Vechten[9] that there are more than sufficient vacancies in all types of GaAs and thus they should be taken into account in a DX-center model, the presence of vacancies to explain DX-center properties is no longer considered in most models in the past decade. It is generally accepted that the transport properties are dominated by the donor charge states (d^+,d^0,DX^-); however, vacancies can be responsible for some carrier trapping, which becomes very important in creating a dipole system and a TSDC measurable signal, since vacancies do exist in the sample, as assured by Van Vechten.

The samples used in this work were grown by molecular-beam epitaxy on an undoped, semi-insulating GaAs substrate. The direct band-gap $Al_xGa_{1-x}As$ sample has $x\cong 0.32$ and a Si impurity donor concentration of 1×10^{18} cm^{-3}. The indirect band-gap sample has $x\cong0.50$ and a Si doping of 5×10^{17} cm^{-3}. In order to prevent a two-dimensional electron-gas formation at the interface, since we are interested in the bulk properties itself, samples have the following structure: 0.25 μm of undoped GaAs buffer layer plus 0.25 μm of undoped $Al_xGa_{1-x}As$ that is compositionally graded from $x=0$ to $x\cong0.32$ (or $x\cong0.50$), 0.25 μm of undoped $Al_{0.32}Ga_{0.68}As$ (or $Al_{0.50}Ga_{0.50}As$), and the 2.0-μm active layer.

In usual TSDC experiments, a voltage is applied to the sample at room temperature in the dark while the temperature is decreased to about 10 K. Then the polarization voltage is removed, the temperature is allowed to increase at a

0163-1829/95/51(19)/13864(4)/$06.00 © 1995 The American Physical Society

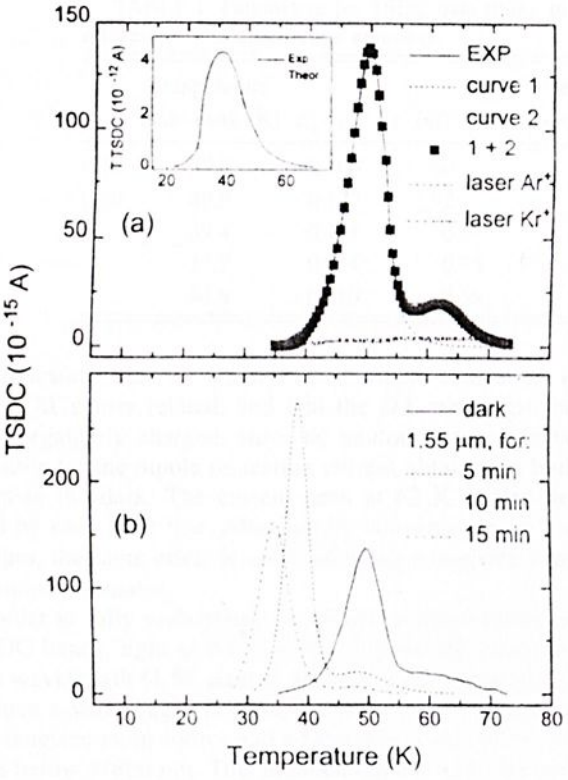


FIG. 1. (a) Thermally stimulated depolarization current in the darkness for $Al_{0.50}Ga_{0.50}As$ and influence of monochromatic light in TSDC bands. Broken line: Kr^+-laser excitation line (647 nm). Dotted line: Ar^+-laser excitation line (488 nm). Inset: TSDC in the darkness for $Al_{0.32}Ga_{0.68}As$. (b) Recorded TSDC bands after irradiating 1.55-μm excitation line for 5, 10, and 15 min in the indirect band-gap sample.

fixed rate, and the current is measured with an electrometer and recorded. The same contacts are used to measure the depolarization current. Dipoles present in the sample are polarized during cooldown and relax to their original random distribution as the temperature is increased.[5] Since no light reaches the sample, no electron is photoexcited to the conduction band when the temperature increases.

Figure 1(a) shows recorded TSDC bands for direct and indirect band-gap $Al_xGa_{1-x}As$. The inset in Fig. 1(a) is a usual TSDC result for the direct band-gap sample, which is about 30 times higher than the current of the indirect band-gap sample, which is shown in the major part of Fig. 1(a). The measured current of Fig. 1(a) is clearly not electronic,[5] considering its order of magnitude. Besides, there is no voltage applied to the sample when the temperature is increased. No known process could cause the release of a few electrons to the conduction band at low temperature and recapture at higher temperature in the dark. Our interpretation is that the observed current is due to electric-dipole reorientation.[5,6] The fitted curves are obtained using Havriliak-Negami relaxation-time distribution approach.[10] A distribution of relaxation times and activation energies is needed in order to fit the data, since we have a dipole-length distribution and the Al atoms are randomly distributed around the defect.[5] The obtained average activation energies are $E_a \cong 0.108$ eV for direct band-gap and $E_a \cong 0.132$ eV for indirect band-gap material, respectively. These values are both very close to the DX-center binding energy.[11] There is another peak in the $Al_{0.50}Ga_{0.50}As$ TSDC curve, with activation energy $E_a \cong 0.165$ eV and lower intensity. Since we have many vacancies in the $Al_xGa_{1-x}As$ sample,[9] we expect that they could trap electrons to become V_{As}^-. The 30-times-higher depolarization current in the direct band-gap sample is reasonable, since there are many more DX^--related dipoles even though the Si doping is only twice as high. The V_{As} unoccupied level is resonant with the conduction band, while the occupied level relaxes to a bound state in the gap.[7] In an As vacancy there are three "dangling" electrons;[8] two of them populate the s-like (a_1) state and the third one belongs to the threefold degenerate t_2 state. The extra electron of the charged vacancy (V_{As}^-) would also belong to this state. A ground state of t_2 symmetry is a candidate for a Jahn-Teller distortion.[8,12] This distortion in the V_{As}^- ion position could be responsible for the dipole system that relaxes at higher temperature, as shown by the smaller TSDC band in Fig. 1(a).

In our indirect band-gap $Al_xGa_{1-x}As$ sample, when monochromatic light is used to excite electrons from the DX center to the conduction band (X valley) at temperatures below $\cong 60$ K, the sample does not exhibit the PPC phenomenon. Electrons are immediately captured metastably by the X-valley effective-mass state.[13,14] Hence indirect band-gap material is suitable for testing the origin of TSDC bands by illuminating the sample with monochromatic light at low temperature in combination with regular TSDC. Since no electronic current is photogenerated in the indirect band-gap sample, it assures that the measured thermally stimulated current comes from relaxing dipoles.

Here we summarize our ideas before going any further: In the direct band-gap sample, as the temperature is lowered to 10 K in the dark, there is an electron freezeout at DX centers, and the TSDC band seen in the inset of Fig. 1(a) is observed. In the indirect band-gap sample, there are three states responsible for trapping the electrons: the X-valley effective mass, the DX center, and the As vacancy. Their occupation obeys some statistical distribution. The first is a neutral state (d^0), which cannot generate a TSDC band. The other two give rise to electric dipoles, which generate the two peaks shown in Fig. 1(a). This is quite consistent with the much lower current magnitude in the indirect band-gap sample depolarization, if compared to the direct band-gap sample.

Figure 1(a) also shows the effect of monochromatic light of two distinct wavelengths in the TSDC band. Light is applied as follows: The sample is electrically biased at room temperature by applying an electric field of 15.7 V/cm (the same as used in the regular TSDC procedure). Then the temperature is decreased slowly to about 10 K, when monochromatic light irradiates the sample for 5 min. The sample is returned to darkness and the electric field is removed. Then the temperature is increased at a fixed rate. The only modification to what we call here regular TSDC is the light excitation of the sample at the lowest temperature. We use $\lambda = 488$ nm from an Ar^+ laser line, which is above the band-gap transition or $\lambda = 647$ nm from a Kr^+ laser line, which is below the band-gap energy but well above the DX-center threshold photoionization energy (about 0.8 eV independent of aluminum mole fraction).[15] Either laser line destroys the TSDC bands obtained in the dark [Fig. 1(a)]. This is a very

TABLE I. Parameters for TSDC data fitting in $Al_xGa_{1-x}As$ using the Havriliak-Negami asymmetric relaxation-time distribution approach.

x	Temperature main peak (K)	E_a (eV)	τ (10^{-14} sec)	Temperature sec. peak (K)	E_a (eV)	τ (10^{-14} sec)	Obs.
0.32	39.0	0.108	90				dark
0.50	49.8	0.132	92	62.1	0.165	97	dark
	39.4	0.121	0.5	48.6	0.132	97	$\lambda = 1.55$ μm, 5 min
	37.7	0.114	0.75	52.7	0.143	97	$\lambda = 1.55$ μm, 10 min
	34.6	0.110	0.59	47.7	0.129	97	$\lambda = 1.55$ μm, 15 min

good indication that the main electric-dipole relaxation is actually DX-center related, and that the DX-center ground state is negatively charged, since no neutral state could be responsible for the dipole relaxation current obtained in both samples in the dark. The current peak at 62 K is also destroyed by each laser line. Although by convenience we use laser lines, the same effect is obtained using a tungsten lamp and a monochromator.

In order to fully understand the photoionization influence on TSDC bands, light at the DX-center threshold photoionization wavelength (1.55 μm) is applied to the sample for 5 min. Such a wavelength is obtained from a monochromator with a tungsten lamp source and a filter which cuts off wavelengths below $\cong 800$ nm. This monochromatic light does not destroy the TSDC band but induces a shift of the main current peak from 50 K (regular TSDC) to 39 K (light induced), corresponding to an average activation energy for dipole relaxation of 0.121 eV. There remains some dipole relaxation current with average activation energy of 0.132 eV, caused by a relaxing dipole system of reduced concentration (proportional to the area under the curve). This is seen in Fig. 1(b). For 5 min of illumination, the main peak becomes much narrower and higher, meaning that the dipole distribution is not as wide as in the darkness, but concentrated around a specific dipole system. Illuminating the sample at this wavelength for longer times gives results also shown in Fig. 1(b). All the parameters used to fit these data are given in Table I. The longer the illumination time, the lower the peak temperature and the lower the average activation energy of the main peak. It is interesting to notice that independent of illumination time, there is always a secondary peak that remains in a position very close to the TSDC band obtained in the dark, which means that some portion of the original dipole system distribution has not been completely destroyed after 15 min of illumination. Another feature is that τ_0, the average constant relaxation time has the same order of magnitude ($\cong 10^{-12}$ sec) for the measurements in the dark in both samples and for all the secondary bands in the experiments using 1.55-μm monochromatic light (Table I). Main bands obtained after light irradiation for different exposure times also have τ_0 with the same order of magnitude ($\cong 5 \times 10^{-15}$ sec), which is more than two orders of magnitude lower than the bands obtained in the dark. Mooney *et al.*[15] show that although 0.8 eV is the DX-center threshold photoionization energy, there is a variation of several orders of magnitude in the photoionization cross section when the photon energy changes from 0.8 to 2.0 eV, depending on the alloy composition. Then we do not expect the TSDC band to be destroyed when the sample is illuminated with 1.55-μm monochromatic light. However, the shift in the current peak is rather unexpected and suggests that the influence of monochromatic light of this wavelength is not only depleting electrons from DX^- centers. Actually, we believe that vacancies are very important to understanding the recombination process that takes place in our modified TSDC experiment.

In Fig. 2, we present a sketch of a configurational coordinate diagram proposed for the DX-center transition. Illuminating the sample with 0.8-eV monochromatic light, the DX^- center is taken to a postulated activated state (denoted as DX^* in Fig. 2). This state can release electrons to the X valley (conduction-band minimum) due to its parabolic potential. Such a possibility is in agreement with Mooney *et al.*,[15] since 0.8 eV is too low to completely photoexcite the DX center, particularly at $x \cong 0.50$, where the photoionization cross section increases over six orders of magnitude when the excitation light energy goes from 0.8 to 2.0 eV. Some electrons can populate the conduction band and be metastably trapped by the X-valley effective-mass state. The 1.55-μm wavelength also depletes occupied vacancies since the peak obtained at 62 K is destroyed. Lang, Logan, and

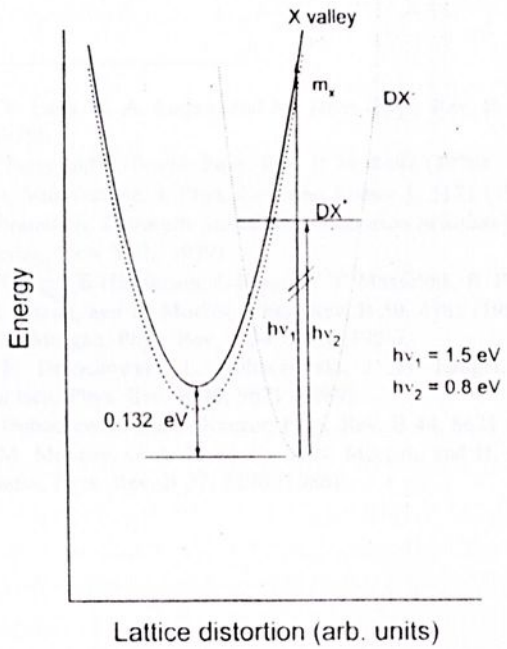


FIG. 2. Sketch of the configurational coordinate diagram involving DX^- electron thermal ionization and optical excitation to the conduction band in the indirect band-gap $Al_xGa_{1-x}As$ (X valley), also showing the X-valley effective-mass state (m_X) and the DX^* activated level.

Jaros[7] suggest a Franck-Condon shift of about 0.8 eV for their DX-center model transition. In this model, the DX center is basically an As vacancy, since the overall properties of the defect, such as energy and wave function, are quite similar to an isolated vacancy. Then, we believe that a transition to an unoccupied vacancy level is observed. However, the most important effect observed in the TSDC spectrum is the generation of a much more defined dipole system, concentrated around a specific system. Van Vechten[9] claims a tendency for a V_{As} center to be formed close to a donor in well-annealed samples. If such is the case, we believe that our excited DX center (DX^*) is able to give electrons to vacancies located close to a d^+ center and a more localized d^+-V_{As}^- dipole system is generated, being responsible for the peak observed in Fig. 1(b) after 5 min of illumination with 1.55-μm monochromatic light. This assumption is reinforced by the fact that light is applied in conjunction with the electric field, which could drive the electrons from DX centers to vacancies. As the illumination time increases, electrons populate more vacancies, leading to a broader TSDC band, since the dipole-length distribution and aluminum neighborhood widens the distribution. We should also mention that there are two possible kinds of V_{As}-related dipoles: V_{As}^--d^+ and distorted V_{As}^-, since the occupied As vacancy state is subject to a Jahn-Teller distortion.

Another possibility is that the activated DX^* state is frozen in this metastable configuration, giving rise to a dipole system such as DX^*-d^+, which is also helped by the electric field maintained during the sample illumination. It would also decrease the depolarization energy, as observed by the TSDC spectrum. We shall notice that this activated state must have a negative charge, since a neutral state would not lead to any measurable current, for there would not be a charge dislocation when it relaxes to a more stable configuration. Besides, the increase in the area under the TSDC curve assures that the transition via a DX^0 intermediate state is improbable, because fewer dipoles would be expected, and a DX^0 state, although still placed in an interstitial site, does not lead to any depolarization current when the temperature is increased, since there is no ion movement. The increase in the area under the curve means that charged states are being created and more dipoles are generated.

In conclusion, electric dipoles present in $Al_xGa_{1-x}As$ have relaxing characteristics that are strongly influenced by monochromatic light. The way wavelength affects the TSDC band is in close relation with photoionization cross-section curves as obtained by Mooney *et al.*[15] In other words, in the saturation region of DX center photoionization, light destroys the dipole current, which does not happen when the monochromatic light wavelength is near the DX-center photoionization threshold energy. Although we cannot assure that the dipoles are O'Reilly's DX^--d^+ pairs, our results strongly suggest that a DX^- ground state is responsible for the main dipole relaxation current peak obtained in the dark. The presence of vacancies in $Al_xGa_{1-x}As$ is also verified, since a secondary peak is always present in the TSDC spectrum, either in the dark or after illumination with 0.8-eV monochromatic light.

These samples were grown at Oregon State University. L.V.A.S. would like to thank Professor John Arthur and Professor John Wager for the hospitality and technical support during his stay in Corvallis. The authors acknowledge Brazilian financial agencies CNPq, CAPES, FAPESP, and FINEP.

[1] D. J. Chadi and K. J. Chang, Phys. Rev. B **39**, 10 063 (1989).
[2] E. P. O'Reilly, Appl. Phys. Lett. **55**, 1409 (1989).
[3] E. Buks, M. Heiblum, and H. Shtrikman, Phys. Rev. B **49** 14 790 (1994).
[4] C. Ghezzi, A. Parisini, and V. Dallacasa, Phys. Rev. B **50**, 2166 (1994).
[5] L. V. A. Scalvi, L. Oliveira, E. Minami, and M. Siu L., Appl. Phys. Lett. **63**, 2658 (1993).
[6] L. V. A. Scalvi, L. Oliveira, and M. Siu Li, in *Physics and Applications of Defects in Advanced Semiconductors*, edited by M. O. Manasreh, H. J. von Bardeleben, G. S. Pomrenke, and M. Lannoo, MRS Symposia Proceedings No. 325 (Materials Research Society, Pittsburgh, 1994), p. 285.
[7] D. V. Lang, R. A. Logan, and M. Jaros, Phys. Rev. B **19**, 1015 (1979).
[8] M. Jaros and S. Brand, Phys. Rev. B **14**, 4494 (1976).
[9] J. A. Van Vechten, J. Phys. Condens. Matter **1**, 5171 (1989).
[10] P. Bräunlich, *Thermally Stimulated Relaxation in Solids* (Springer Verlag, New York, 1979).
[11] N. Chand, T. Henderson, J. Klem, W. T. Masselink, R. Fischer, Y. C. Chang, and H. Morkoç, Phys. Rev. B **30**, 4481 (1984).
[12] T. N. Morgan, Phys. Rev. B **34**, 2664 (1986).
[13] J. E. Dmochowski, L. Dobaczewski, J. M. Langer, and W. Jantsch, Phys. Rev. B **40**, 9671 (1989).
[14] L. Dobaczewski and P. Kaczor, Phys. Rev. B **44**, 8621 (1991).
[15] P. M. Mooney, G. A. Northrop, T. N. Morgan, and H. G. Grimmeiss, Phys. Rev. B **37**, 8298 (1988).

Light and Thermal Excitation of Depolarization Current in Indirect Bandgap $Al_xGa_{1-x}As$

Luis V. A. Scalvi and L. Oliveira

Departamento de Física, Universidade Estadual Paulista, campus Bauru, Caixa Postal 473, Bauru, SP, 17033-360 Brazil

M. Siu Li

Departamento de Física e Ciência dos Materiais, Instituto de Física de São Carlos - USP Caixa Postal 369, São Carlos, SP, 13560-970, Brazil

Received August 25, 1995

Monochromatic light excitation in conjunction with thermally stimulated depolarization current measurements are applied to indirect bandgap $Al_xGa_{1-x}As$. The obtained average activation energy for dipole relaxation is in very close agreement with the DX center binding energy. Monochromatic light induces state transition in the defect and makes possible the identification of dipoles observed in the dark. Charge relaxation currents are destroyed by photoionization of $Al_{0.5}Ga_{0.5}As$ using either 647 nm Kr^+ or 488 nm Ar^+ laser lines, which are above the DX center threshold photoionization energy. It suggests that correlation may exist among charged donor states DX^--d^+. Sample resistance as a function of temperature is also measured in the dark and under illumination and shows the probable X valley effective mass state participation in the electron trapping. Ionization with energies of 0.8 eV and 1.24 eV leads to striking current peak shifts in the thermally stimulated depolarization bands. Since vacancies are present in this material, they may be responsible for the secondary band observed in the dark as well as participation in the light induced recombination process.

I. Introduction

The striking properties of the well-known DX center in $Al_xGa_{1-x}As$ has led many scientists to spend a good deal of work in its investigation in the past two decades. Although most of physics of this deep level has already been established, the peculiar situation by which the defect most likely presents a non-neutral ground state[1] has provided explanation for some new phenomena in $Al_xGa_{1-x}As$ based structures[2,3]. The presence of electric dipoles in $Al_xGa_{1-x}As$ has recently been demonstrated in direct bandgap sample[4] as well as indirect bandgap material[5] by using thermally stimulated depolarization current measurements (TSDC). The close agreement of dipole activation energy with the DX center binding energy and the use of asymmetric distribution of energies and dipole lengths has led us to associate them with DX centers (impurity donor placed at interstitial site and negatively charged). O'Reilly[6] stated that mobility data in GaAs under hydrostatic pressure can only be explained if DX^--d^+ correlations are taken into account, where d^+ means the substitutional impurity donor after releasing one electron. Preliminary measurements using TSDC in combination with monochromatic light excitation[7] indicates that this DX^--d^+ interaction can actually be the case, but there is also some possibility of carrier trapping by vacancies, which becomes very important in creating another dipole system, since vacancies do exist in $Al_xGa_{1-x}As$ as assured by Van Vechten[8]. In this paper we present results of thermally stimulated depolarization current in conjunction with monochromatic light of several wavelengths in an indirect bandgap $Al_xGa_{1-x}As$ sample. Monochromatic light excitation does not produce persistent photoconductivity (PPC) in this material. Then it is expected that no electronic current is photoinduced, due to absence of PPC, and moreover, TSDC bands obtained in the dark should

vanish because DX center-related dipoles are destroyed by this experimental procedure.

II. Light induced dipole relaxation in indirect bandgap $Al_xGa_{1-x}As$

The sample used in this work has been described elsewhere[4,7] and it is basically a molecular beam epitaxy (MBE) grown $Al_xGa_{1-x}As$ structure on a semi-insulating GaAs substrate. The active layer has 2 μm of $Al_xGa_{1-x}As$ where $x \approx 0.50$, doped with 5×10^{17} cm^{-3} Si.

In usual TSDC experiments, a voltage is applied to the sample at room temperature in the dark. It is used an electric field of 15.7 V/cm. Then the temperature is decreased to about 10 K, where the polarization voltage is removed and the temperature is allowed to increase at fixed rate. Using the same contacts where the voltage is applied, the current is now measured with an electrometer. Electric dipoles are polarized during cool down and relax to their original random distribution as the temperature is increased[4]. Since in usual TSDC procedure no light is shined on the sample, there is no photoionization of electrons to the conduction band when the temperature increases.

Fig. 1 shows recorded TSDC bands for $Al_{0.5}Ga_{0.5}As$. The inset in Fig. 1 is the usual TSDC procedure for this sample, where all the data is recorded keeping the sample in the dark The measured current is clearly not electronic, considering its low magnitude and because no voltage is applied to the sample when the temperature is increased. No known process could be responsible for releasing a few electrons to the conduction band at low temperature and recapture at higher temperature in the dark. Our interpretation is that observed current is due to electric dipole reorientation[4,5]. In order to fit the data we use Havriliak-Negami relaxation time distribution approach[9], which is shown in the inset in Fig. 1 by the continuos line. A distribution is needed since we have dipole-length distribution and Al atoms are randomly distributed around the defect[4], which suggests distinct activation energies due to distinct neighborhood. There is two bands in the inset of Fig. 1, reproduced by stars in the main figure. The major one has average activation energy $E_a \approx 0.132$ eV and the other current peak with lower intensity has $E_a \approx 0.165$ eV. Although both peaks have activation energy value very close to the DX center binding energy for this Aluminum composition[10], our results with direct bandgap material[4] and the preliminary investigation with monochromatic light excitation in dipole relaxation[7] indicate that the main peak is the DX center related one. We also expect a negatively charged DX center ground state, since no neutral state could be responsible for the obtained dipole relaxation current. Since there are many vacancies in the $Al_xGa_{1-x}As$ sample[8], we believe that they could trap electrons to become V_{As}^-. The V_{As} unoccupied level is resonant with the conduction band, while the occupied level relaxes to a bound state in the gap[11]. V_{As}^- presents a Jahn Teller distortion in its position[12] and could be responsible for the dipole system that generates the lower TSDC band shown in Fig. 1. This figure also shows the effect of monochromatic light of two distinct wavelengths in the TSDC band, that we call modified TSDC. This procedure can be shortly explained as being the same of usual TSDC with the only modification that when the temperature is at its minimum value ($\approx$ 10 K), monochromatic light irradiates the sample for some time. The sample is returned to darkness and the electric field is removed. Then, the temperature is increased at fixed rate. We use $\lambda = 488$ nm from an Ar^+ laser line, which is above the bandgap transition or $\lambda = 647$ nm from a Kr^+ laser line, which is below the bandgap energy but well above the DX center threshold photoionization energy (about 0.8 eV independent of aluminum mole fraction[13]). The irradiation time is 5 minutes. Either laser line destroys the TSDC bands shown in Fig. 1. This is the expected behavior for a dipole system DX center-related. The current peak at 62 K is also destroyed by each laser lines. The same effect is obtained using a tungsten lamp and a monochromator.

In Fig. 1 it is also presented the effect of illuminating the sample with $\lambda = 1.55\mu$m, the DX center threshold photoionization energy, for different exposure times. This is obtained from a monochromator with a tungsten lamp source and a filter which cuts off wavelengths below $\approx$ 800 nm. This light does not destroy the TSDC bands but induces a shift of the main current peak from

50 K (regular TSDC) to another temperature, which is the lower the longer the exposure time.

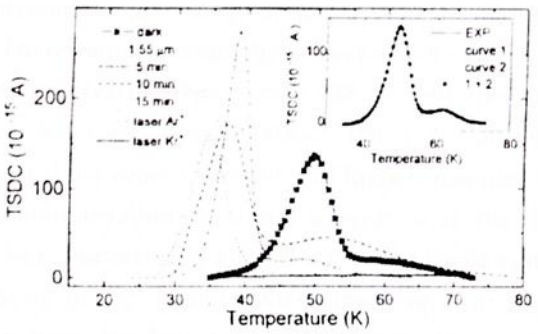


Figure 1. Thermally stimulated depolarization current in the darkness for $Al_{0.5}Ga_{0.5}As$ and influence of monochromatic light in TSDC bands for Ar^+ laser excitation line (488 nm), Kr^+ laser excitation line (647 nm) and TSDC bands after irradiating 1.55 μm excitation line for 5 to 15 minutes. Inset - TSDC obtained in the dark and data fitting using Havriliak-Negami approach.

We chose an indirect bandgap sample because when monochromatic light is used to excite electrons from DX centers to the X valley conduction band, below ≈ 60 K, the sample does not show PPC, because electrons are immediately trapped metastably by the X valley effective mass state[14–16]. Fig. 2 shows the resistance as a function of temperature for this sample in the dark and under illumination with $\lambda = 488$ nm Ar^+ laser line and with $\lambda = 1.55\mu$m. In the dark, the resistance increases as the temperature is lowered down, which is a expected behavior in $Al_xGa_{1-x}As$ of any Al composition, due to electron freezeout at DX centers, which is more effective above 150 K to about 60 K, when the resistance becomes practically constant. The temperature lowering is slow enough (≈ 5 hours) to prevent any sort of metasbility. Keeping the laser line illuminating the sample during the cooling, electrons remain in the conduction band, mainly due to photoexcitation of DX centers. The increase in resistance, starting about 60 K is a very good indication of the participation of the X valley effective mass state in the recombination process. Results of transient decay of persistent photoconductivity presented earlier[17] show the existence of this type of trapping. The illumination with $\lambda = 1.55\mu$m has an intermediate photoexcitation, as expected, since 0.8 eV is too low to completely photoexcite the DX center, particularly in this composition where the photoionization cross-section increases over 6 orders of magnitude when the excitation light energy goes from 0.8 eV to 2.0 eV [13]. Therefore, below ≈ 60 K, indirect bandgap $Al_xGa_{1-x}As$ is suitable for testing the origin of TSDC bands, since no electronic current is photogenerated in this sample. It assures that even after monochromatic light excitation, the measured thermally stimulated current comes from relaxing dipoles. The X-valley effective mass state after trapping electrons metastably, does not induce a new TSDC band because it is a neutral state (d^0) placed at a substitutional site.

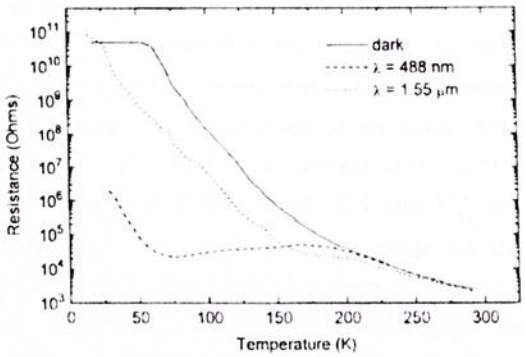


Figure 2. Resistance as a function of temperature in the dark and under constant illumination of Ar^+ laser excitation line (488 nm) and 1.55 μm excitation line.

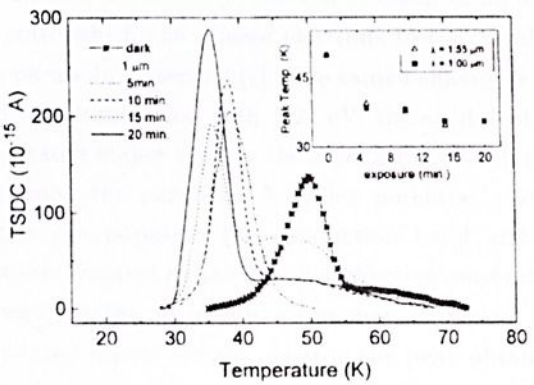


Figure 3. Influence of irradiating $\lambda = 1.0\mu$m excitation line in TSDC bands for $Al_{0.5}Ga_{0.5}As$, for 5 to 20 minutes. Inset-main peak temperature for several exposure times for 1.55 μm and 1.0 μm excitation lines.

Fig. 3 shows the effect of illumination with another wavelength, $\lambda = 1.0\mu$m, which is above the DX center threshold energy, but not yet in the saturation region[13,18]. The results are similar to those obtained for illumination with $\lambda = 1.55\mu$m, where the main current peak is shifted to a lower temperature. The results obtained from numerical simulation of TSDC bands shown in Figs. 1 and 3 are summarized in table I. The illumination with 5 minutes of monochromatic

light of 1.55 μm induces a shift ofthe main peak from 50 K, obtained in the dark to 39 K, corresponding to an average activation energy for dipole relaxation of 0.121 eV. There remains some dipole relaxation current with average activation energy of 0.132 eV, but this dipole system has lower concentration. For $\lambda = 1.55\mu$m the main peak becomes narrower and higher, meaning that the dipole distribution is not as wide as in the darkness, but concentrated around a specific dipole system. As shown in Fig. 1 and table I, the longer the illumination time, the lower the peak temperature and the lower the average activation energy of the main peak. No matter how long the exposure time with 1.55 μm illumination, there is always a remaining peak in position very close to the TSDC band obtained in the dark, which means that the original dipole system has not been completely destroyed even after 15 minutes of illumination. It is also interesting to notice that τ_0, the average constant relaxation time has the same order of magnitude ($\approx 10^{-12}$ sec) for the TSDC band obtained in the dark and for all the secondary current peaks after illumination. This is clearly described in table I. Main bands obtained after 1.55 μm light irradiation for different exposure times also have τ_0 with the same order of magnitude ($\approx 5 \times 10^{-15}$sec), which is more than two orders of magnitude lower than the band obtained in the dark. Also in table I are the results of exposure to $\lambda = 1.0\mu$m at 10 K. The bands are in very good agreement with results obtained for $\lambda = 1.55\mu$m, since the main peak for illumination with 1.0 μm is shifted to a lower temperature and the average activation energy is even lower than those obtained from data fitting of the main peaks shown in Fig. 1. It is expected since 1.24 eV is fairly higher than the DX center threshold photoionization energy, but not in the saturation region. Then the 1.0 μm excitation line drives the bands to a lower dipole relaxation energy, but does not destroy the band, unlike laser lines excitation. τ_0 has a value ($\approx 5 \times 10^{-14}$ sec) between the value calculated for the main band and the values for the secondary bands of Fig. 1. In the case of 1.0 μm we still have secondary peaks with activation energies and average constant relaxation time coincident with the main peak obtained in the dark. It means that the dipole system with $E_a \approx$ 0.132 eV is not completely destroyed by illumination with this wavelength, a similar result to what happens when the monochromatic light has $\lambda = 1.55\mu$m. There is a tendency for driving the main peak position to lower temperature as the exposure time gets longer, either for 1.0 μm curves or 1.55 μm curves. This is seen in the inset of Fig. 3. It seems that the temperature is going to steady at some limiting value, since the peak position seems to have exponential-like behavior.

Our interpretation for the recorded shifted bands is as follows: in indirect bandgap $Al_xGa_{1-x}As$, there are three states responsible for trapping the electrons, the X-valley effective mass state, the DX center and the As vacancy, the occupation obeys some statistical distribution. The first is a neutral state (d^0) which can not generate a TSDC band. DX and V_{As}^- are negatively charged and could be responsible for the two peaks obtained in the dark and seen in Fig. 1. This is quite consistent with the much lower dipole current magnitude recorded in this sample, if compared to direct bandgap $Al_xGa_{1-x}As$[4,5], which does not present a double TSDC band. The DX^- ground state can be photoexcited, releasing electrons to the conduction band. When excited with 0.8 eV, the DX is taken to an activated state which can release electrons to the X valley due to parabolic potential [7]. The same behavior is expected for illumination with 1.24 eV, the excited state being located higher than in the case of Fig. 1, but still not crossing the parabolic X valley potential. Some electrons can populate the conduction band and be metastably trapped by the X valley effective mass state. Both wavelengths, although not enough to deplete the DX^- related dipole system, destroy the peak obtained at 62 K. Lang *et al*[11] suggest a Franck-Condon shift of about 0.8 eV for the vacancy transition between occupied and unoccupied states. We believe that the peak at 62 K is destroyed by the V_{As}^- transition to an unoccupied vacancy level. In both cases, of illumination with 1.55 μm and 1.0 μm, there is generation of a much more defined dipole system, concentrated around a specific system, after some exposure time. The excited DX level is able to give electrons to vacancies located close to d^+ center, since there is a tendency for a V_{As} to be formed close to a Si donor[8]. Then a more localized $d^+ - V_{As}^-$ dipole system is generated. This is observed in Fig. 1 with 5 minutes of illumination. This assumption is reinforced by the fact that light is applied in

Table I - Parameters for TSDC data fitting in $Al_{0.5}Ga_{0.5}As$ using Havriliak-Negami assymetric relaxation time distribution approach.

Temperature main peak (K)	E_a (eV)	τ (10^{-14} sec)	Temperature sec. peak (K)	E_a (eV)	τ (10^{-14} sec)	OBS.
49.8	0.132	92	62.1	0.165	97	dark
39.4	0.121	0.5	48.6	0.132	97	λ=1.55μm - 5 minutes
37.7	0.114	0.75	52.7	0.143	97	λ=1.55μm - 10 minutes
34.6	0.110	0.59	47.7	0.129	97	λ=1.55μm - 15 minutes
38.3	0.104	30.0	—	—	—	λ=1.0μm - 5 minutes
38.2	0.109	6.0	48.5	0.133	97	λ=1.0μm - 10 minutes
35.6	0.102	5.0	46.3	0.132	97	λ=1.0μm - 15 minutes
35.5	0.102	4.5	48.7	0.133	97	λ=1.0μm - 20 minutes

conjunction with the electric field, which could drive the electrons from DX centers to vacancies. There is another kind of V_{As} related dipole, since the occupied V_{As} is subject to a Jahn-Teller distortion.

For excitation with 0.8 eV, as the illumination time gets longer than 5 minutes, electrons populate more vacancies leading to the broader TSDC band observed, since the dipole length distribution and aluminum neighborhood widens the distribution. For excitation with 1.24 eV, after 15 minutes of illumination the secondary peak becomes fairly high, reaching almost half of the main peak height. When the exposure time is 20 minutes, the secondary peak becomes very low and the main peak is the highest recorded for this excitation line, the area under the curve remaining practically constant. Once again the more localized dipole $d^+ - V_{As}^-$ system is generated and the number of similar pairs seems to increase with the exposure time. There is also the possibility that the excited DX center state has negative charge and could form pairs with vacancies[7].

Conclusion

Electric dipoles present in $Al_xGa_{1-x}As$ have relaxing characteristics strongly influenced by the wavelength of irradiation light. The way wavelength affects TSDC bands is in close agreement with measurements of resistance as a function of temperature, under influence of $\lambda = 488$ nm Ar^+ laser line and $\lambda = 1.55\mu$m monochromatic light. In the saturation region of DX center photoionization[13], light destroys the dipole current, which does not happen when the excitation energy is about the DX center photoionization threshold energy, neither higher than this energy, since it is still below the saturation region. The presence of the X-valley effective mass state is also verified in the curve of resistance under illumination. Results presented here, reinforced by results obtained for direct bandgap $Al_xGa_{1-x}As$[4,5] strongly suggests that a DX ground state is related to TSDC bands obtained in the dark. This dipole system could be DX^--d^+ pairs as predicted by O'Reilly[6]. The presence of vacancies in these samples is also verified, since a secondary peak is always present in the TSDC spectrum, either in the dark or after illumination with 0.8 eV or even with 1.24 eV monochromatic light.

Acknowledgments

This sample was grown at Oregon State University, U.S.A.. Luis V.A. Scalvi would like to thank profs. John Arthur and John Wager for the hospitality and technical support during his stay in Corvallis. The authors acknowledge Brazilian financial agencies: CNPq, CAPES, FAPESP and FINEP.

References

1. D. J. Chadi and K. J. Chang, Phys. Rev. **B39**, 10063 (1989).
2. E. Buks, M. Heiblum and H. Shtrikman, Phys. Rev. **B49**, 14790 (1994).
3. C. Ghezzi, A. Parisini and V. Dallacasa, Phys. Rev. **B50**, 2166 (1994).
4. L. V. A. Scalvi, L. Oliveira, E. Minami and M. Siu Li, Appl. Phys. Lett. **63**, 2658 (1993).

5. L. V. A. Scalvi, L. Oliveira and M. Siu Li, Mat. Res. Soc. Symp. Proc. **325**, 285 (1994).
6. E. P. O'Reilly, Appl. Phys. Lett. **55**, 1409 (1989).
7. L. V. A. Scalvi, L. Oliveira and M. Siu Li, Phys. Rev. B **51**, 13864 (1995).
8. J. A. Van Vechten, J. Phys. Condens. Matter **1**, 5171 (1989).
9. P. Bräunlich, *Thermally Stimulated Relaxation in Solids*, (Springer Verlag, New York 1979).
10. N. Chand, T. Henderson, J. Klem, W. T. Masselink, R. Fischer, Y.C. Chang and H. Morkoç, Phys. Rev. **B30**, 4481 (1984).
11. D. V. Lang, R. A. Logan and M. Jaros, Phys. Rev. **B19**, 1015 (1979).
12. M. Jaros and S. Brand, Phys. Rev. **B14**, 4494 (1976).
13. P. M. Mooney, G. A. Northrop, T. N. Morgan and H. G. Grimmeiss, Phys. Rev. **B37**, 8298 (1988).
14. J. E. Dmochowski, L. Dobaczewski, J. M. Langer and W. Jantsch, Phys. Rev. **B40**, 9671 (1989).
15. L. Dobaczewski and P. Kaczor, Phys. Rev. **B44**, 8621 (1991).
16. P. Séguy, M. Zigone and G. Martinez, Phys. Rev. Lett. **68**, 518 (1992).
17. L. V. A. Scalvi, L. Oliveira, E. Minami, M. H. Degani and M. Siu Li, Braz. J. Phys. **24**, 379 (1994).
18. R. Legros, P. M. Mooney and S. L. Wright, Phys. Rev. **B35**, 7505 (1987).

Radiation Effects & Defects in Solids, Vol. 146, pp. 175–186 © 1998 OPA (Overseas Publishers Association) N.V.
Reprints available directly from the publisher
Photocopying permitted by license only
Published by license under
the Gordon and Breach Science
Publishers imprint
Printed in India

INVESTIGATION OF TEMPERATURE INFLUENCE ON PHOTO-INDUCED CONDUCTIVITY IN N-TYPE $Al_xGa_{1-x}As$

MARCO H. TAQUECITA [a,b], LUIS V.A. SCALVI [a,*], L. OLIVEIRA [a], M. SIU LI [c] and S.B. PARREIRA [a,b]

[a] *Departamento de Física – FC, Universidade Estadual Paulista, Cx. Postal 473, Bauru, SP 17033-360, Brazil;* [b] *Departamento de Engenharia Elétrica – FET, Universidade Estadual Paulista, Cx. Postal 473, Bauru, SP 17033-360, Brazil;* [c] *Instituto de Física de São Carlos, Universidade de São Paulo, Cx. Postal 369, São Carlos, SP 13560-970, Brazil*

(Received 27 October 1997)

We present conductance as function of temperature ($G \times T$) under influence of monochromatic light in the range 0.5–1.5 μm for direct as well as indirect bandgap n-type $Al_xGa_{1-x}As$. Results obtained below 60 K in indirect bandgap sample show the presence of another level of trapping, besides the DX centre, probably a X-valley effective mass state. In direct bandgap samples, these $G \times T$ curves show that above bandgap light increases conductivity to higher values than at room temperature and below bandgap light is not enough to avoid trapping. Photoconductivity spectra in indirect bandgap $Al_xGa_{1-x}As$ show that above ≅120 K, the absence of persistent photoconductivity contributes for a very clean spectrum. The mobility of $Al_xGa_{1-x}As$ is modelled considering dipole scattering. Data of transient decay of persistent photoconductivity is simulated using this approach.

Keywords: Aluminium gallium arsenide; III–V semiconductors; DX centre; Photoconductivity; Dipoles

1 INTRODUCTION

To an effective understanding of the combination of electrical and optical properties of $Al_xGa_{1-x}As$ one must decrease the temperature,

* Corresponding author.

since at room temperature thermal generation of charge carriers does not allow the verification of transitions between bands. However, temperature lowering induces electron trapping at a defect known as DX centre [1]. Although most of the physics of this deep level has already been established, the peculiar situation by which the defect most likely presents a non-neutral ground state [2] has provided explanation for some transport properties in new $Al_xGa_{1-x}As$ based structures [3–5], since it may have correlations with positive charge centres present into the sample. The negatively charged DX^- state is located at an interstitial position, stabilised by strong electron–phonon coupling. In this work we present conductance as function of temperature measured under influence of monochromatic light and variation of photoconductivity excitation with wavelength for indirect bandgap $Al_xGa_{1-x}As$ measured at several temperatures. We investigate the effect of temperature and the presence of deep levels, mainly the DX centre. Samples used in this work have been described elsewhere [6].

To maintain charge neutrality in the sample, one must have the same amount of DX^- and d^+ centres, where the first means the substitutional donor with one extra electron in its configuration and located at an interstitial position, d^+ means the same impurity after releasing one electron and still located in the substitutional site. Based on this charge neutrality, O'Reilly [7] has explained mobility data in GaAs under hydrostatic pressure, stating that correlation among DX^- and d^+ impurities must be taken into account in order to fully understand the transport properties. Thermally stimulated depolarisation current measurements (TSDC) performed in $Al_xGa_{1-x}As$ samples leads to relaxation processes with DX^- related feature [6,8,9]. A few years ago transient decay of persistent photoconductivity (TDPPC) was simulated and it was found that the best fit to experimental data is obtained with a trapping kinetics model based on Chadi and Chang's DX centre model [2,10]. However a perfect data fitting was only obtained if one postulates the existence of a shallower donor, whose trapping becomes very important for long decay times. Up to now, the nature of such a level remains obscure. The possibility of dipole formation in $Al_xGa_{1-x}As$, brought by TSDC results, yields new possibilities for the simulation, since DX^- related dipoles will be less efficient electron scatters than the isolated DX^- impurity and the mobility shall increase. The overall effect is the increase in the sample conductivity for longer decay times, exactly

what is observed in TDPPC experimental data [10]. In this paper we also present a discussion of dipole scattering in $Al_xGa_{1-x}As$ based on TDPPC data and O'Reilly's $DX^- - d^+$ interaction hypothesis, taking into account the initial formation of the shortest dipoles in the capture process.

2 LIGHT INDUCED CONDUCTIVITY MEASUREMENTS IN $Al_xGa_{1-x}As$

Monochromatic light plays a very important role in the electrical conduction of $Al_xGa_{1-x}As$ samples at low temperature. Figure 1 shows the conductance as a function of temperature for $Al_xGa_{1-x}As$ samples in the dark and under steady illumination with several wavelengths. For indirect bandgap sample, Fig. 1(a), the conductance decreases as the temperature is lowered down, in the dark, due to regular bandgap recombination and mainly due to electron freezeout at DX centres, which is stronger below $\cong 120$ K. Temperature lowering is slow enough ($\cong 5$ h) to prevent any sort of metastability. Illuminating the sample with $\lambda = 1.55\,\mu$m, very little modification of the curve in the dark is obtained, only below $\cong 120$ K a noticeable shift is observed. This photon energy (0.8 eV) is the DX centre photoionisation threshold energy [11]. The same behaviour is obtained from illumination with $\lambda = 1.00\,\mu$m, which is above the DX centre photoionisation threshold energy but not yet in the saturation region [11]. In all the measurements done under illumination, we have used a tungsten lamp in conjunction with a monochromator. When $\lambda = 488$ nm monochromatic light is kept shining the sample during cooling down, the conductance follows the same behaviour as seen in the dark until about 180 K, when photoexcitation starts to take place in the sample. In the range 180–300 K nothing is observed, although this photon energy is high enough to excite bandgap transition and electrons trapped at impurities. There is a local minimum in conductance about 170 K and again an increase in conductance as the temperature is further decreased until about 70 K when it starts to decrease. This last decrease in conductance is a very good indication of the existence of the X-valley effective mass state, which has a very important participation in the recombination process at very low temperatures. Figure 1 must be seen as a dynamical process of

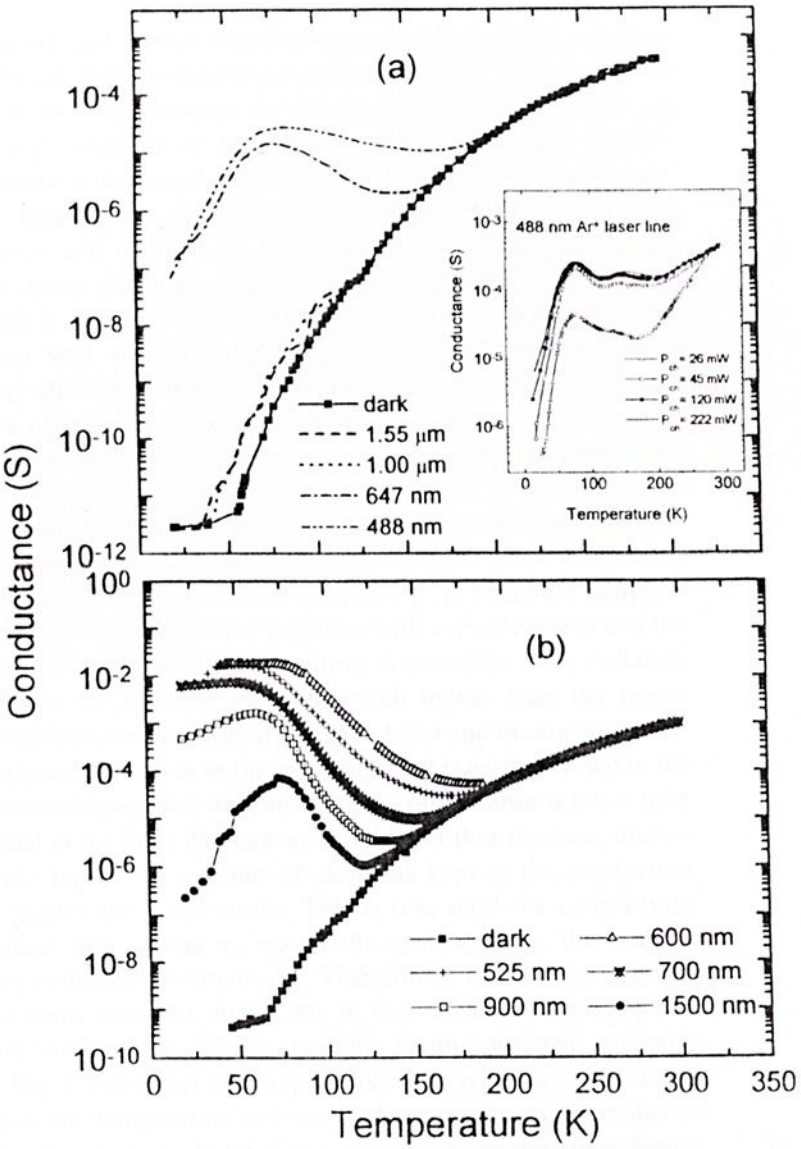


FIGURE 1 (a) Conductance as a function of temperature under steady illumination with several wavelengths, according to the legend, for indirect bandgap $Al_xGa_{1-x}As$. All lines obtained from a tungsten lamp plus a monochromator. Inset – Conductance × temperature for illumination with $\lambda = 488$ nm Ar^+ laser line with varying power. (b) Conductance × temperature for direct bandgap $Al_xGa_{1-x}As$ (lamp plus monochromator).

thermal capture and photoexcitation which are taking place simultaneously. The curve shape depends on the light energy and also in how efficient it is to keep electrons in the conduction band against the thermal "force" which drives the electrons towards the traps, since as the temperature is decreased, traps becomes the most thermodynamically stable location for the conducting electrons. So if the light has enough energy and intensity, it may create a metastable conducting state, where more electrons are kept in the conduction band. A very similar result is obtained with illumination of 647 nm, which is below bandgap but well above the DX centre threshold photoionisation energy, since the curve shape is about the same, and the overall conductance is always lower, which is expected since we do not have bandgap transition with this excitation. The local minimum takes place at about 140 K and, again, it must be understood as the dynamical combination of thermal trapping and photoionisation from DX centres. The influence of light intensity in creating a more conducting metastable state is confirmed in the inset of Fig. 1, where the sample is illuminated with $\lambda = 488$ nm Ar^+ laser line with variable power and the conduction as a function of temperature is measured. The radiation power used in the inset of Fig. 1 is much higher than the power obtained with the combination of tungsten lamp and monochromator, used to generate the curves in the main Fig. 1. It is easily verified in the curve for illumination with 488 nm that the conductance is lower than those plotted in the inset. We can see in the inset that the more intense the light the higher the amount of electrons kept in the conduction band, no matter the temperature. This is true until the temperature reaches about 70 K, where no matter the light intensity, the conductance starts to decrease dramatically. Therefore, if the X valley effective mass state traps electrons metastably in this range of temperature as reported in the literature [12,13], it cannot be photoexcited, as clearly shown in Fig. 1. For direct bandgap sample, Fig. 1(b), the conductance decreases as the temperature is lowered down in the dark, similar to indirect bandgap sample. In the curves with steady illumination there is a local minimum between 100 and 200 K. The local minimum with higher temperature ($\cong$186 K) corresponds to illumination with 600 nm ($\cong$2.06 eV), a very close value to bandgap transition and then the illumination is a much more efficient process in this case. The aluminum composition in this sample is about 32% [8]. It is important to

mention that intensity is kept constant by controlling the lamp current. For the curves with illumination with $\lambda = 900\,\text{nm}$ and $\lambda = 1500\,\text{nm}$ there is another decrease in conductance for temperatures lower than $\cong 70\,\text{K}$, which does not happen for the other curves, with higher energy illumination. This is different from what is observed in Fig. 1(a), where even for above bandgap illumination this conductance decrease is observed. These results indicates that although this level of trapping is stronger in indirect bandgap $Al_xGa_{1-x}As$, it also occurs in direct bandgap samples.

Figure 2 shows variation of photoconductivity excitation with wavelength for an indirect bandgap $Al_xGa_{1-x}As$ at several temperatures. The inset in Fig. 2 shows the measurement at 200 K, which would be hard to visualise if plotted with the other curves in the main figure. The scanning rate is 0.5 nm/s from higher to lower wavelength. This figure illustrates the influence of DX centre, since at 40 and 80 K, the transition has no well defined end, because optical excitation as well as thermal capture are slow processes and then the energy value where transition ends cannot be seen clearly. Bandgap transition is better seen

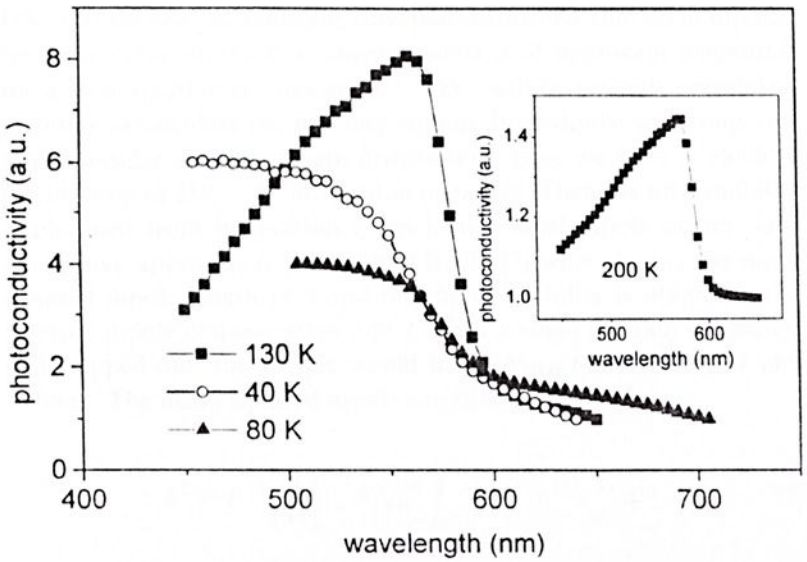


FIGURE 2 Variation of photoconductivity excitation with wavelength for indirect bandgap $Al_xGa_{1-x}As$ at several temperatures.

for temperatures higher than 120 K. Even at 200 K, although the optical excitation is not so efficient (the maximum value is only 1.5 times the minimum value), the transition is clearly seen. With curves obtained at several temperatures we can estimate [14] the Al composition in the sample and obtained $\cong 56\%$.

3 DIPOLE SCATTERING IN N-TYPE $Al_xGa_{1-x}As$

Correlations among charged impurities contribute to increasing the sample mobility, since ion pairs are much less effective electron scatters than the isolated charged impurity. In $Al_xGa_{1-x}As$ samples, impurities are randomly distributed throughout the sample and the probability that the nearest defect centre lies inside a shell of distance r from a d$^+$ centre, short enough to be considered a dipole, is rather small [15]. In a sample held at low temperature, the probability that the nearest defect to a d$^+$ centre is a DX^- is even lower. However in a capture process, electrons may not be trapped randomly, but their capture may be driven by electrostatic forces. O'Reilly [7] argues that the initial formation of DX^- centres involves replacing close pairs of positive charges by dipoles, since the extra electrostatic energy gained is of significant magnitude for a large fraction of sites and d$^+$–DX^- will be strongly correlated. In order to calculate the mobility coming from dipole scattering, one must consider a dipole length distribution, since we have a random distribution of DX^- – d$^+$ interaction distances. Then the total mobility is obtained from integration of each individual dipole scatter. One alternative approach is given by O'Reilly [7] who obtains the mean squared dipole length (L^2) and the dipole mobility is obtained considering dipole concentration and L^2. For a small fraction of carriers (f) trapped out, the sample would have ($N_{DOP}f/2$) dipoles per unit volume. The mean squared dipole length is given by [7]

$$L^2 = f^{-1}\left[\frac{3}{4\pi}\right]^{2/3} N_{DOP}^{2/3} \int_0^{-\ln(1-f)} y^{2/3} e^{-y}\, dy, \qquad (1)$$

where N_{DOP} is the doping concentration. In the following calculation, O'Reilly's approach is used.

Stratton [16] derives the scattering cross section for a screened dipole and obtains the relation between ionised impurity scattering and dipole scattering [16]:

$$\gamma = \frac{N_{ii}\mu_{ii}}{N_{DIP}\mu_{DIP}} = 2(k_1 L)^2 g(\eta)\frac{F_2}{F_1}, \tag{2}$$

where N_{ii} and μ_{ii} are the ionised impurity concentration and the ionised impurity mobility respectively. N_{DIP} and μ_{DIP} are the electric dipole concentration and the dipole mobility respectively. k_1 is the wavenumber of an electron with energy kT. $g(\eta)$ is a function of the normalised Fermi Level η, measured from the bottom of the conduction band, as given by Stratton. F_1 and F_2 are Fermi Dirac integrals of order 1 and 2 respectively. Figure 3 shows numerical simulation results of transient decay of persistent photoconductivity, compared to experimental data at 85 K. Initially impurities are isolated either in the form DX^- or d^+ at 85 K in the dark. Then the sample is illuminated with sub bandgap light (900 nm), which corresponds to about 1.36 eV, well below the bandgap transition. When conductance reaches saturation, the illumination is removed and trapping takes place. A d^+ centre located close to another d^+ centre traps two electrons becoming DX^- in agreement with Chadi and Chang's model, and resulting in a $DX^- - d^+$ dipole. It is easily calculated from Eq. (2) that mobility due to dipole scattering is much higher than mobility due to ionised impurity scattering in this range of temperature. It is possible to conclude that scattering is completely dominated by isolated ionised impurities, and the mobility is given by Brooks–Herring equation [10]. The crucial point to be understood is that although the dipole scattering by $DX^- - d^+$ correlated impurities does not contribute for the overall mobility, the amount of isolated d^+ or DX^- decreases significantly and then the dominating ionised impurity scattering is changed by the association of impurities in pairs. In Brooks–Herring equation mobility is inversely proportional to the ionised impurity concentration. The overall effect is the increase in mobility as a function of time in TDPPC if compared to Chadi and Chang's negative U model, where the amount of isolated ionised impurities remains practically constant during the whole measurement, either in the state d^+ or DX^-. As a consequence the sample conductivity shall decrease slower than obtained if only isolated

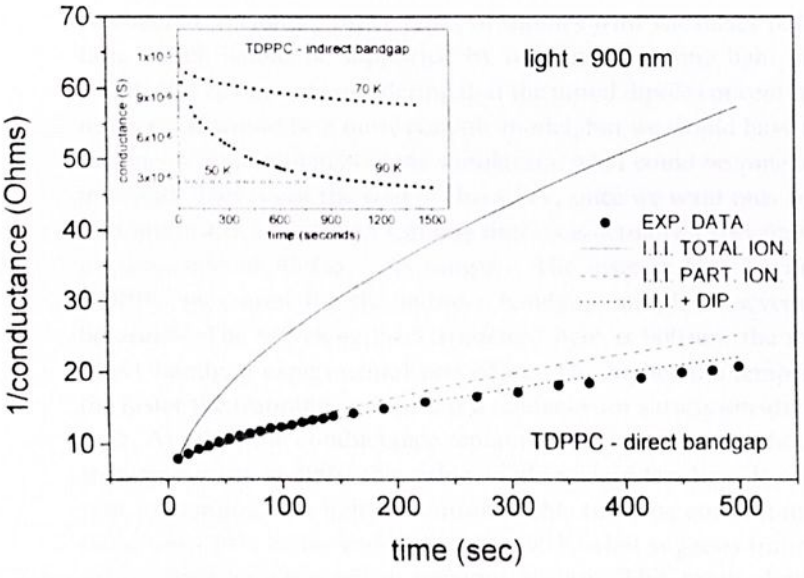


FIGURE 3 Data fitting of TDPPC data of $Al_{0.32}Ga_{0.68}As$ at 85 K. Full line – initial free carrier concentration = 1×10^{17} cm^{-3}, considering only isolated ionised impurity (I.I.I.) scattering. Broken line – initial free carrier concentration = 2.2×10^{17} cm^{-3}, only I.I.I. scattering. Dotted line – initial free carrier = 2.2×10^{17} cm^{-3}, I.I.I. plus dipole correlation. Inset – TDPPC for indirect bandgap $Al_xGa_{1-x}As$.

scattering centres are considered. In Fig. 3 is seen experimental data of TDPPC for the $Al_{0.32}Ga_{0.68}As$ sample, and numerical simulation based on Chadi and Chang's model, considering three cases: (1) all the impurities ionised at the beginning with only isolated ionised impurity scattering, (2) ionised impurity scattering with initial free carrier concentration of 2.2×10^{17} cm^{-3}, (3) including dipole formation with the same initial free electron concentration. It is important to notice that the only adjustable parameter is the initial free electron concentration. Capture by Chadi and Chang's model gives good fit in the beginning of the decay, but not for longer times where the calculated conductivity is lower than the measured one. A rather different result is obtained when dipole formation is taken into account, as can be seen in Fig. 3. Although dipole scattering does not contribute for the mobility, as already mentioned, it decreases the amount of isolated charged impurities, increasing the overall mobility. However a perfect fit was not obtained with such a simple approach. A more complex model could be

considered, including other types of dipoles with vacancies participation, which would be supported by our findings using light induced TSDC [6,17], or even considering that the initial dipole concentration is not zero. It would be a more realistic model, but we would have also to include more parameters in the simulation, what could become hard to interpret. This is not the goal of this work, since we want only to show that impurities association forming dipoles is actually a very important phenomenon in $Al_xGa_{1-x}As$ samples. The inset in Fig. 3 represents TDPPC measured for the indirect bandgap sample at several temperatures. The wavelength of irradiated light is 900 nm, the same of direct bandgap experimental procedure. The higher the temperature, the faster the trapping and there is a tendency for saturation after some time. At 50 K, the conductance remains for a long time. Although we stop measuring at 800 s, this value would remain for days. It is important to mention that light excitation is able to excite conductance to a value only 20% of the excited value at 90 K what suggests trapping by other levels as discussed in previous section. This result shows that there is PPC in indirect bandgap $Al_xGa_{1-x}As$ below 60 K, even though it has lower magnitude if compared to direct bandgap samples, unlike we had concluded previously [6,17].

4 CONCLUSION

Conductance as function of temperature under steady illumination shows the decrease in conductance for temperatures below $\cong$60 K, which demonstrates the small influence of light in transport properties in indirect bandgap $Al_xGa_{1-x}As$ in this range of temperature. This is a good indication of the metastable trapping by X-valley effective mass state. The same kind of conductance decrease is observed in direct bandgap samples, but only for illumination with below bandgap monochromatic light. Variation of photoconductivity excitation with wavelength of indirect bandgap $Al_xGa_{1-x}As$ measured at several temperatures is reported for the first time and shows the influence of deep levels in this measurement.

Ionised impurities present in the sample correlate among themselves and the number of effective scattering centres decreases. The overall effect is higher mobility in a trapping process. Our comparison of the

decay of persistent photoconductivity data with Chadi and Chang's trapping kinetics yields a better agreement when correlation among negatively charged centres such as DX^- and positively charged centres such as d^+, is considered in calculating the mobility. Although a perfect fit was not obtained, the improvement of adding dipole scattering to the simulation is clear and besides, only one adjustable parameter is used. A more complex model would yield a perfect fit to the data, by considering other dipole systems or other adjustable parameters such as the initial dipole concentration. The presence of competing trapping centres increases the possibilities of electron capture and the formation of dipole systems. All of these traps and dipoles shall give a contribution to indirect bandgap $Al_xGa_{1-x}As$ conductivity and a very complex model could be thought of, but this is matter for future work.

Acknowledgements

These samples were grown at Oregon State University, USA. Luis V.A. Scalvi would like to thank Professor John Arthur and John Wager for the hospitality and technical support during his stay in Corvallis. The authors acknowledge Brazilian financial agencies: CNP_q, CAPES, FINEP, PRONEX 402/96 and FAPESP. Luis V.A. Scalvi thanks specially FAPESP for the financial support of his participation in 15th General Conference of Condensed Matter Division of European Physical Society, where discussions with several scientists allow to finish this paper.

References

[1] P.M. Mooney, *J. Appl. Phys.* **67**, R1 (1990).
[2] D.J. Chadi and K.J. Chang, *Phys. Rev. B* **39**, 10063 (1989).
[3] E. Buks, M. Heiblum and H. Shtrikman, *Phys. Rev. B* **49**, 14790 (1994).
[4] C. Ghezzi, A. Parisini and V. Dallacasa, *Phys. Rev. B* **50**, 2166 (1994).
[5] J.M. Shi, P.M. Koenraad, A.F.W. van de Stadt, F.M. Peeters, J.T. Devreese and J.H. Wolter, *Phys. Rev. B* **54**, 7996 (1996).
[6] L.V.A. Scalvi, L. Oliveira and M. Siu Li, *Phys. Rev B* **51**, 13864 (1995).
[7] E.P. O'Reilly, *Appl. Phys. Lett.* **55**, 1409 (1989).
[8] L.V.A. Scalvi, L. Oliveira, E. Minami and M. Siu Li, *Appl. Phys. Lett.* **63**, 2658 (1993).
[9] L.V.A. Scalvi, L. Oliveira and M. Siu Li, *Mat. Res. Soc. Symp. Proc.* **325**, 285 (1994).
[10] T.W. Dobson, L.V.A. Scalvi and J.F. Wager, *J. Appl. Phys.* **68**, 601 (1990).
[11] P.M. Mooney, G.A. Northrop, T.N. Morgan and H.G. Grimmeis, *Phys. Rev. B* **37**, 8298 (1988).

cm 1 2 3 4 5 6 7 unesp 1 12 13 14 15 16 17 18

[12] J.E. Dmochowski, L. Dobaczewski, J.M. Langer and J. Jantsch, *Phys. Rev. B* **40**, 9671 (1989).
[13] L. Dobaczewski and P. Kaczor, *Phys. Rev. B* **44**, 8621 (1991).
[14] S. Adachi, *J. Appl. Phys.* **58**, R1 (1985).
[15] H. Reiss, C.S. Fuller and F.J. Morin, *Bell System Tech. J.* **35**, 535 (1956).
[16] R. Stratton, *J. Phys. Chem. Solids* **23**, 1011 (1962).
[17] L.V.A. Scalvi, L. Oliveira and M. Siu Li, *Brazilian J. Phys.* **26**, 239 (1996).

J. Phys.: Condens. Matter 11 (1999) 425–433. Printed in the UK PII: S0953-8984(99)94966-4

Photo-induced electron trapping in indirect bandgap $Al_xGa_{1-x}As$:Si at low temperature

Luis V A Scalvi†, Marco H Taquecita†‡ and Bárbara A V Vega†§

† Departamento de Física—FC, Universidade Estadual Paulista, Cx. Postal 473, 17033-360 Bauru SP, Brazil

‡ Departamento de Engenharia Elétrica—FET, Universidade Estadual Paulista, Cx. Postal 473, 17033-360 Bauru SP, Brazil

§ Departamento Computação—FC, Universidade Estadual Paulista, Cx. Postal 473, 17033-360 Bauru SP, Brazil

Received 10 June 1998, in final form 18 September 1998

Abstract. A variation of photoconductivity excitation with wavelength is applied to Si-doped $Al_{0.56}Ga_{0.44}As$ (indirect bandgap material) for a wide range of temperature. The lower the temperature the lower the photocurrent below 70 K. In the range 13–30 K there is a decrease in the photoconductivity spectrum slightly above the bandgap transition energy, followed by another increase in the conductivity. We interpret these results in the light of existing models and confirm the trapping by the X-valley effective mass state, which is responsible for attenuation of persistent photoconductivity below 70 K. A DX^0 intermediate state which has non-negligible lifetime is proposed as responsible for the decrease in the photoconductivity with about 561 nm of wavelength of exciting light, in the investigated 13–30 K range.

1. Introduction

In the last twenty years many efforts have been concentrated towards the understanding of $Al_xGa_{1-x}As$ physical properties, since this alloy has wide application in opto-electronic devices. A deep level known as the DX centre is dominant for the electrical properties of this alloy and most of its physics has already been established [1]. A lot of good work was published on the physics of this deep level and its influence on the performance of opto-electronic devices, mainly on direct bandgap $Al_xGa_{1-x}As$. In 1988 Chadi and Chang [2] published their work which was accepted by most DX centre researchers. In their model, the DX centre is the substitutional donor atom itself which traps two electrons and moves towards an interstitial position, becoming negatively charged (DX^-). One of the most striking DX centre characteristics is the persistent photoconductivity (PPC), where the photoexcited conductivity at low temperature lasts for a long time, the lower the temperature, the longer the persistent photoconductivity. In 1989, Dmochowski *et al* [3] concluded that in indirect bandgap $Al_xGa_{1-x}As$, below 60 K, PPC has much lower magnitude since the shallow effective mass donor state is populated after photoexcitation of DX levels. After direct–indirect crossover the X-like state must participate in a carrier repopulation. The existence of an effective-mass-like level was demonstrated by Séguy and co-workers [4] using Raman scattering experiments. They detected bound phonons associated with electrons trapped at this level and did not find persistent photoconductivity effects. Based on the absence of PPC, a light induced experiment of thermally stimulated depolarization current (TSDC) [5] was proposed, and the existence

0953-8984/99/020425+09$19.50 © 1999 IOP Publishing Ltd

of DX^--related electric dipoles in indirect bandgap $Al_xGa_{1-x}As$ was identified. Correlation among opposite charges such as DX^-–d^+, where d^+ means the substitutional donor after releasing an electron to the conduction band, have been proposed by some authors [6–8] in order to understand the electrical behaviour of samples containing DX centres. According to O'Reilly [6], in an electron capture process, the initial formation of DX^- centres involves replacing close pairs of positive charges by dipoles, because the capture is driven by electrostatic forces. Then for a large fraction of sites, d^+–DX^- are strongly correlated. These correlation effects may enhance the mobility and have been used to explain striking characteristics of $Al_xGa_{1-x}As$ based structures of complex geometries [9–11]. No great attention was given to indirect bandgap $Al_xGa_{1-x}As$ since the X valley (lowest energy in indirect bandgap material) has much lower mobility than the Γ valley, and then most of the work on DX centre in $Al_xGa_{1-x}As$ films were carried out in direct bandgap samples. Torres-Delgado and co-workers [12] measured the photoluminescence of indirect bandgap $Al_xGa_{1-x}As$ and concluded that for $x < 0.60$ the donor level may be related to the L valley rather than to the X valley, because the Si donor ionization energy is quite large. In this communication we report the variation of photoconductivity excitation with wavelength for indirect bandgap $Al_xGa_{1-x}As$ for a wide temperature range. A photoinduced electron trapping takes place for energy slightly higher than the bandgap transition below $\cong$34 K, and the spectra are DX centre dominated for temperatures higher than that, until about 120 K.

The sample used in this work was grown by molecular beam epitaxy on an undoped, semi-insulating GaAs substrate. In order to prevent a two-dimensional electron gas formation at the interface, since we are interested in the bulk properties, the sample has the following structure: 0.25 μm of undoped GaAs buffer layer, 0.25 μm of undoped $Al_xGa_{1-x}As$ that is compositionally graded from $x = 0$ to $x \cong 0.50$, 0.25 μm of undoped $Al_xGa_{1-x}As$ with $x \cong 0.50$ and 2.0 μm of indirect bandgap material ($x \cong 0.50$) active layer, that is 5×10^{17} cm^{-3} Si doped. Variation of photoconductivity excitation is obtained by scanning a monochromator at a fixed rate. The light source is a tungsten lamp. Although we have not monitored the photon flux, the light source spectrum intensity in the used wavelength range is rather uniform and we have precisely controlled the current of the light source at 10 A, with 10^{-2} A of precision, using a 68831 Radiometric power supply from Oriel Corporation. The scanning as well as the data acquisition from the electrometer are controlled by a microcomputer. All the spectra presented here are obtained with wavelength being scanned from higher to lower value.

2. Variation of photoconductivity excitation with wavelength and temperature

In figure 1 we show variation of photoconductivity excitation with wavelength for indirect bandgap $Al_xGa_{1-x}As$ for several temperatures. We start irradiating the sample with light with the beginning of scanning about 600 nm (or slightly different in some cases). Then the wavelength is decreased slowly which is controlled by a microcomputer. The scanning speed is about 9.8 nm min^{-1} from higher to lower wavelength. At 13 K there is a peak in the photoconductivity about 566 nm (2.19 eV) and the conductivity starts to decrease until about 561 nm (2.21 eV), where there is a local minimum and then there is another increase and another peak about 550 nm where a new decrease starts to take place. The first peak and the last decrease are expected since they correspond to the regular photoconductivity spectrum type of $Al_xGa_{1-x}As$, but the local minimum is rather unexpected. We can associate the peak at 566 nm with the bandgap transition, which is consistent with results for other temperatures since the peak wavelength position increases slightly with temperature as predicted by Adachi [13]. In figure 1(a) we apply 50 mV of voltage and measure the current. As the temperature is increased the current magnitude increases. It is not possible to measure the current with

cm 1 2 3 4 5 6 7 unesp 1 12 13 14 15 16 17 18

50 mV at 17 K (figure 1(b)). Then we apply 100 mV. Since $Al_xGa_{1-x}As$ is very sensitive to the presence of light, there are oscillations in the measured current for this voltage, although the result is even worse for 50 mV (not shown). These oscillations are probably related to complex generation–recombination processes, since electrons coming from bandgap transitions have very short lifetime and are metastably kept in the conduction band by the presence of light. We record a very clean spectrum for 20 K using 100 mV (figure 1(c)), but as the temperature increases it becomes hard to control the oscillations in current as we can see in figure 1(d) at 25 K. Therefore we decrease once more the applied voltage and use 50 mV to carry out measurements at 34 K (figure 1(e)). The local minimum about 561 nm, observed at low temperature, vanishes about 34 K, leaving only a short plateau region around this wavelength.

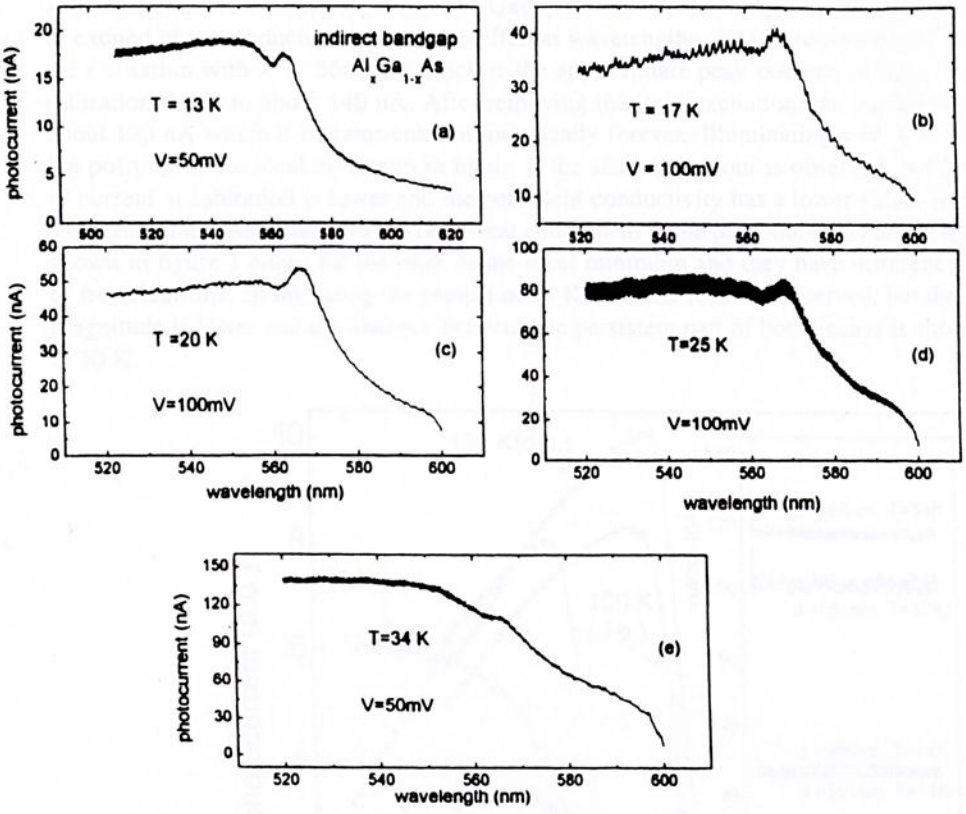


Figure 1. Variation of photoconductivity excitation with wavelength for indirect bandgap $Al_xGa_{1-x}As$ at several temperatures. Wavelength scanning speed = 9.8 nm min^{-1}. (a) 13 K, (b) 17 K, (c) 20 K, (d) 25 K, (e) 34 K.

For higher temperature there is no local minimum around 561 nm and the photoconductivity keeps increasing for energies higher than the bandgap transition as we can see in figure 2 for 40 K. This behaviour is very similar for all the spectra measured in the range 34–120 K, since the transport properties are dominated by DX centres in this range of temperature. It is not possible to evaluate the bandgap transition in this range since the beginning as well the end of the photoconductivity transition rate is not clearly observed in this range of temperature. In the beginning of the photoconductivity spectra, the monochromatic light has energy enough to excite electrons from DX centres and the excitation depends on time

of exposure and does not depend on the absolute value of energy, since it is much higher than the DX centre threshold photoionization energy [14]. As the bandgap transition is approached the photo-excitation rate is increased since we now have two combined processes: excitation from DX centres and bandgap transition. Therefore the photoconduction at the peak comes from electron–hole pairs generated from the bandgap transition and electrons coming from DX centres. As the wavelength becomes shorter the generation of electron–hole pairs is inhibited, but the photoconduction does not decrease, because electrons coming from DX centres, responsible for most of the transport, are under the PPC phenomenon. Above $\cong$120 K, the transition excitation rate is much easier to observe as seen from the photoconductivity spectrum at 130 K, also shown in figure 2, since PPC is negligibly short. We estimate the Al composition as $x \cong 56\%$ in this sample [13], which is far from the direct–indirect crossover and in the indirect bandgap region for $Al_xGa_{1-x}As$. In the inset of figure 2 we show the decay of excited photoconductivity using two different wavelengths and two temperatures. At 30 K the excitation with $\lambda = 566$ nm (which is the approximate peak position in figure 1), until saturation, leads to about 140 nA. After removing the light excitation, the current decays to about 120 nA where it remains constant practically forever. Illuminating with $\lambda = 561$ nm, the position of the local minimum in figure 1, the same behaviour is observed, but the value of current at saturation is lower and the persistent conductivity has a lower value, $\cong$100 nA. This result indicates that there is a persistent component in the photoinduced current spectrum shown in figure 1 either for the peak or the local minimum and they have different amounts of free electrons. Illuminating the sample at 14 K a similar result is observed, but the current magnitude is lower and the distance between the persistent part of both decays is shorter than at 30 K.

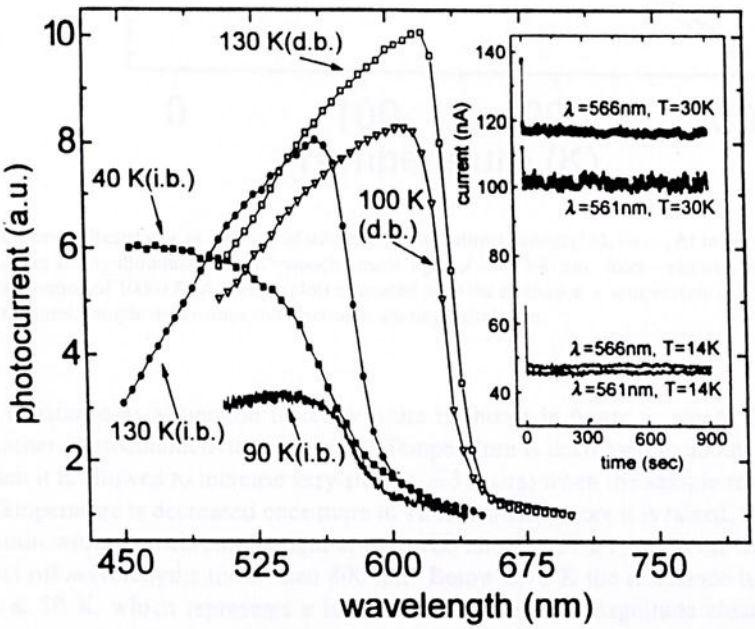


Figure 2. Variation of photoconductivity excitation with wavelength for indirect bandgap $Al_xGa_{1-x}As$ ($x \cong 0.56$) at 40 K, 90 K and 130 K. Results for a direct bandgap (d.b.) $Al_xGa_{1-x}As$ sample ($x \cong 0.32$) are also shown for comparison. Inset—decay of photoexcited current at low temperature. The temperature and excitation light of saturation are indicated.

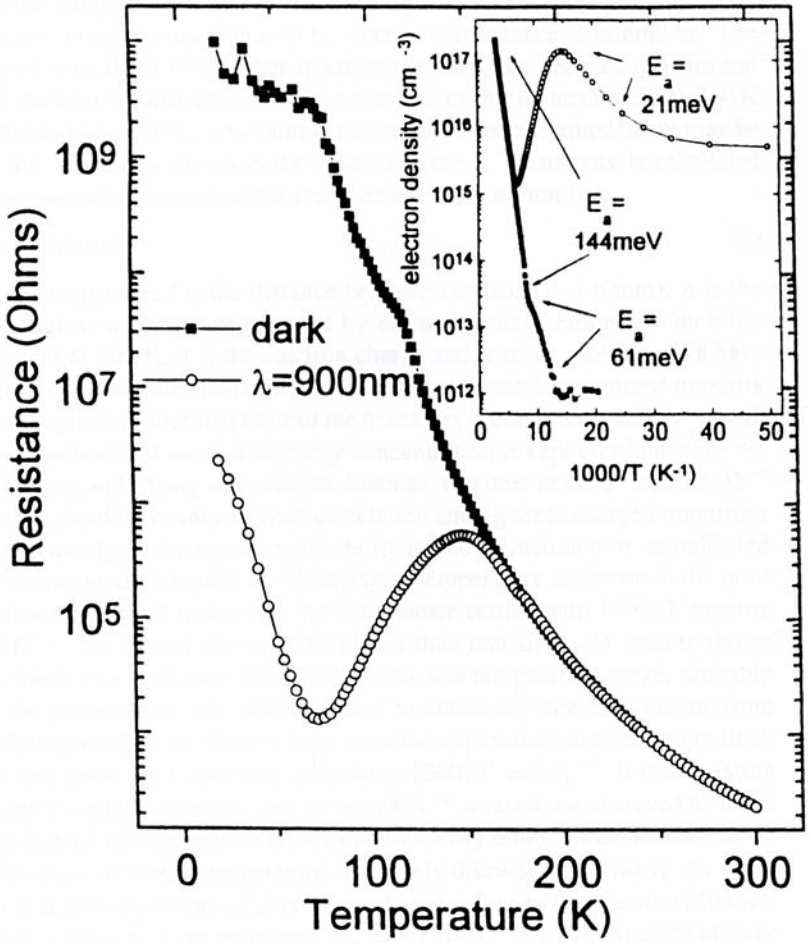


Figure 3. Resistance as function of temperature for indirect bandgap $Al_xGa_{1-x}As$ in the dark and under steady illumination with monochromatic light of $\lambda = 900$ nm. Inset—electron density as a function of $1000/T$ (Arrhenius plot) estimated from the resistance × temperature (RT) data of the inset, sample dimensions and electron scattering calculation.

Measured resistance as a function of temperature is shown in figure 3, where data are obtained by another photoconductivity procedure. Temperature is decreased to about 12 K in the dark and then it is allowed to increase very slowly ($\cong$3 hours) when the sample resistance is measured. Temperature is decreased once more to 12 K and once more it is raised, this time under illumination with monochromatic light of $\lambda = 900$ nm ($\cong$1.37 eV), with the help of a filter which cuts off wavelengths lower than 800 nm. Below $\cong$70 K the resistance is higher than the value at 70 K, which represents a local minimum and has magnitude close to the value at room temperature. Since 1.37 eV is much lower than the bandgap transition energy, we believe that we have DX centre excitation since this illumination energy is much higher than the DX centre threshold photoionization energy [14], since DX centres were populated when the temperature was decreased in the dark. However the magnitude of photo-induced conductivity below $\cong$70 K is lower, since there is trapping by another level. This result is in good agreement with figure 1 for the lower the temperature the lower the magnitude of

photoconductivity. As the temperature is raised this trapping becomes less important and the photoconductivity reaches its maximum about 70 K, where the resistance is minimum. The resistance increases again until about 150 K when it has maximum value, decreasing again and approaching the dark value of resistance about 200 K, which means that in the range 200–300 K light has very little influence on $Al_xGa_{1-x}As$ sample resistance. Free electron density may be estimated from these RT curves, as shown in the inset of figure 3. Resistivity is calculated from sample dimensions in order to estimate the free carrier concentration (n):

$$n = l[RAq\mu(n)]^{-1} \tag{1}$$

where R is the measured resistance, l is the distance between contacts (= 1.6 mm), A is the cross-sectional area, which is a parameter adjusted by electron concentration and mobility obtained by the Hall effect at 300 K, q is the electron charge and μ is the mobility. We have considered two electron scattering mechanisms [15] to obtain the mobility: ionized impurity scattering [16] and polar optical scattering [17] and the necessary parameters given by Adachi [13]. It is important to mention that ionized impurity concentration is kept constant since we are using the model of Chadi and Chang where the Si donor exists either in the d^+ state or DX^- state. A better estimation should take into account correlation among these charged impurities [6, 7]. Solving self-consistently all the equations (mobility is also a function of n, as indicated in equation (1)), we obtain electron density as a function of temperature as shown in the inset of figure 3. For resistance measured in the dark we have shown results with $1000/T$ ranging from 3.3. K^{-1} to 20 K^{-1}. We do not show results higher than that since RT results shown in the inset of figure 3 lead to a oscillatory behaviour in the low temperature range, probably due to limitations of the electrometer, and then it is hard to obtain any new information from the Arrhenius plot. Mizuta and Mori [18] have done a similar experiment in Si-doped indirect bandgap $A_xGa_{1-x}As$ and show the result only until about $1000/T = 8$ K^{-1}. It is interesting to note that the dark curve changes its slope very close to 8 K^{-1}, a result not observed by those researchers that claim that at low temperature the dark conductivity is too low to measure, as we agree, but our troubles were for lower temperature, as already discussed. For the range 3.3 to $\cong$8 K^{-1} our calculated activation energy (E_a) is 144 meV, very close to their result (136 meV [18]) and in the range $\cong$8–13 K^{-1} we estimated $E_a \cong 61$ meV. For the experiment done under steady illumination of $\lambda = 900$ nm we have an activation energy of 21 meV in the range 16–25 K^{-1}. Considering that our experimental procedure is rather different from Mizuta and Mori and the aluminium composition and Si doping are slightly different from their sample, both data are very consistent. They have used non-monochromatic light and illumination at 4 K with measurement in the dark whereas we have used $\lambda = 900$ nm monochromatic light and steady illumination while the temperature is raised. Therefore the minimum in the RT curve takes place at a lower temperature in our case.

3. Participation of the X-valley effective mass state, the DX^0 intermediate state and other levels in the recombination process

The variation of photoconductivity excitation with wavelength seen in figure 1 must be understood as follows: light at 600 nm has energy enough to excite electrons from DX centres, which is slowly excited since there is low photoionization rate (the amount of free carriers depends on exposure time). When the energy increases, bandgap transition is approached and the ionization rate becomes higher. The lower the temperature, the lower the photoconductivity signal which means that as electrons are excited from DX centres, they are retrapped at another level, which may be the X-valley effective mass state. The depth of the Si–X-like level might be of a similar order of magnitude as the $\cong$40 meV Te–X-like level [3]. The peak position in

figure 1 should not be associated with the bandgap transition energy since its location depends on scanning speed and the DX centre photoionization rate. One must be careful in associating the peak in photoconductivity spectral response with bandgap transition energy, since it is not a straightforward process. This maximum in photoconductivity occurs at a wavelength slightly longer than that corresponding to the absorption edge [19]. Even from the absorption spectral response curve the estimation of the energy gap is not a simple process, for transitions are subject to certain selection rules [20]. Moreover, one must account for the change in both energy and momentum since our sample has an indirect bandgap transition, which requires a two step process involving the participation of phonons that may be emitted or absorbed. Then around 566 nm there is a combination of electron–hole pairs generated from the bandgap transition and electrons from DX^- centres. As the exciting energy is increased, there is a decrease in the photocurrent, which may be associated with some kind of trapping. The X-valley effective mass state has an influence on the current magnitude at low temperature as shown in figures 1 and 3. The lower PPC magnitude found by Dmochowski and co-workers [3] for Te-doped $Al_xGa_{1-x}As$ is in good agreement with our results. Then the photoinduced trapping at $\cong$561 nm must have another explanation.

For high temperature, the DX^- centre is photoionized, according to the reaction [2]:

$$DX^- \rightarrow d^+ + 2e^-. \tag{2}$$

This reaction means that besides releasing two electrons to the conduction band, the DX^- centre relaxes back to its original position, substitutional in a Ga site. For lower temperature, there is another reaction probable:

$$d^+ + DX^- \rightarrow d^0 + DX^+ + 1e^- \tag{3}$$

where DX^+ means the Si dopant after releasing two electrons to the conduction band but before relaxing to the substitutional position. This reaction means that one of the two electrons released by the DX^- state is captured by a X-valley effective mass state of another atom. According to our data this reaction is more probable as the temperature gets lower, since the excited photocurrent becomes lower. However the photoconductivity spectrum at low temperature presents a decrease in the current magnitude about 560 nm, which suggests another mechanism of trapping. We believe that at temperature as low as 13 K, the thermal energy is low and does not allow relaxation immediately. The DX^+ state is highly unstable and it is located $\cong$20 meV above the conduction band minimum. Then it is able to recapture one electron from electron–hole pairs of the bandgap transition and becomes DX^0 according to the reaction

$$DX^+ + 1e^- \rightarrow DX^0. \tag{4}$$

For illuminating energies higher than the DX^+ level, we have bandgap transition (although less efficient) and DX^- excitation by reactions (2) and (3). In both cases there is a release of electrons to the conduction band. As the temperature is raised the DX^+ lifetime becomes shorter and a decrease in the photoconductivity is no longer observed. A DX^0 state has been already proposed by some authors [21–23] and has been used again in a very recent paper [24]. In indirect bandgap $Al_xGa_{1-x}As$, in the range 13–30 K, the thermal energy is quite low and the DX^0 intermediate state has a lifetime long enough to be responsible for the local minimum in the photoconductivity curve. The experimental decay of photoexcited current shows that even at 14 or 30 K the current is excited to a higher value by using $\lambda = 566$ nm and the persistent part is also higher in this case; however the distance between the persistent current after excitation with 566 nm and 561 nm is larger at 30 K than at 14 K. This result means that after removing the light, bandgap transitions immediately take place, but states d^0 and DX^0, generated by reactions (2) and (3), are metastably kept by the low temperature. The reason



for the similarity in persistent part at 14 K is probably that, at this low temperature, impurity states of A_1 symmetry as proposed by Dmochowski *et al* [25] may be taking part in the capture process.

Another interesting point is that the energy of the photoconductivity local minimum is just above the bottom of the conduction band. It is well known that As vacancies (V_{As}) have an unoccupied level resonant with the conduction band [26, 27]. Van Vechten [28] predicts the participation of vacancies in the defects present in the sample, since there is a tendency for a V_{As} centre to be formed close to a donor. Thermally stimulated depolarization current measurements under the influence of monochromatic light [5] have revealed the possibility of V_{As} participation in the recombination process at low temperature. Therefore, the local minimum in the photoconductivity response may be related to trapping by As vacancies located close to DX^- centres.

4. Conclusion

We have confirmed the X-valley effective mass state as responsible for the low PPC signal below $\cong$70 K, for Si-doped $Al_xGa_{1-x}As$, similarly to that observed previously for the Te donor [3]. The lower the temperature the lower the induced photocurrent, unlike what occurs for direct bandgap material. In the range 13–30 K we have found a decrease in the photoconductivity excitation with energy slightly higher than the bandgap transition, followed by another increase. We have interpreted this behaviour as capture by a DX^0 intermediate state, which in this case would be photoinduced. However the actual nature of such a local minimum in the photoconductivity needs further research.

Acknowledgments

The samples were grown at Oregon State University, USA Luis V A Scalvi would like to thank Professor John Arthur and John Wager for the hospitality and technical support during his stay in Corvallis. We are also grateful to Professor M Siu Li and L Oliveira for important discussions. The authors acknowledge the Brazilian financial agencies CNPq, FAPESP and MCT-PRONEX 402/96.

References

[1] Mooney P M 1990 *J. Appl. Phys.* **67** R1
[2] Chadi D J and Chang K J 1988 *Phys. Rev. Lett.* **61** 873
Chadi D J and Chang K J 1989 *Phys. Rev.* B **39** 10063
[3] Dmochowski J E, Dobaczewski L, Langer J M and Jantsch W 1989 *Phys. Rev.* B **40** 9671
[4] Séguy P, Zigone M and Martinez G 1992 *Phys. Rev. Lett.* **68** 518
[5] Scalvi L V A, Oliveira L and Siu Li M 1995 *Phys. Rev.* B **51** 13 864
[6] O'Reilly E P 1989 *Appl. Phys. Lett.* **55** 1409
[7] Wilamowski Z, Kossut J, Suski T, Wisniewski P and Dmowski L 1991 *Semicond. Sci. Technol.* **6** B34
[8] Wilamowski Z, Kossut J, Jantsch W and Ostermayer G 1991 *Semicond. Sci. Technol.* **6** B38
[9] Buks E, Heiblum M and Shtrikman H 1994 *Phys. Rev.* B **49** 14 790
[10] Ghezzi C, Parisini A and Dallacasa V 1994 *Phys. Rev.* B **50** 2166
[11] Shi J M, Koenraad P M, van de Stadt A F W, Peeters F M, Devreese J T and Wolter J H 1996 *Phys. Rev.* B **54** 7996
[12] Torres-Delgado G, Castanedo-Perez R, Diaz-Arencibia P, Mendoza-Alvarez J G, Orozco-Vilchis J L, Murillo-Lara M and Serra-Jones A 1995 *J. Appl. Phys.* **78** 5090
[13] Adachi S 1985 *J. Appl. Phys.* **58** R1
[14] Mooney P M, Northrop G A, Morgan T N and Grimmeiss H G 1988 *Phys. Rev.* B **37** 8298

cm 1 2 3 4 5 6 7 unesp 1 12 13 14 15 16 17 18

[15] Saxena A K and Mudares M A L 1985 *J. Appl. Phys.* **58** 2795
[16] Chattopadhyay D and Queisser H J 1981 *Rev. Mod. Phys.* 53 745
[17] Putley E H 1968 *The Hall Effect and Semiconductor Physics* (New York: Dover) p 142
[18] Mizuta M and Mori K 1988 *Phys. Rev.* B **37** 1043
[19] Bube R H 1960 *Photoconductivity of Solids* (New York: Wiley) p 230
[20] Pankove J I 1971 *Optical Processes in Semiconductors* (New York: Dover) p 34
[21] Theis T N and Mooney P M 1990 *Mater. Res. Soc. Symp. Proc.* vol 163 (Pittsburgh, PA: Materials Research Society) p 729
[22] Dobaczewski L and Kaczor P 1991 *Phys. Rev.* B **44** 8261
[23] Sampaio J F, Chaves A S, Ribeiro G M, Guimarães P S S, Carvalho R P and Oliveira A G 1991 *Phys. Rev.* B **44** 10 933
[24] Ghosh S and Kumar V 1997 *Solid State Commun.* **104** 781
[25] Dmochowski J E, Wang P D and Stradling R A 1991 *Semicond. Sci. Technol.* **6** 118
[26] Jaros M and Brand S 1976 *Phys. Rev.* B **14** 4494
[27] Lang D V, Logan R A and Jaros M 1979 *Phys. Rev.* B **19** 1015
[28] Van Vechten J A 1989 *J. Phys.: Condens. Matter* **1** 5171

Capítulo II

Caracterização de SnO_2 Depositado Via Sol-Gel

Óxido de estanho tem sido obtido na forma de filmes finos de alta transparência e boa condutividade elétrica. Em sua forma não dopada, SnO_2 é um semicondutor do tipo n, devido à alta concentração de vacâncias de oxigênio e átomos de Sn intersticiais, que agem como doadores de elétrons. O processo sol-gel de produção destes filmes tem sido usado para deposição em substratos de grandes dimensões e formas complexas [1-4]. Em geral a camada de SnO_2 depositado via sol-gel tem condutividade menor que filmes depositados por outros métodos [5-8], a qual é atribuída aos efeitos do contorno de grão dos cristalitos. A dopagem com Sb^{5+} ou Nb^{5+} aumenta a concentração de portadores porém limita o crescimento do cristalito. Com isso mais átomos de oxigênio podem ser adsorvidos no contorno de grão o que torna a barreira de potencial na interface bastante relevante para o espalhamento de elétrons, levando a uma menor mobilidade no contorno de grão e consequentemente a uma maior resistividade do filme.

Dióxido de estanho tem sido amplamente utilizado para produção de sensores de gás, eletrodos tranparentes e outros dispositivos [9]. O objetivo geral de nossa investigação é a melhoria nas propriedades de transporte elétrico do filme, mantendo-se a boa transparência, visando-se com isso a produção de eletrodos transparentes para aplicação em dispositvos.

II.1 A RESISTIVIDADE DE SnO_2

Os primeiros experimentos que realizamos nas amostras estão relacionados aos tipos de contatos que forneciam melhores resultados, além de medidas de resistência em função da temperatura. Nossa intenção era proceder a uma investigação similar à que havíamos feito para $Al_xGa_{1-x}As$, e com isso aproveitar a experiência adquirida com aquele semicondutor. Assim poderíamos identificar o possíveis defeitos presentes na amostra e contribuir para o entendimento dos processos de transporte elétrico neste material semicondutor.

A investigação com os contatos mostrou que os melhores resultados eram obtidos com filmes de In evaporados na superfície, que passou então a ser o material utilizado para confecção de contatos nos trabalhos subsequentes. As medidas de resistência em função da temperatura, feitas em um filme de SnO_2 dopado com 2%Sb, mantida no escuro, mostrou uma forte diminuição na condutividade conforme a temperatura era abaixada, característico da captura por níveis profundos. Iluminação desta amostra com luz de energia superior ao bandgap, ou seja λ=305 nm, advindo de uma fonte de mercúrio acoplada com um monocromador, mostrou aumento da condutividade a baixa temperatura e um aumento ainda maior quando a temperatura era levada de volta à ambiente. Novas experimentos de irradiação de luz mocromática de 305nm a baixa temperatura propiciaram novos aumentos na condutividade, desde que a amostra fosse mantida em vácuo. Ao contrário de nossa experiência anterior, este material tinha um comportamento que não era uma função única da temperatura, mas dependia do histórico da amostra. A condutividade era continuamente aumentada pela sequência de iluminações em conjunto com o aumento de temperatura, que sugeria que este tratamento estava induzindo uma transformação permanente nos filmes de SnO_2. Um tratamento térmico a 200°C, feito sob vácuo, levou o filme a um aumento ainda maior na condutividade, que chegou a 4 ordens de magnitude em relação ao comportamento inicial da amostra. Após todo esse ciclo de tratamentos óticos e térmicos, a amostra foi deixada em repouso à temperatura ambiente, e observou-se um progressivo aumento na resistividade, ainda que a mesma não voltasse a condição inicial. Efeito similar de aumento da resistência do filme era observado se o tratamento fosse realizado em ar. Este efeito pode ser compreendido ao se considerar a geração de pares elétron-buraco no filme e a existência de alguma espécie gasosa que era adsorvida ou dessorvida dependendo da pressão no criostato, e

unesp

que tinha contribuição direta para a concentração de portadores de carga. Elétrons e buracos fotogerados recombinam com este gás [10] deixando uma concentração líquida de elétrons que conduz a corrente elétrica. Fomos levados a pensar que este gás seria oxigênio, hipótese esta totalmente consistente com os experimentos que foram feitos desde então.

II.2 FOTOCONDUTIVIDADE DE SnO_2

A influência da presença de ar para a condutividade do filme, nos levou a realizar experimentos sobre a variação espectral da fotocondutividade sob diferentes condições. A excitação da condutividade de uma amostra amostra não-dopada, feita a 300K, utilizando uma lâmpada de tungstênio mostra um pico a 380nm. Quando a amostra é mantida em ar durante o experimento, existe um retorno ao valor inicial da condutividade, o que não é observado se o filme é mantido em vácuo. Este comportamento está relacionado à adsorção química e a fotodessorção de oxigênio na superfície do filme e contorno de grão. Pares elétron-buraco são gerados por luz monocromática de energia acima da transição de bandgap, que podem reagir com oxigênio de acordo coma s reações:

$$SnO_{2-x} \xrightarrow{-h\nu\rightarrow} h^{+} + e^{-} \qquad \text{(II.1)}$$

$$e^{-} + \tfrac{1}{2}\, O_2 + SnO_{2-x} \rightarrow O_{ads}^{-}(SnO_{2-x}) \qquad \text{(II.2)}$$

$$h^{+} + O_{ads}^{-}(SnO_{2-x}) \rightarrow \tfrac{1}{2}\, O_2 + SnO_{2-x} \qquad \text{(II.3)}$$

onde : SnO_{2-x} – filme não estequiométrico de dióxido de estanho

O_2 – espécie gasosa de oxigênio

$O_{ads}^{-}(SnO_{2-x})$ – átomo de oxigênio adsorvido, carregado negativamente

Sob vácuo, a concentração de O_2 é mais baixa e a quantidade de O^{-} produzido pela ração II.2 é diminuída. A reação II.3 acontece com maior intensidade. O efeito global é uma concentração líquida de elétrons livres que podem transportar a corrente elétrica.

Experimentos de fotocondutividade também foram realizados com outras fontes de luz, Xenônio e Deutério. Os experimentos com uma lâmpada de xenônio a 300 K mostra que o efeito predito pelas reações II.1 a II.3 é também observado e a clareza na observação da transição do bandgap depende da quantidade de oxigênio adsorvido no filme. Após um

cm 1 2 3 4 5 6 7 unesp 1 12 13 14 15 16 17 18

tratamento térmico em ar a 200°C o espectro da fotocondutividade mostra um pico a 290nm. Novas medidas confirmam este resultado, porém a magnitude da corrente vai aumentando com o número de medidas até que não seja mais possível observar esta transição com clareza. Tratamentos térmicos feito em vácuo mostram grande aumento na magnitude de corrente e impedem a visualização clara do pico a 4,2eV.

Todos os resultados obtidos com uma lâmpada de deutério mostram um pico em torno de 230nm (5,4eV), valor que é muito maior qualquer transição de bandgap publicada e maior que nossa estimativa de $E_g \cong 3,5eV$ [4].

A energia do pico obtida com diferentes fontes de luz mostra o efeito da fonte de luz no espectro da fotocondutividade e do processo de recombinação de pares elétron-buraco com o oxigênio adsorvido. Adsorção e dessorção de oxigênio parecem ser processos muito mais lentos que recombinação elétron-buraco, desde que dependem da difusão atômica no filme e velocidade de deslocamento de oxigênio gasoso na superficie. Se o aumento na condutividade fosse somente devido a geração e posterior recombinação de pares elétron-buraco com energia nas proximidade do bandgap, sua posição seria independente da fonte de luz. Mesmo bem acima da energia da transição do gap a condutividade continua aumentando, conforme observado em nossos experimentos com a lâmpada de deutério.

II.3 – ESPALHAMENTO DE ELÉTRONS NO CONTORNO DE GRÃO

A importância deste assunto foi detectado ao nos depararmos com a alta resistividade dos filmes de SnO_2 obtido via sol-gel e os pequenos cristalitos existentes neste material. Dióxido de estanho não dopado é um semicondutor do tipo n onde o principal nível doador é formado pelas vacâncias de oxigênio [11]. No processo de deposição e no tratamento térmico, oxigênio gasoso é adsorvido na superficie e contorno de grão. O mecanismo de redução da resistência é o tratamento térmico em vácuo, o que remove oxigênio do contorno de grão. A adsorção de oxigênio acontece tipicamente na faixa 200-400°C [12], na forma de espécies iônicas que capturam elétrons livres da banda de condução, diminuindo a condutividade do filme. A contribuição mais importante para a condutividade é a barreira de potencial no

unesp

contorno de grão. Os efeitos internos do cristalito e do contorno de grão para a resistividade devem ser separados. A mobilidade da região neutra ("bulk") é dada por :

$$(\mu_{bulk})^{-1} = (\mu_{opt})^{-1} + (\mu_{ii})^{-1} \qquad \text{(II.4)}$$

onde μ_{opt} é a mobilidade devido ao espalhamento polar óptico [13] e μ_{ii} é mobilidade devido ao espalhamento por impurezas ionizadas [14]. Embora Zhang e Ma [15] argumentem que o espalhamento no contorno de grão tem pequena contribuição para a mobilidade de filmes de boa qualidade, este efeito não pode ser desconsiderado em filmes depositados via sol-gel. A resistividade pode variar diversas ordens de magnitude, dependendo dos tratamentos térmicos e fotoexcitação a que o filme foi submetido, conforme já discutido. Aliado às pequenas dimensões dos cristalitos dos filmes obtidos via sol-gel (3-10nm em nosso caso), estas evidências nos fazem acreditar que a formação da barreira de potencial é o mecanismo mais relevante para a condutividade do filme.

Como um resultado das desordem atômica, a região intergrãos contém muitos defeitos, o que resulta na formação de armadilhas com uma densidade Q_t [16]. Se N_d é a concentração de portadores na região neutra (proporcional a densidade de sítios doadores ionizados – vacâncias de oxigênio e átomos dopantes, em nosso caso), a concentração efetiva de portadores N_a (que seria obtida por efeito Hall) é menor que N_d , devido ao aprisionamento de portadores no contorno de grão. Cada grão é depletado sobre uma distância menor ou igual a $L_g/2$, isto é metade do tamanho de grão. Se o grão for totalmente depletado, $Q_t = N_d . L_g$ e nenhum portador estaria disponível para a condução. N_a pode ser considerado como a concentração média de elétrons sobre um grão [17]. Definindo x como uma quantidade adimensional igual à fração de carga aprisionada no contorno de grão com respeito a carga total disponível no grão, temos que :

$$x = Q_t . (L_g N_d)^{-1} \qquad \text{(II.5)}$$

onde esta fração x representa a razão da largura da região de depleção para o diâmetro do grão L_g. A resistividade através do contorno de grão (ρ_g) é dada por [16]:

$$\rho_g = k\,(qA^*\,T\,L_g)^{-1} . \mathrm{Exp}(\varphi_a/kT) \qquad \text{(II.6)}$$

onde φ_a é a altura da barreira, A^* é a constante de Richardson [16] e k é a constante de Boltzmann.

A resistividade geral do filme torna-se a média ponderada das duas contribuições:

$$\rho = x.\rho_g + (1-x)\rho_{bulk} \qquad \text{(II.7)}$$

onde ρ_{bulk} [$=(q.N_a\mu_{bulk})^{-1}$] é a resistividade da região neutra.

Assim valores de resistividade podem ser ajustados resolvendo-se todas as equações envolvidas de forma auto-consistente, tanto no meio do cristalito (região neutra) como na região de depleção do contorno de grão. O parâmetro de ajuste é a resistividade experimental e obtém-se N_a e x em função da temperatura ou comprimento de onda, dependendo do resultado experimental que é simulado. Resultados preliminares destes cálculos foram apresentados na "14th International Conference on Defects in Insulating Materials" (ICDIM200) na África do Sul e foram publicados no artigo em anexo [Scalvi et. al., Radiation Effects and Defects in Solids **156**, 145 (2001)]. No entanto a obtenção de um modelamento mais completo é parte de nosso trabalho atual, sendo uma das metas para se obter maior compreensão dos mecanismos de transporte em filmes finos de SnO_2.

REFERÊNCIAS DESTE CAPÍTULO

[1] – Orel, B.; Lavrencic-Stangar, U.; Crnjak-Orel, Z; Bukovek P. e Koosec, M., J. Non-Cryst. Solids **167**(3), p. 272-288, 1994

[2] – Terrier, C.; Chatelon, J. P. e Roger, J. A., Thin Solid Films **295**, p. 95-100, 1997

[3] – Souza, A E.; Monteiro, S. H.; Santilli, C.V. e Pulcinelli, S. H., J. Mat. Sci.:Mat. Electron. **8** (4), p. 265-270, 1997

[4] – Scalvi, L. V. A; Messias, F. R.; Souza, A E.; Siu Li, M.; Santilli, C. V. e Pulcinelli, S.H., J. Sol-Gel Sci. Technol. **13**, p. 793-798, 1998

[5] – Jarzebski, Z. M. e Marton, J.P., J Electrochem. Soc. 123, p. 199C-310C, 1976

[6] – Shanthi, E.; Banerjee, A; Dutta, V e Chopra, K. L., J. Appl. Phys. **53 (3)**, p. 1615-1621, 1982

[7] – Sanon, G.; Rup, R. e Mansingh, A., Phys. Rev. B **44** (11), p. 5672-5680, 1991

[8] –Prado, F.; Meyer, G. e Saura, J., J. Phys.: Condens. Matter **5**, p. A351-A352, 1993

[9] – Park, S. S. e Mackenzie, J. D., Thin Solid Films **258**, p. 268-273, 1995

[10] – Morrison, S. R., *The Chemical Physics of Surfaces*, Plenum Press, New York, 1990

[11] – Watson, J.; Ihokura, K. e Coles, G. S.V, Meas. Sci. Technol. **4**, p. 711-719, 1993

[12] – Yamazoe, N.; Fuchigami, J.; Kishikawa, M. e Seiyama, T., Surf. Sci. **86**, p. 335-344, 1979

[13] –Putley, E. H. *The Hall Effect and Semiconductor Physics*, Dover, New York, 1960

[14] – Chattopadhyay, D. e Queisser, H.J., Rev. Modern Phys. **53** (4), p. 745-768, 1981

[15] – Zhang, D.H. e Ma, H. L., Appl. Phys. A **62**, p. 487-492, 1996

[16] – Bruneaux, J.; Cachet, H.; Froment, M. e Messad, A, Thin Solid Films **197**, p. 129-142, 1991

[17] – Seto, J. Y. W., J. Appl. Phys. **46**(12), p. 5247-5254, 1975

II.4 – ARTIGOS PUBLICADOS SOBRE O ASSUNTO (anexados na sequência)

II.4.1. - **Scalvi, L. V. A;** Messias, F. R.; Souza, A E.; Siu Li, M; Santilli, C.V. e Pulcinelli, S.H., *Improved Conductivity Induced by Photodesorption in SnO_2 Thin Films Grown by a Sol-Gel Dip Coating Technique*, J. Sol-Gel Sci. Technol. **13**, p. 793-798, 1998

II.4.2 – Messias, F.R.; **Scalvi, L. V A;** Siu Li, M.; Santilli, C.V.; e Pulcinelli, S.H.; *Photodesorption and Electron Trapping in n-type SnO_2 Thin Films Grown by Dip-coating Technique*, Rad. Eff. & Def. in Solids **146**, p. 199-206, 1998

II.4.3 – Messias, F.R.; Vega, B. A V.; **Scalvi, L. V A**; Siu Li, M.; Santilli, C.V. e *Pulcinelli, S. H., Electron Scattering and Effects of Sources of Light on Photoconductivity of SnO_2 Coatings Prepared by Sol-gel,* J. Non Crystalline Solids **247**, p. 171-175, 1999

II.4.4. - Messias, F.R.; **Scalvi, L. V A;** Siu Li, M.; Santilli, C.V. e *Pulcinelli S.H., Oxygen Related Defects and Photoconductivity Dependence of SnO_2 Sol-gel Films with Several Light Sources*, Rad. Eff. & Def. in Solids **150**, p. 391-395, 1999

II.4.5 - **Scalvi**, L.V. A; Geraldo, V.; Messias, F.R.; Siu Li, M.; Santilli, C. V. e Pulcinelli, S.H., *Contribution of Oxygen Related defects to the Electronic Transport in SnO_2 Sol-gel Films*, Rad. Eff. & Def. in Solids **156**, p. 145-149, 2001

cm 1 2 3 4 5 6 7 unesp 11 12 13 14 15 16 17 18

Journal of Sol-Gel Science and Technology 13, 793–798 (1998)
© 1998 Kluwer Academic Publishers. Manufactured in The Netherlands.

Improved Conductivity Induced by Photodesorption in SnO_2 Thin Films Grown by a Sol-Gel Dip Coating Technique

LUIS V.A. SCALVI
Departamento de Física, FC, UNESP, Caixa Postal 473, 17033-360 Bauru SP, Brazil

FÁBIO R. MESSIAS
Instituto de Física de São Carlos, U.S.P., Caixa Postal 369, 13560-970 São Carlos SP, Brazil

A.E. SOUZA
Instituto de Química, UNESP, Caixa Postal 355, 14801-907 Araraquara SP, Brazil

M. SIU LI
Instituto de Física de São Carlos, U.S.P., Caixa Postal 369, 13560-970 São Carlos SP, Brazil

C.V. SANTILLI AND S.H. PULCINELLI
Instituto de Química, UNESP, Caixa Postal 355, 14801-907 Araraquara SP, Brazil

Abstract. Thin films of undoped and Sb-doped SnO_2 have been prepared by a sol-gel dip-coating technique. For the high doping level (2–3 mol% Sb) *n*-type degenerate conduction is expected, however, measurements of resistance as a function of temperature show that doped samples exhibit strong electron trapping, with capture levels at 39 and 81 meV. Heating in a vacuum and irradiation with UV monochromatic light (305 nm) improve the electrical characteristics, decreasing the carrier capture at low temperature. This suggests an oxygen related level, which can be eliminated by a photodesorption process. Absorption spectral dependence indicates an indirect bandgap transition with $E_g \cong 3.5$ eV. Current-voltage characteristics indicate a thermionic emission mechanism through interfacial states.

Keywords: thin films, impurities in semiconductors, electronic transport, recombination and trapping

Introduction

Undoped SnO_2 is an *n*-type, wide bandgap semiconductor [1]. A high concentration of antimony as a dopant leads to quasimetallic behaviour while maintaining its transparency [2]. This is an interesting optoelectronic property, exploited in electro-optical devices [3]. Electrical properties of undoped SnO_2 depend mainly on deviation from the stoichiometric composition. Either oxygen vacancies or interstitial tin atoms are expected to be donors in pure SnO_2 [1]. Sb doping increases the *n*-type conductivity since Sb^{5+} is incorporated into the lattice substituting for Sn^{4+} [4]. Another important feature is the mechanism of chemisorption of oxygen on the SnO_2 surface which provides electron transfer from the conduction band to an acceptor level introduced by the adsorbed atoms [5]. Bandgap transitions change electron and hole concentrations at the semiconductor surface [6]. Photoproduced electrons will induce oxygen adsorption, but photoinduced holes will induce oxygen desorption, so that the net effect depends on the

rate constants and on the sample properties in the dark.

By the methods typically used to prepare SnO_2 films it is hard to coat large surfaces and control stoichiometry [7]. Coatings of large and complex-shaped substrates have been obtained by means of the dip-coating sol-gel process, using both organic and inorganic precursors [8–10]. Alkoxides are expensive and sensitive to moisture, producing inhomogeneous SnO_2 layers [8]. The colloidal suspensions prepared via inorganic sol-gel route developed in our laboratory [9] have been the preferred way of making SnO_2 layers by dip coating [10] because these disadvantages are absent. In this communication we show electrical and optical properties of undoped and Sb-doped SnO_2 thin films. Our conclusions help sample preparation and the understanding of electrical transport properties of SnO_2 thin films prepared by a sol-gel dip-coating technique.

Experimental

Films were deposited as follows: borosilicate glass substrates were dipped vertically into a suspension of SnO_2 prepared from the hydrolysis of $SnCl_4 \cdot 5H_2O$ in aqueous solution [9]. Sb doping was obtained by dissolution of $SbCl_3$ in a $SnCl_4$ aqueous solution. The dipping rate was 6 cm/min and the resulting thickness after 30 dips was 300 nm. Samples were annealed at 550°C for 1 hour in air. Films presented 80% transmission in the visible and were uniform over the whole surface, being polycrystalline with an average grain size of 3 nm and porosity of about 35%.

Electrical measurements were performed in a parallel orientation to the coating, using evaporated In electrodes, annealed to 150°C for 30 min. The resistance was measured as a function of temperature in the range 77–300 K using an electrometer and the conductivity (σ) was calculated considering the distance between electrodes and film thickness. Optical absorption coefficients were determined by UV-Vis spectroscopy.

Results and Discussion

Figure 1 shows conductivity as a function of temperature for a Sb-doped (2 mol%) SnO_2 sample, both in the dark and under illumination with $\lambda = 305$ nm monochromatic light. The lower curve represents the measurement carried out in the dark: the sample was taken to 77 K and then the temperature was allowed to increase very slowly. There was a pronounced increase in the sample conductivity as the temperature was raised, suggesting a carrier freezeout of defects. Taking the sample to 77 K again and illuminating steadily with monochromatic light of $\lambda = 305$ nm, the $\sigma \times T$ curve suggests that whatever is causing the carrier freezeout has its concentration decreased by exposure to monochromatic light above the bandgap. It is important to mention that below bandgap light had no effect on the resistance with the same procedure. Repeating several times the procedure of illuminating the sample continuously with $\lambda = 305$ nm as the temperature was increased, resulted in the conductivity keeping on increasing. It seems that there is a tendency for saturation, but at low temperature at least, this saturation has not yet been reached. Subsequently, the temperature was increased to 200°C for about 5 min in a vacuum and cooled to room temperature. Once more the sample was taken to 77 K and the resistance measured during the increase of temperature in the dark. The strong decrease in conductivity, observed in the first measurement in the dark no longer existed and the conductivity dependence with temperature can hardly therefore be associated with deep levels. The cycling procedure had eliminated most of the traps which were present in the beginning. Although Fig. 1 represents data recorded for an Sb-doped sample, the same behavior is also observed for a pure SnO_2 film. The only difference is the absolute value of resistance, which is higher for the pure SnO_2 film than for the Sb-doped sample, as expected. In order to interpret these results we performed the same measurement after annealing the sample to 200°C, but keeping the sample in air this time. Low conductivity and electron trapping behavior was recovered, being quite similar to the curve in the dark shown in Fig. 1.

The inset in Fig. 1 is an Arrhenius plot related to the data of the upper and the lower curves of Fig. 1. Before any photo- or thermal processing, the curve can be approximated by two straight lines with good correlation coefficients. These two regions have activation energy of about 39 and 81 meV, for the lower and higher temperature ranges, respectively, which may be related to two levels: a Sb donor level and an oxygen vacancy level (the deeper one) [11]. Considering that our samples were polycrystalline, the scattering at grain boundaries [12] should contribute to the discrepancies between single crystal data [11] and our data. This change in slope has been predicted by Blakemore [13] for semiconductors dominated by several localized

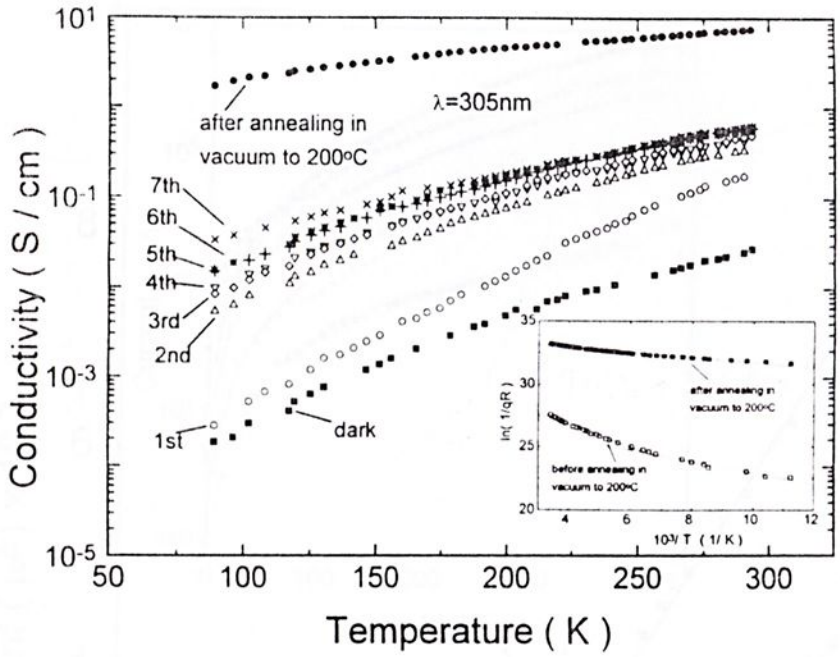


Figure 1. Conductivity of an Sb-doped (2 mol%) SnO_2 thin film as function of temperature in the dark and under steady illumination with λ = 305 nm monochromatic light during several cycles. The upper curve represents data obtained after annealing in vacuum at 200°C. Inset: Arrhenius plot for the curve obtained in the dark and after all of the cycling process.

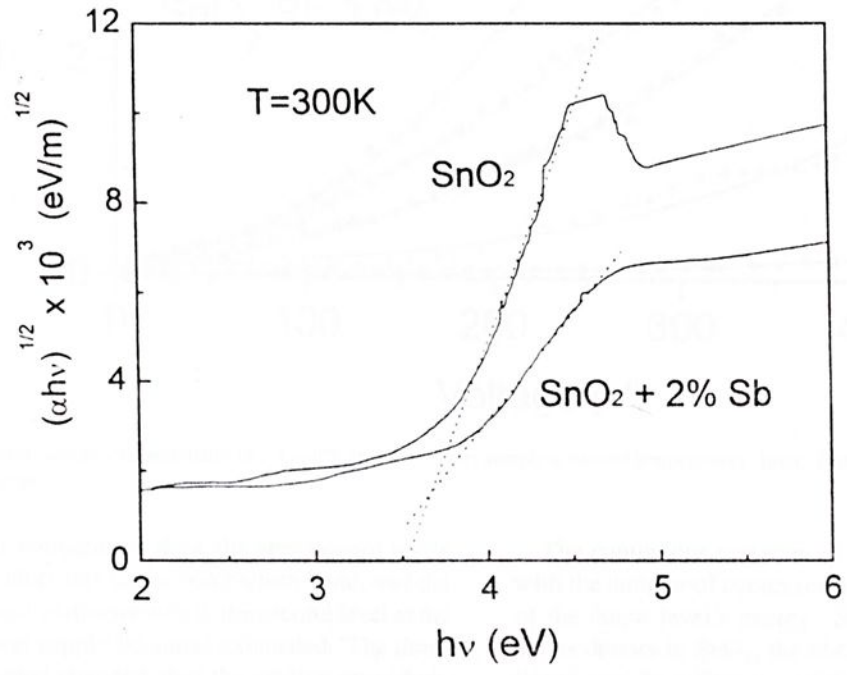


Figure 2. Test for indirect bandgap transition for pure SnO_2 and 2 mol% Sb doped. Data calculated from optical absorption.

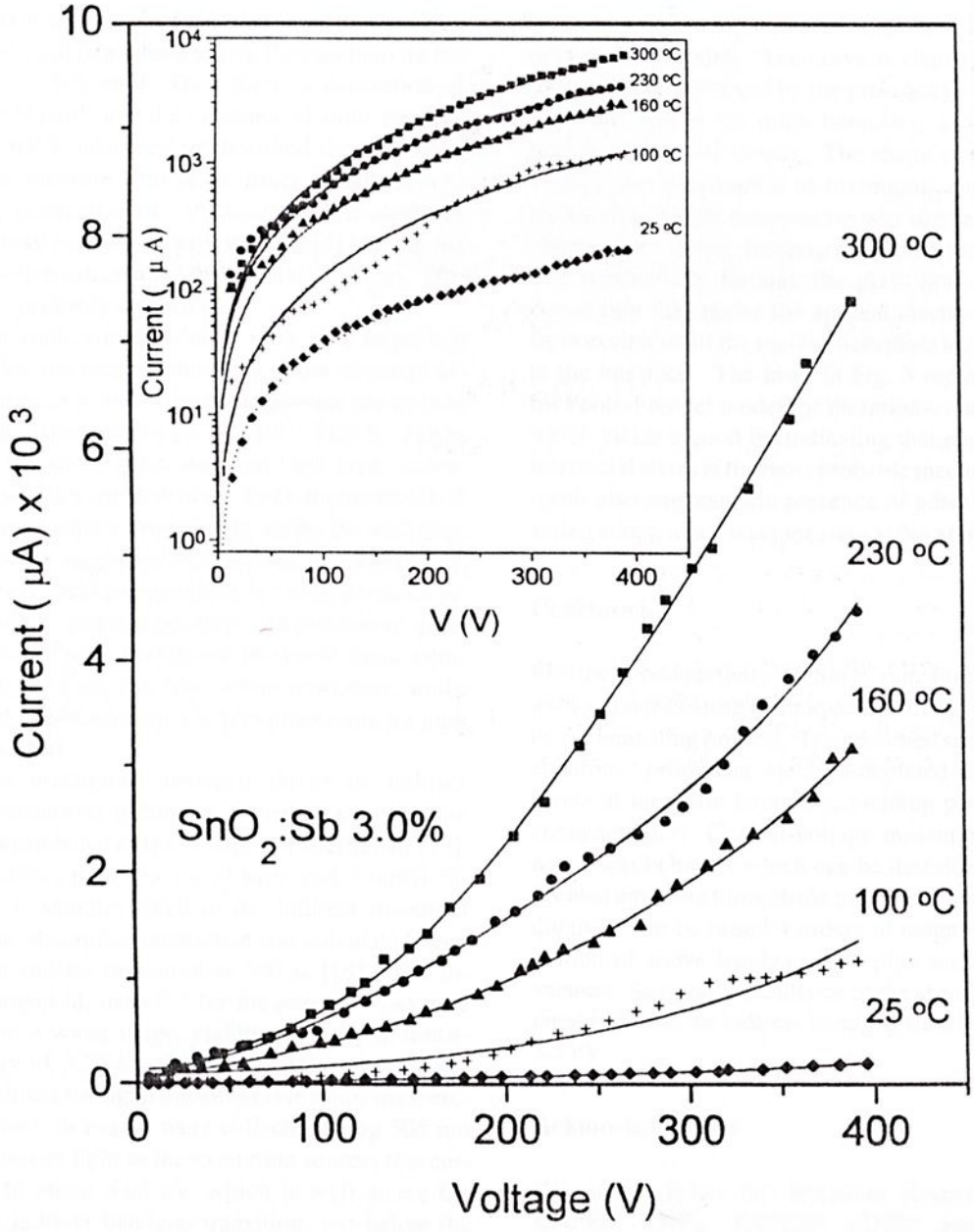


Figure 3. Current-voltage characteristics of a 3 mol% Sb-doped SnO_2 sample at several temperatures. Inset: Test for Poole-Frenkel model for thermionic emission.

levels. As the temperature rises, the upper donor levels release their electrons to the conduction band, and the Fermi level moves downwards to the second level as the shallower level supply becomes exhausted. The dominant donor level changed after the cycling procedure, resulting in a single Arrhenius behavior (upper curve) with an activation energy of about 18 meV, which is rather low.

The continuous variation of the $\sigma \times T$ curve slope with the number of cycles seems to indicate a decrease of the donor level's energy. Since oxygen vacancies act as donors in SnO_2, the observed behavior may be interpreted as a decrease of the donor ionization energy with increasing donor concentration, which has been observed previously [1]. Indeed, it seems consistent to attribute this behavior to the elimination of

traps at grain interface. This can be understood by considering light irradiation above the bandgap on the sample (λ = 305 nm). Then there is generation of electron-hole pairs, and the existence of some gaseous specimen that is adsorbed or desorbed depending on the cryostat pressure, and has a direct contribution to the carrier concentration. Photo-generated electrons and holes may recombine with this gas [6] leaving net electrons which can conduct the electrical current. This gas is most probably oxygen [5].

From an applications point of view, it is important to notice that the best conductivity value obtained after the treatment is one order of magnitude lower than the best published values [8, 12, 14]. This is mainly related to the small grain size and high layer porosity of the samples studied here. Such microstructural characteristics can be improved by using the multidipping procedure suggested by Park and Mackenzie [8], which should yield precipitation of small particles inside the pores, reducing porosity and promoting grain coalescence. Photo-desorption proposed here, combined with the Park and Mackenzie procedure, probably would yield easier and cheaper processing for high quality material.

We can distinguish between direct or indirect bandgap transitions in SnO_2 samples by studying the spectral dependence of the absorption coefficient [15]. Figure 2 shows the behavior of pure and 2 mol% Sb doped SnO_2 samples filled to the indirect transition model. The absorption coefficient was calculated from absorption spectra measured at 300 K [16]. The indirect bandgap fit, $(\alpha h\nu)^{1/2}$ for the pure SnO_2 sample is better for a wider range, yielding a bandgap transition energy of 3.52 eV. Another strong point to support an indirect bandgap transition is that our measurements, shown in Fig. 1, were collected using 305 nm monochromatic light as the excitation source; this corresponds to about 4.05 eV, which is well above the estimated indirect bandgap transition, but below the value estimated from fitting the direct transition model (4.15 eV, not shown in Fig. 2). The inclusion of Sb doping in SnO_2 decreases the indirect bandgap transition to 3.35 eV. This decrease may be related to the high doping level, which can modify the band structure diagram, or to the electron-impurity interaction which can shift the absorption edge to a lower photon energy [15].

Figure 3 represents current-voltage curves for an SnO_2 sample doped with 3 mol% of Sb. This sample exhibited a high resistivity, which may be explained by this measurement being taken prior to any thermal or photo-processing. The curve is clearly non-linear, which can be explained by the presence of an electron-depleted layer at the grain boundary, and the formation of a potential barrier. The shape of the current-voltage curves is typical of thermionic emission over the barrier. As the temperature was increased, the deviation from ohmic behaviour became more evident. The conductivity through the grain boundary of the doped thin film under the applied electric field came from excitation of the ionized acceptors localized close to the interface. The inset in Fig. 3 represents a test for Poole-Frenkel model for thermionic emission [17], which yields a good fit, indicating that emission from interfacial states is the most probable mechanism. This result also suggests the presence of adsorbed oxygen acting acting as an acceptor state at the grain boundary.

Conclusion

Electrical conductivity of SnO_2 thin films grown by a sol-gel dip-coating technique are strongly influenced by the annealing process. The adsorbed specimen traps electrons, producing electron-depleted space-charge layers at the grain boundary, yielding poor electrical characteristics. Current-voltage measurements show non-linear behavior which can be described by Poole-Frenkel emission through the grain boundary. The conductivity can be raised 4 orders of magnitude by irradiation of above bandgap light plus annealing under vacuum. Spectral dependence of the absorption coefficient indicates an indirect bandgap transition of about 3.5 eV.

Acknowledgments

We acknowledge the Brazilian financial agencies CAPES, CNPq, FAPESP, FINEP and PRONEX 402/96.

References

1. Z.M. Jarzebski and J.P. Marton, J. Electrochemical Society **123**, 199C and 299C (1976).
2. K.C. Mishra, K.H. Johnson, and P.C. Schmidt, Phys. Rev. B **51**, 13972 (1995).
3. G. Sanon, R. Rup, and E.A. Mansingh, Phys. Rev. B **44**, 5672 (1991).
4. C. Terrier, J.P. Chatelon, R. Berjoan, and J.A. Roger, Thin Solid Films **263**, 37 (1995).

5. F. Prado, G. Meyer, and J. Saura, J. Phys.: Condens. Matter **5**, A351 (1993).
6. S.R. Morrison, *The Chemical Physics of Surfaces* (Plenum Press, New York, 1990), p. 341.
7. K. Chopra, S. Major, and D.K. Pandya, Thin Solid Films **102**, 1 (1983).
8. S.S. Park and J.D. Mackenzie, Thin Solid Films **258**, 268 (1995).
9. R.S. Hiratsuka, S.H. Pulcinelli, and C.V. Santilli, J. Non-Cryst. Solids **121**, 76 (1990).
10. B. Orel, U. Laurencie-Stangar, Z. Crnjak-Orel, P. Bukovec, and M. Kosec, J. Non-Cryst. Solids **167**, 272 (1994).
11. C.G. Fonstad and R.H. Rediker, J. Appl. Phys. **42**, 2911 (1971).
12. E. Santhi, V. Dutta, A. Banerjee, and K.L. Chopra, J. Appl. Phys. **51**, 6243 (1980).
13. J.S. Blakemore, *Semiconductor Statistics* (Dover Publications, New York, 1987), p. 159.
14. T.D. Senguttuvan and L.K. Malhotra, Thin Solid Films **289**, 22 (1996).
15. E.A. Johnson, in *Semiconductors and Semimetals*, edited by R.K. Willardson and A.C. Beer (Academic Press, New York, 1967), Vol. 3, p. 153.
16. G. Campet, C. Geoffroy, J.P. Manaud, J. Portier, Z.W. Sun, J. Salardenne, and P. Keou, Materials Sci. and Engr. **B8**, 45 (1991).
17. T.K. Gupta, J. Am. Ceram. Soc. **73**, 1817 (1990).

Radiation Effects & Defects in Solids, Vol. 146, pp. 199–206 © 1998 OPA (Overseas Publishers Association) N.V.
Reprints available directly from the publisher
Photocopying permitted by license only
Published by license under
the Gordon and Breach Science
Publishers imprint.
Printed in India

PHOTODESORPTION AND ELECTRON TRAPPING IN n-TYPE SnO_2 THIN FILMS GROWN BY DIP-COATING TECHNIQUE

FÁBIO R. MESSIAS[a,*], LUIS V.A. SCALVI[b], M. SIU LI[a], C.V. SANTILLI[c] and S.H. PULCINELLI[c]

[a] *Instituto de Física de São Carlos – U.S.P., Caixa Postal 369, São Carlos SP 13560-970, Brazil;* [b] *Departamento de Física-FC – UNESP, Campus Bauru, Caixa Postal 473, Bauru SP 17033-360, Brazil;* [c] *Instituto de Química – UNESP, Campus Araraquara, Caixa Postal 355, Araraquara SP 14801-907, Brazil*

Thin films of undoped and Sb-doped (2 atg%) SnO_2 have been prepared by sol-gel dip-coating technique on borosilicate glasses. Variation of photoconductivity excitation with wavelength and optical absorption indicate indirect bandgap transition with energy of $\cong 3.5$ eV. Conductance as function of temperature indicates two levels of capture with 39 and 81 meV as activation energies, which may be related to an Sb donor and oxygen vacancy respectively. Electron trapping by these levels are practically destroyed by UV photoexcitation (305 nm) and heating in vacuum to 200°C. Gas analysis using a mass spectrometer indicates an oxygen related level, which may not be desorbed in the simpler O_2 form.

Keywords: Tin dioxide; Wide gap semiconductor; Optical absorption; Photoconductivity; Oxygen vacancy; Traps

1 INTRODUCTION

Tin dioxide has wide application as transparent electrodes [1], electro-optical devices and solar collectors [2,3]. In its undoped form SnO_2 is an n-type semiconductor and its structure is represented by one tin atom at a centre of six oxygen atoms placed approximately at the corners of a

* Corresponding author.

regular octahedron [4]. Since oxygen vacancies or interstitial tin atoms act as donors in SnO_2, the electrical properties depend on the deviation from stoichiometric composition and interstitial tin atoms concentration. It has been observed that Sb doping increases the *n*-type conductivity since Sb is incorporated into the lattice in substitution to Sn atoms [5], which means the exchange of Sn^{4+} by Sb^{5+}. Another very important feature is the mechanism of chemisorption of oxygen on the SnO_2 surface. Bandgap transitions change electron and hole concentrations at the semiconductor surface [6]. Photoproduced electrons will induce oxygen adsorption, but photoinduced holes will induce oxygen desorption, so that the net effect depends on the rate constants and on the sample properties in the dark.

In this communication we show some electro-optical properties of pure and Sb-doped SnO_2 thin film samples, based on chemisorption of an acceptor atom on the surface. In order to find out what this atom is, we have done gas analysis during annealing in vacuum and we present the most probable forms of desorption. We also observe a light induced increase in the sample conductivity in vacuum, pointing to a metastable effect related to this gas adsorption.

2 EXPERIMENTAL

Samples used in this work were grown by sol-gel dip-coating technique. Borosilicate glass substrates are dipped vertically into a suspension of SnO_2 prepared from hydrolysis of $SnCl_4 \cdot 5H_2O$ in aqueous solution [7]. The Sb doped sample (2 atg%) is obtained by dissolution of $SbCl_3$ in $SnCl_4$ aqueous solution. The dipping rate is 6 cm/min and the resulting thickness after 30 dips is 3000 Å. Afterwards samples are annealed to 550°C for one hour in air. Films present good transparency (80% in the visible) and are uniform over the whole surface, being polycrystalline with average grain size of 3 nm and porosity of about 35%.

Electrical measurements were performed in samples with evaporated In electrodes, annealed to 150°C for 30 min. Variation of photocurrent excitation with wavelength is done using a tungsten lamp of 470 watt plus a monochromator. Electrical data are recorded using an electrometer and a microcomputer. For variation of conductance with temperature data, we have used a 305 nm line of a UV Hg lamp. Optical

absorption coefficient were determined by UV-visible spectroscopy. For gas analysis is used a mass spectrometer which is able to measure several gases inside the cryostat until 64 a.m.u.

3 RESULTS AND DISCUSSION

Figure 1 shows results of conductivity in function of wavelength of exciting light, at room temperature. Although it presents a broad spectrum around the bandgap transition, a maximum value can be seen at 339 nm, which corresponds to about 3.64 eV. The inset in Fig. 1 represents indirect bandgap transition test for pure and Sb doped samples. The absorption coefficient (α) is calculated from absorption spectra at 300 K [8]. Although the polycrystalline structure of our samples leaves the definition of transition rather obscure, indirect

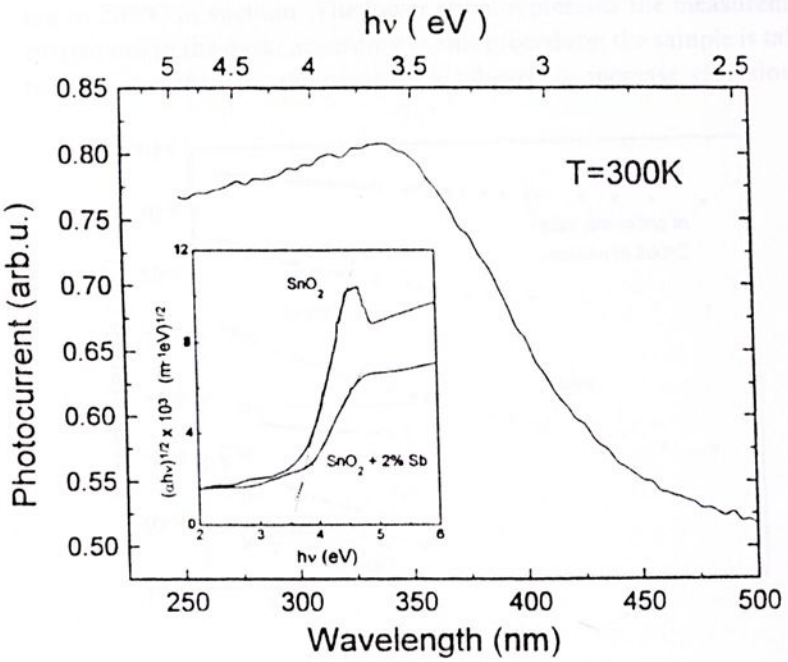


FIGURE 1 Variation of photoconductivity excitation with wavelength for Sb-doped (2 atg%) SnO_2 at 300 K. Inset – Test for indirect bandgap transition for undoped and 2% Sb-doped. Absorption coefficient calculated from UV-visible spectroscopy.

bandgap fit, $(\alpha h\nu)^{1/2}$ for pure SnO_2 sample is more convenient for a wider range (h – Planck constant, ν – frequency of irradiating light), yielding bandgap transition energy of 3.52 eV. The inclusion of Sb doping in SnO_2 decreases the indirect bandgap transition to 3.35 eV. This decrease may be related to the high doping level, which can modify the band structure diagram, or to the electron impurity interaction which can shift the absorption edge to a lower photon energy [9], and then, a precise bandgap transition could only be estimated if a correction for this shift is taken into account. The maximum in photocurrent has a longer wavelength than that corresponding to the absorption edge, what is expected since for wavelengths shorter than this maximum in photocurrent, the radiation is being strongly absorbed and produces excitation only near the surface [10].

Figure 2 shows results of conductance as function of temperature for the Sb-doped sample in three situations: (1) in the dark, (2) using excitation with $\lambda = 305$ nm monochromatic light and (3) after annealing to 200°C in vacuum. The lower curve represents the measurement carried out in the dark, according to this procedure: the sample is taken to 77 K and then the temperature is allowed to increase very slowly.

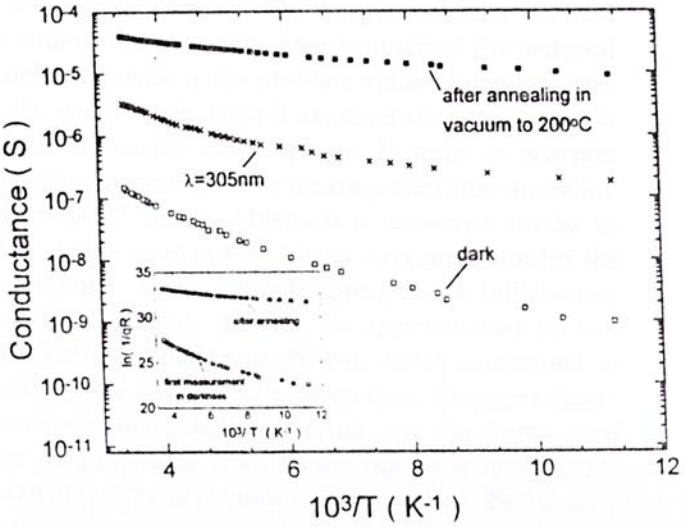


FIGURE 2 Conductance of Sb-doped (2 atg%) SnO_2 thin film as function of temperature in the dark, under steady illumination with $\lambda = 305$ nm light and after annealing to 200°C in vacuum. Inset – Arrhenius plot for the lower and upper curve.

when data are recorded. There is a sharp decrease in the sample conductivity as the temperature is lowered, suggesting a carrier freezeout at defects, whose energy levels are in the sample bandgap because if the doping generates only a shallow level in the forbidden gap, this conductivity curve is not expected. The high doping level leads to a highly degenerate oxide semiconductor and the temperature dependence of the conductance would be much weaker than the observed. Taking the sample to 77 K again and illuminating steadily with monochromatic light of $\lambda = 305$ nm, the conductance × temperature curve suggests that whatever is causing the carrier freezeout, has its concentration decreased. The curve shown in Fig. 2 results from repeating several times the procedure of taking the sample to 77 K and illuminating during the increase of temperature. These conductance values are practically light induced saturation values. Then the temperature is increased to 200°C for about 5 min in vacuum and cooled down to room temperature. The sample is taken to 77 K again and the conductance is plotted during the increase of temperature. The strong decrease in conductance observed in the first measurement in the dark no longer exist and the smooth variation can hardly be associated to deep levels. The combination of optical and thermal procedure has eliminated most of the traps. Although Fig. 2 represents data recorded for an Sb-doped sample, the same behaviour is observed for undoped SnO_2 film. The only difference is the absolute value of conductance, that is lower for the pure sample, what is expected since the doping is supposed to increase the carrier concentration. In order to interpret these results we have performed the same measurement after annealing the sample in air to 200°C. Low conductance is recovered, similar to lower curve of Fig. 2. The inset in Fig. 2 is an Arrhenius plot for the upper and the lower curve. Using a simple approach, the initial curve can be divided in two portions, that can be approximated by two straight lines with good correlation coefficient, which correspond to two distinct trapping levels. As the temperature rises, the upper donor releases its electrons to the conduction band and the Fermi level moves downward to the second level, as the shallower level supply becomes exhausted [11]. The activation energies are 39 and 81 meV and may be associated to a Sb donor level and an oxygen vacancy level respectively [12]. Discrepancies between crystal data [12] and our data are probably related to grain boundary scattering [13], since our

samples are polycrystalline. The Arrhenius plot for the upper curve can be approximated by only one straight line and activation energy is 18 meV which is rather shallow.

Since vacancies act as donors in SnO_2, the result observed in Fig. 2 may be interpreted as a decrease of donors level ionisation energy with increasing donor concentration [4]. However, it seems consistent to associate this conductance increase with the elimination of adsorbed traps from grain interface. Irradiation of above bandgap light generates electron-hole pairs, which can recombine with this adsorbed specimen. Following the model of oxygen surface recombination [6], photo-generated electrons and holes recombine with this gas as follows:

$$e^- + G \rightarrow G^-, \quad (1)$$

$$h^+ + G^- \rightarrow G, \quad (2)$$

where e^- is one electron, h^+ is one hole and G means one atom of the interacting specimen in the gaseous phase (G) or adsorbed and ionised (G^-). Since we obtain an increase in the *n*-type sample conductivity we believe that relation 2 is the dominant mechanism and the monochromatic light irradiation with above bandgap light leaves an effect of net electrons which can conduct the electrical current. Although G atom is most probably oxygen [14], we perform an analysis of gases being desorbed during the annealing. Figure 3 represents the analysis of the most important gases probably being desorbed from the sample. Experimental procedure is repeated for the cryostat either without the sample or loaded with the sample. Cryostat is under vacuum for 80 min ($\cong 10^{-5}$ Torr) as shown in Fig. 3 and then we start heating up the system until about 260 min, when the temperature reaches 200°C. Although the time previous to annealing is the same, there are some differences in absolute pressure for most of these gases between these two situations. Considering a normalised partial pressure (relative to the value at the beginning in these two cases), we can see the increase in partial pressure for O_2 and H_2O in the inset of Fig. 3. Although O_2 desorption is the most expected mechanism, H_2O also has a very significative increase in the partial pressure in the cryostat with the sample, if compared to the empty cryostat, mainly during the annealing. It suggests that oxygen vacancies are actually responsible for increase in sample conductivity.

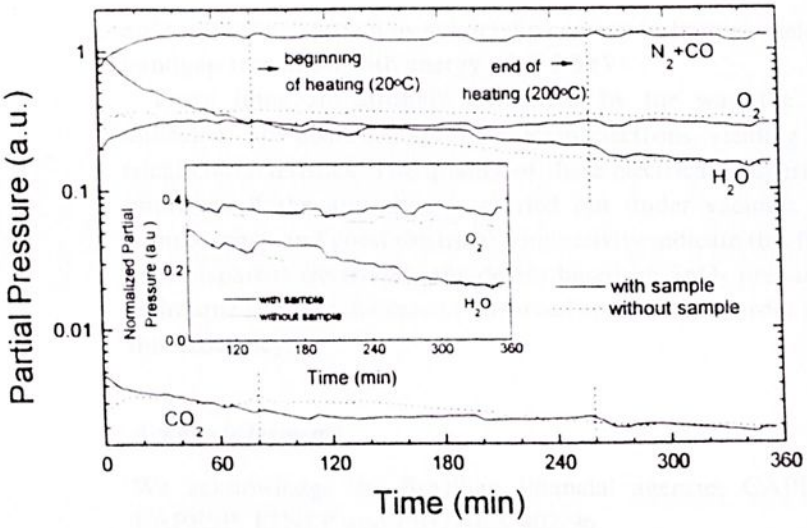


FIGURE 3 Gas analysis with mass spectrometer during the heating cycle of the cryostat with the sample and without the sample. Inset – Normalised partial pressure for O_2 and H_2O.

but the way oxygen is desorbed from the sample may not be the simpler O_2 form, but associated with hydrogen. Indeed, superficial OH groups which induce structuration of water molecules by the extensive formation of H-bridges has been found previously [15]. There is another possibility of association with carbon during the desorption process [16], but the partial pressure of CO_2 seen in Fig. 3 is too small and we find hard to conclude anything about it based on Fig. 3. Although we have been very careful in doing this experiment, the amount of gas adsorbed on the sample is low and then Fig. 3 must be seen as a qualitative result. In order to make sure how oxygen is adsorbed or desorbed from the surface and grain boundaries, we are carrying out some experiments using atmospheres rich in specific gases and our conclusions shall be published opportunely.

4 CONCLUSION

Conductivity as function of wavelength and optical absorption were carried out at room temperature for undoped and Sb-doped (2 atg%)

SnO_2 thin films, grown by sol-gel dip coating technique, yields indirect bandgap transition with energy of $\cong 3.5\,eV$.

These films are strongly influenced by the way the sample is annealed. The adsorbed specimen traps electrons, yielding poor electrical characteristics. The quality of these electrical properties can be improved if the annealing is carried out under vacuum. Although transparency and good electrical conductivity indicate this film for use as transparent electrodes, any device based on SnO_2 prepared by this technique should take care of adsorbed specimens in order to improve this efficiency.

Acknowledgements

We acknowledge the Brazilian financial agencies CAPES, CNPq, FAPESP, FINEP and PRONEX 402/96.

References

[1] K.C. Mishra, K.H. Johnson and P.C. Schmidt, *Phys. Rev. B* **51**, 13972 (1995).
[2] H. Hoheisel, S. Hellerm, C. Mrotzek and A. Mitwalsky, *Solid State Comm.* **76**, 1 (1990).
[3] G. Sanon, R. Rup and E.A. Mansingh, *Phys. Rev. B* **44**, 5672 (1991).
[4] Z.M. Jarzebski and J.P. Marton, *J. Electrochemical Society* **123**, 199C and 299C (1976).
[5] C. Terrier, J.P. Chatelon, R. Berjoan and J.A. Roger, *Thin Solid Films* **263**, 37 (1995).
[6] S.R. Morrison, *The Chemical Physics of Surfaces* (Plenum Press, New York, 1990), p. 341.
[7] R.S. Hiratsuka, S.H. Pulcinelli and C.V. Santilli, *J. Non-Cryst. Solids* **121**, 76 (1990).
[8] G. Campet, C. Geoffroy, J.P. Manaud, J. Portier, Z.W. Sun, J. Salardenne and P. Keou, *Materials Sci. and Engr.* **B8**, 45 (1991).
[9] E.A. Johnson, in: *Semiconductors and Semimetals*, Vol. 3, ed. by R.K. Willardson and A.C. Beer (Academic Press, New York, 1967), p. 153.
[10] R.H. Bube, *Photoconductivity of Solids* (John Wiley & Sons, New York, 1960), p. 230.
[11] J.S. Blakemore, *Semiconductor Statistics* (Dover Publications, New York, 1987), p. 159.
[12] C.G. Fonstad and R.H. Rediker, *J. Appl. Phys.* **42**, 2911 (1971).
[13] E. Santhi, V. Dutta, A. Banerjee and K.L. Chopra, *J. Appl. Phys.* **51**, 6243 (1980).
[14] F. Prado, G. Meyer and J. Saura, *J. Phys.: Condens. Matter* **5**, A351 (1993).
[15] S.J.L. Ribeiro, C.V. Santilli, S.H. Pulcinelli, F.L. Fortes and L.F.C. Oliveira, *J. Sol-Gel Sci. Technol.* **2**, 263 (1994).
[16] H. Windischmann and P. Mark, *J. Electrochem. Soc.* **26**, 627 (1979).

Reprinted from

JOURNAL OF
NON-CRYSTALLINE SOLIDS

Journal of Non-Crystalline Solids 247 (1999) 171–175

Electron scattering and effects of sources of light on photoconductivity of SnO_2 coatings prepared by sol–gel

F.R. Messias [a], B.A.V. Vega [b], L.V.A. Scalvi [b,*], M. Siu Li [a], C.V. Santilli [c], S.H. Pulcinelli [c]

[a] *Instituto de Física de São Carlos, USP. C.P. 369, 13560-970 São Carlos, SP, Brazil*
[b] *Departamento de Física, FC, UNESP. C.P. 473, 17033-360 Bauru, SP, Brazil*
[c] *Instituto de Química, UNESP. C.P. 355, 14801-970 Araraquara, SP, Brazil*

ELSEVIER

ELSEVIER

Journal of Non-Crystalline Solids 247 (1999) 171–175

JOURNAL OF NON-CRYSTALLINE SOLIDS

Electron scattering and effects of sources of light on photoconductivity of SnO_2 coatings prepared by sol–gel

F.R. Messias [a], B.A.V. Vega [b], L.V.A. Scalvi [b,*], M. Siu Li [a], C.V. Santilli [c], S.H. Pulcinelli [c]

[a] *Instituto de Física de São Carlos, USP. C.P. 369, 13560-970 São Carlos, SP, Brazil*
[b] *Departamento de Física, FC, UNESP, C.P. 473, 17033-360 Bauru, SP, Brazil*
[c] *Instituto de Química, UNESP, C.P. 355, 14801-970 Araraquara, SP, Brazil*

Abstract

Electro-optical properties of sol–gel derived 2 mol% antimony or niobium doped tin dioxide films have been measured. The electron density has been calculated considering all the relevant scattering mechanisms and experimental conductivity data measured in the range −197 to 25°C. The results support the hypothesis that both ionised impurity scattering and grain boundary scattering have comparable effects in the resistivity of coatings, for free electron density $\cong 5 \times 10^{19}$ cm^{-3}. We have measured variation of photoconductivity excitation with wavelength using xenon and deuterium lamp as light sources. Results show that the main band in the photoconductivity spectrum is dependent on the spectral light source emission, the excitation peak reaching 5 eV (deuterium lamp). This band is due to the recombination process involving oxygen species and photogenerated electron–hole pairs. © 1999 Elsevier Science B.V. All rights reserved.

1. Introduction

Tin dioxide has been used for making transparent and electrically conductive coatings of large surface glass substrates by means of the dip-coating sol–gel process [1–4]. In general, the sol–gel coating has smaller conductivity compared with those reported for SnO_2 coatings prepared by other deposition techniques [5–8]. This smaller conductivity is attributed to grain boundary effects of the crystallites in sol–gel derived SnO_2 [3]. Moreover, doping with electronic donors such as Sb^{5+} or Nb^{5+} increases the carrier concentration and limits the crystallite sizes yielding a larger overall grain boundary resistivity [3]. The interpretation of the conductance changes caused by grain boundary effects in doped SnO_2 is complex due to the contribution of several scattering processes [9] and the effect of adsorbed species such as oxygen [8], which decrease the concentration of point defects (oxygen vacancies and interstitial tin atoms) responsible for the n-type conduction of tin dioxide.

In a recent paper [4], we pointed out the effects of ultra-violet light irradiation on the desorption of oxygen species and increase of the electric conductivity of undoped SnO_2 coatings. This phenomena was attributed to the recombination process involving oxygen and photogenerated electron–hole pairs, leading to an increase in the number of conduction electrons. To exploit such phenomena for improving sol–gel processing of

* Corresponding author. Tel.: +55-14 230 2111; e-mail: scalvi@bauru.unesp.br

0022-3093/99/$ – see front matter © 1999 Elsevier Science B.V. All rights reserved.
PII: S0022-3093(99)00085-X

SnO_2 based coatings, we investigated the effect of light sources with different ultra-violet spectral emission on 2 mol% antimony or niobium doped films grown by sol–gel dip coating technique. Electron density calculation based on electron scattering mechanisms is also presented to better understand the grain boundary effects of these films.

2. Experimental

Films were deposited in laboratory ambient conditions (25°C, relative humidity of 60%), as follows: borosilicate glass substrates were dipped vertically into a colloidal suspension of SnO_2 prepared from hydrolysis of $SnCl_4 \cdot 5H_2O$ (BDH) in bidistilled water solution [3]. Sb or Nb 2%mol doping was obtained by dissolution of $SbCl_5$ (Merck) or $NbCl_5$ (Merck) in $SnCl_4$ aqueous solution. Films were drawn with a lifting rate of 6 cm/min, resulting in a 300 nm thickness after 30 dips [3]. Samples were annealed at 550°C for 1 h in air. These samples had a transparency of 80% in the 400–800 nm range which was invariant over the whole surface, being polycrystalline with average grain size of 3 nm and porosity of about 35% [3].

Photocurrent spectral dependence was measured in a parallel orientation to the coating, using evaporated In electrodes, annealed at 150°C for 30 min. We used light sources: a 450 W xenon lamp, which does not emit at wavelengths <290 nm and a deuterium lamp from a spectrophotometer (Cary), with decreasing intensity in the range 250–200 nm. In these cases the wavelength was selected by a computer controlled monochromator and the scanning was from larger to smaller wavelength.

3. Results

Electron density was calculated from conductivities ($\sigma = q\mu(n)n$. The symbols are: q the electron charge, $\mu(n)$ the mobility and n the free electron density) measured at different temperatures, assuming that the dominant scattering mechanisms which determine the mobility (μ) are

$$\mu^{-1} = \mu_n^{-1} - \mu_g^{-1} - \mu_{po}^{-1}, \quad (1)$$

where μ_n is the mobility due to ionised impurity scattering [10], μ_g is the mobility due to grain boundary scattering [9] and μ_{po} is the polar optical scattering [11]. Solving self-consistently all the equations involved, we evaluate electron density, which is shown in Fig. 1 for three different situations: (i) the lower curve comes from measured resistance in the dark for an as prepared sample (2 mol% Sb-doped SnO_2), (ii) after illumination during the increase of temperature (seven times [4]), and (iii) after annealing in vacuum to 200°C (full line). The inset in Fig. 1 represents the mobility in a calculation based on the three scattering mechanisms. The mobility due to the ionised impurity scattering corresponding to three different free electron densities is indicated in the Fig. 1.

Fig. 2 shows photoconductivity spectral dependence for a 2 mol% Nb and a 2 mol% Sb-doped samples annealed in air at 200°C during 5 min when illuminated with a Xenon lamp. Measurements have been carried out at 25°C at a pressure of 10^{-3} m Torr. Keeping the sample under these conditions, the photoconductivity increases, as

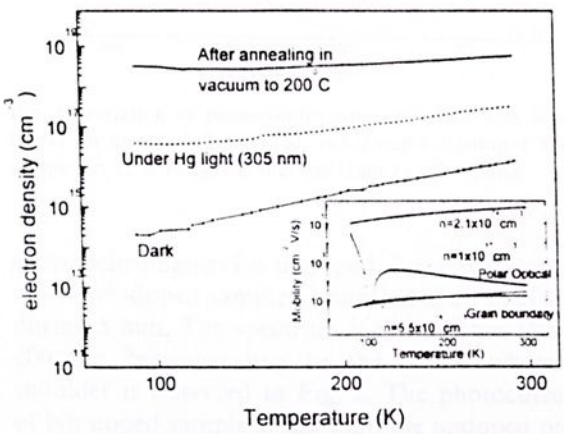


Fig. 1. Electron density for a 2 mol% Sb-doped SnO_2 thin film. Lower curve – measured in the dark, as prepared sample; dotted line – under illumination with $\lambda = 305$ nm monochromatic light, full line – after annealing in vacuum and measured in the dark. Inset – mobility evaluated for polar optical, grain boundary and ionised impurity scattering for electron density of 2.1×10^{14}, 1×10^{15} and 5.5×10^{15} cm^{-3}. Lines are drawn as a guide for the eye.

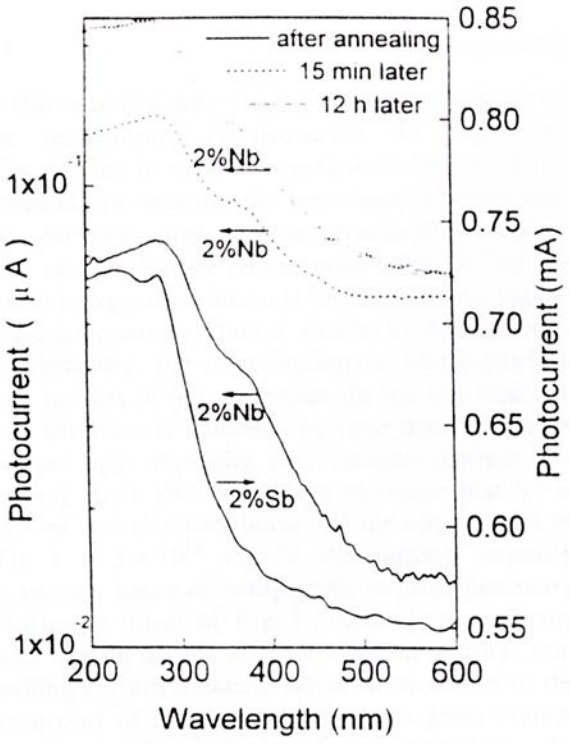


Fig. 2. Variation of photoconductivity excitation with wavelength using a xenon lamp as light source, for 2 mol% Nb-doped and Sb-doped (lower curve) SnO_2 at 25°C, full line – after annealing to 200°C in air, dotted line – 15 min after measurement number 1, triangles – 12 h after measurement 2.

shown by the curves measured at 15 min and 12 h. All curves have a shoulder at about 390 nm as well as a maximum at about 290 nm. When annealing to 200°C is carried out at a pressure of 10^{-3} m Torr and the photoconductivity measured at room temperature, the current magnitude increases about 20 times and oscillations in the current are observed (not shown in Fig. 2). In this case we can not identify any transition in the photoconductivity.

Fig. 3 shows the first derivative of the lower curves of Fig. 2. For the 2 mol% Nb doped SnO_2 sample, two peaks are observed at about 3.2 and 4.0 eV. In the case of the 2 mol% Sb doped sample, just the latter peak is detected. In the case of the Sb-doped sample we observe many oscillations and local maximum, the highest one being located about 3.2 eV.

Fig. 4 shows spectral dependence of photocurrent with wavelength using a deuterium lamp (plus

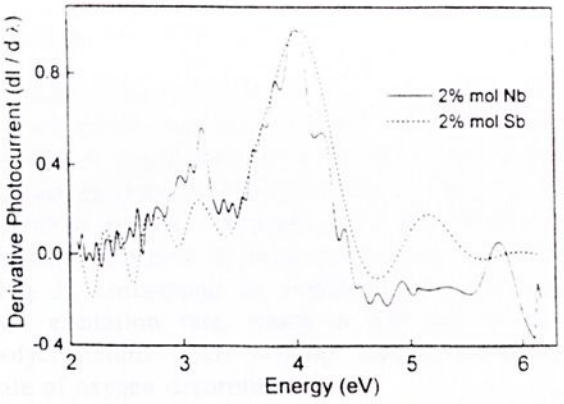


Fig. 3. First derivative of photoconductivity signal after annealing to 200°C in air for 2 mol% Nb and Sb doped-SnO_2 samples.

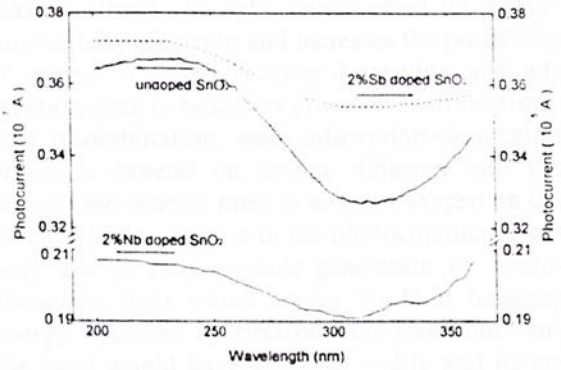


Fig. 4. Variation of photoconductivity excitation with wavelength for undoped, 2 mol% Sb and 2 mol% Nb-doped SnO_2 samples at 25°C using a deuterium lamp as light source.

a monochromator) for undoped, 2 mol% Sb, and 2 mol% Nb-doped samples, annealed in air at 200°C during 5 min. The spectrum is taken from 360 to 200 nm corresponding to the region where a shoulder is observed in Fig. 2. The photocurrent of Nb doped sample is less than the undoped one, whereas the Sb doped sample has a larger current.

4. Discussion

The set of results shows that the as prepared sample has a smaller conductivity than the annealed samples at various times after the anneals.

In this sample a decrease in free electron density as the temperature is decreased was observed (Fig. 1), due to carrier freezeout at defects. After annealing in vacuum, the free electron concentration increases and becomes practically independent of temperature (continuous curve in Fig. 1), which is expected, since it is assumed to be a highly degenerate semiconductor, due to its doping level. Furthermore, the contribution of photo-adsorption process of gas molecules on the free electron concentration is indicated by their dependence on sample light exposure and vacuum thermal annealing. It is also interesting to notice that for a typical free electron density of the upper curve in Fig. 1 (5.5×10^{18} cm^{-3}), the ionised impurity scattering becomes comparable to grain boundary scattering (inset of Fig. 1). According to Zhang and Ma [9] at this level of electron density, tunnelling current makes a major contribution to the transport of electric charges across grain boundaries, since the thickness of grain boundaries decrease by doping.

The dependence of photocurrent with time for sample kept under vacuum at 25°C is due to the exchange of oxygen partial pressure (sample annealed in air, $p_{O2} = 0.21$, and measurements were taken under $p_{O2} \equiv 0.2 \times 10^{-3}$). This effect is only observed as the sample is exposed to radiation energy greater than the bandgap energy. Oxygen pressure has been reported to be responsible for the variations in electrical properties of the SnO_2 thin films [8,12,13]. Results shown in Fig. 2 can be explained by an oxygen reaction with electrons and holes on the film surface [12] and grain boundaries [13]. Electron–hole pairs can be generated by monochromatic light whose energy is about bandgap energy (≅3.5 eV [4]). These charge carriers can react with oxygen according to the reactions

$$e^- + O_2 + SnO_2 \rightarrow O^-_{ads}(SnO_2), \quad (2)$$

$$h^+ + O^-_{ads}(SnO_2) \rightarrow O_2 + SnO_2, \quad (3)$$

where $O^-_{ads}(SnO_2)$ means the adsorbed negatively charged oxygen atom. When the experiment is being carried out under vacuum conditions, there is less gaseous O_2 and the amount of adsorbed O^- decreases. The overall result is a concentration of free electrons that can transport charge. As the number of experiments with the same sample increases, photocurrent increases due to decrease of adsorbed oxygen. The peaks at 3.2 and 4.0 eV on the first derivative of photoconductivity spectrum (Fig. 3), correspond to maximum electron–hole pair excitation rate, which in the case of our polycrystalline SnO_2 samples means maximum rate of oxygen desorption.

All the results obtained with a deuterium lamp (Fig. 4) show a peak about 230 nm (≅5.4 eV), which is much larger than any bandgap transition given in published literature and larger then our estimation ($E_g \cong 3.5$ eV) [4]. The energy of the main peak illustrates the light source affect on photoconductivity spectrum and increases the possibility of oxygen trapping because desorption and adsorption seem to be slower processes than electron–hole recombination, since adsorption–desorption processes depend on atomic diffusion into the sample and motion rates of gaseous oxygen on the surface. If the increase in the photoconductivity is only due to electron–hole generation by monochromatic light whose energy is about bandgap energy, followed by electron–hole recombination, the band would have a smaller width, and its position would be independent of the light source. Even far from the bandgap transition the conductivity keeps increasing as seen in Fig. 4. We suggest that the observed decrease from 360 nm indicates that the shoulder observed in the measurements done with a xenon lamp as light source (Fig. 2) may actually be the tail of another peak whose identification is masked by oxygen photodesorption. This property may be due to capture levels verified by electrical measurements [4].

One should notice that conductivity comes from combined free electron concentration plus formation of space charge layers with concomitant potential barrier at grain boundaries [13]. Both effects are related to O^- adsorption at grain boundaries and determine the observed conductivity. Photoconductivity of SnO_2 single crystal has been reported [14] and there are two peaks, about 3.4 eV and 3.8 eV. Oxygen photodesorption does not allow us to see similar peaks.

unesp

5. Conclusion

We have analysed the electron density from measured conductivities and considering the contribution of ionised impurity, lattice and grain boundary scattering on the mobility. Results show that adsorbed species traps electrons and the electrical conductivities can be increased by annealing under vacuum.

Variation of photoconductivity excitation with wavelength measured with two light sources is consistent with the assumption that oxygen participates in electron–hole recombination. The peak in the photoconductivity spectrum depends on light source, reaching 5.4 eV (deuterium), which means that bandgap identification using photoconductivity spectrum is not a straightforward process, because it depends on electron and hole recombination with oxygen adsorbed species.

Acknowledgements

We acknowledge Brazilian financial agencies: CAPES, CNPq, FAPESP and MCT- PRONEX.

References

[1] B. Orel, U. Lavrencic-Stangar, Z. Crnjak-Orel, P. Bukovek, M. Koosec, J. Non-Cryst. Solids 167 (1994) 272.
[2] C. Terrier, J.P. Chatelon, J.A. Roger, Thin Solid Films 295 (1997) 95.
[3] A.E. Souza, S.H. Monteiro, C.V. Santilli, S.H. Pulcinelli, J. Mater. Sci. Mater. Electron. 8 (1997) 265.
[4] L.V.A. Scalvi, F.R. Messias, A.E. Souza, M. Siu Li, C.V. Santilli, S.H. Pulcinelli, J. Sol–Gel Sci. Technol. 13 (1998) 793.
[5] Z.M. Jarzebski, J.P. Marton, J. Electrochem. Soci. 123 (1976) 199C–299C.
[6] E. Shanthi, A. Banerjee, V. Dutta, K.L. Chopra, J. Appl. Phys. 53 (1982) 1615.
[7] G. Sanon, R. Rup, A. Mansingh, Phys. Rev. B 44 (1991) 5672.
[8] F. Prado, G. Meyer, J. Saura, J. Phys.: Condens. Matter 5 (1993) A351.
[9] D.H. Zhang, H.L. Ma, Appl. Phys. A 62 (1996) 487.
[10] D. Chattopadhyay, H.J. Queisser, Rev. Mod. Phys. 53 (1981) 745.
[11] E.H. Putley, The Hall Effect and Semiconductor Physics, Dover, New York, 1960, p. 142.
[12] S.R. Morrison, The Chemical Physics of Surfaces, Plenum, New York, 1990, p. 341.
[13] J. Watson, K. Ihokura, G.S.V. Coles, Meas. Sci. Technol. 4 (1993) 711.
[14] M. Nagasawa, S. Shionoya, Jpn. J. Appl. Phys. 10 (1971) 727.

Radiation Effects & Defects in Solids, Vol. 150, pp. 391–395 © 1999 OPA (Overseas Publishers Association) N.V.
Reprints available directly from the publisher
Photocopying permitted by license only
Published by license under
the Gordon and Breach Science
Publishers imprint
Printed in Malaysia

OXYGEN RELATED DEFECTS EXCITATION AND PHOTOCONDUCTIVITY DEPENDENCE OF SnO_2 SOL-GEL FILMS WITH SEVERAL LIGHT SOURCES

FABIO R. MESSIAS[a], LUIS V.A. SCALVI[b,*], M. SIU LI[a], C.V. SANTILLI[c] and S.H. PULCINELLI[c]

[a]*Instituto de Fisica de São Carlos, USP, C.P. 369, 13560-970 São Carlos SP, Brazil;* [b]*Departamento de Fisica, FC, UNESP, C.P. 473, 17033-360 Bauru SP, Brazil;* [c]*Instituto de Química, UNESP, C.P. 355, 14801-907 Araraquara SP, Brazil*

(Received 6 July 1998; In final form 20 September 1998)

Since oxygen vacancies act as donors in SnO_2, the electrical properties are related to deviation from stoichiometric composition. Depending on stoichiometry SnO_2 can be highly insulating or may exhibit fairly high n-type conductivity. Since bandgap transitions are in the ultraviolet range, its photoconductivity is strongly dependent on the excitation source. We have measured variation of photoconductivity excitation with wavelength for tin dioxide grown by dip-coating sol-gel technique using several light sources: tungsten lamp, xenon, mercury and deuterium, and present selected results. The main band is obtained in the range 3–4 eV according to light source spectrum in the ultraviolet range. The presence of oxygen in the cryostat also affects the spectrum since electron–hole pairs react with adsorbed oxygen specimens.

Keywords: Tin dioxide; Photoconductivity; Oxygen; Vacancy; Sol-gel

1 INTRODUCTION

Depending on stoichiometric composition, undoped SnO_2 may be an n-type semiconductor or an insulator [1]. Dopants such as niobium increase its conductivity while maintaining its transparency. Another

* Corresponding author.

important feature related to electrical properties is the mechanism of chemisorption of oxygen on the SnO_2 surface and grain boundaries, which promotes reaction with photogenerated electrons and holes [2]. In this communication we show photoconductivity excitation with wavelength in the range 200–600 nm using distinct light sources for SnO_2 thin films grown by sol-gel dip coating technique [3]. Film deposition procedure has been described elsewhere [4].

Photocurrent spectral dependence is measured in a parallel orientation to the coating, using evaporated In electrodes. We have used three light sources: a tungsten lamp of 480 W; a xenon lamp of 450 W, and a deuterium lamp from a Cary spectrophotometer. The wavelength is properly selected and scanned from higher to lower wavelength by a computer controlled monochromator.

2 PHOTOCONDUCTIVITY EXCITATION WITH WAVELENGTH

Spectral dependence of photoconductivity for undoped SnO_2 sample is shown in Fig. 1. Monochromatic light comes from the tungsten excitation source. The conductivity excitation is clearly observed, with a peak around 380 nm, for 300 K data. For the sample kept in air (Fig. 1(b)) there is a return to the initial value of current, which is not observed for the sample under vacuum (Fig. 1(a)). This behaviour is related to the chemical absorption and photodesorption of oxygen on the film surface [5] and grain boundaries [6]. Electron–hole pairs can be generated by monochromatic light of energy about bandgap transition, which can react with oxygen according to the reactions:

$$SnO_{2-x} \xrightarrow{(h\nu)} h^+ + e^- \tag{1}$$

$$e^- + \tfrac{1}{2}O_2 + SnO_{2-x} \rightarrow O^-_{ads}(SnO_{2-x}) \tag{2}$$

$$h^+ + O^-_{ads}(SnO_{2-x}) \rightarrow \tfrac{1}{2}O_2 + SnO_{2-x} \tag{3}$$

where SnO_{2-x} is the non-stoichiometric thin dioxide, O_2 is the gaseous oxygen specimen, $O^-_{ads}(SnO_{2-x})$ means the adsorbed negatively charged oxygen atom. Under vacuum, O_2 concentration is lower and the amount of adsorbed O^- produced by reaction 2 is decreased. Then reaction

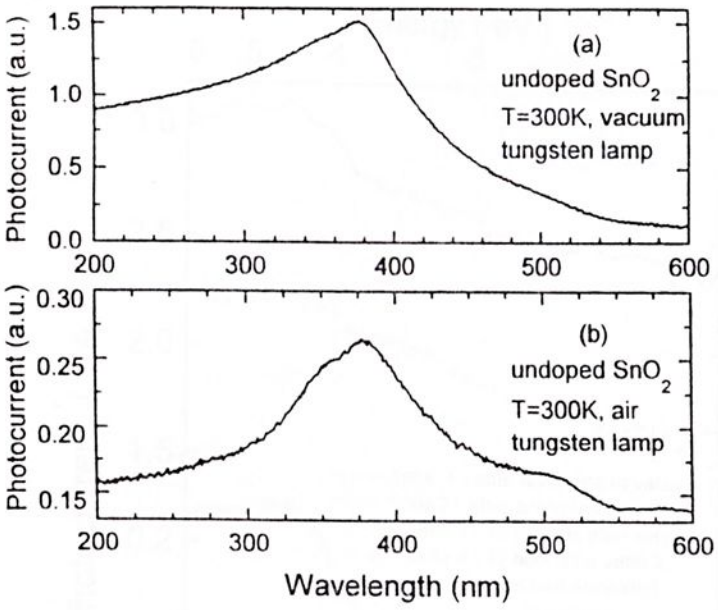


FIGURE 1 Variation of photoconductivity excitation with wavelength for undoped SnO_2 at 300 K: (a) in vacuum, using a tungsten lamp as light source; (b) in air.

number 3 is most probable. The overall result is a net concentration of free electrons that can transport the electrical charge.

Figure 2 shows photoconductivity spectral dependence with a xenon lamp for a 2 atg% Nb-doped sample under several conditions. The first data series (full line) is recorded after annealing under vacuum to 200°C when the adsorbed oxygen species are greatly eliminated. After annealing in air to 200°C the current magnitude decreases and the photoconductivity is as shown by the dashed line (lower curve). A step about 390 nm is seen as well as a peak about 290 nm (4.2 eV). Keeping the sample in vacuum, new measurements are carried out 15 min after the second data series and 12 h after the third measurement. The current magnitude keeps increasing since the oxygen species are being removed. When another annealing under vacuum is carried out, the current magnitude increases again and the photoconductivity is quite similar to what is observed in the measurement number one. Using absorption data we have estimated the bandgap for the Nb-doped sample as 3.4 eV. Measurements using a deuterium lamp have also been carried out and

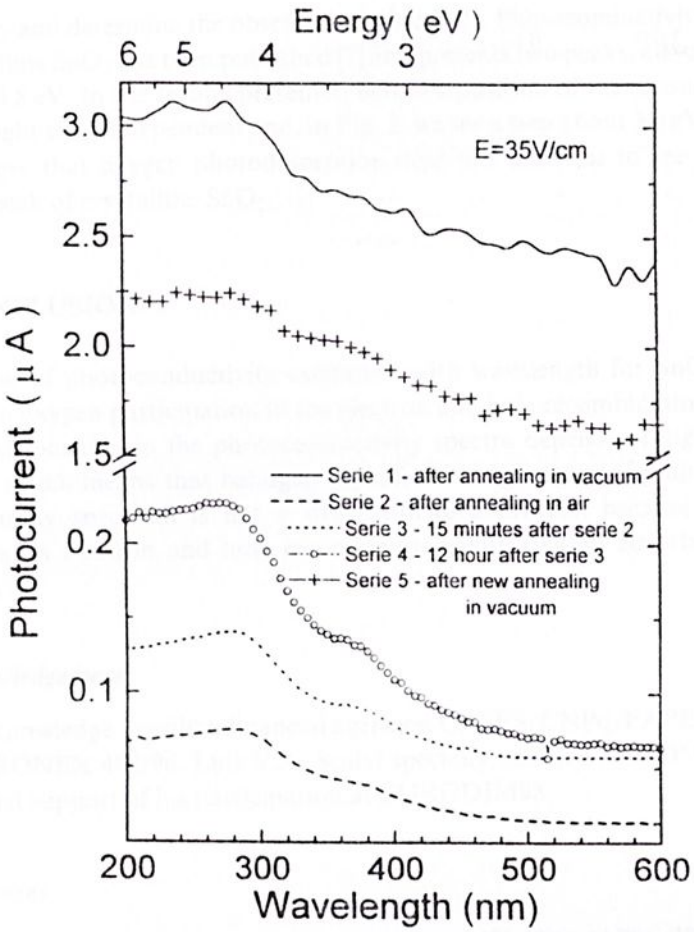


FIGURE 2 Variation of photoconductivity excitation with wavelength using a xenon lamp as light source, for 2 atg% Nb doped SnO_2 at 300 K in sequence, under several conditions, full line – after annealing to 200°C in vacuum, dashed line – after annealing to 200°C in air, dotted line – 15 min after measurement number 2 (dashed), circles – 12 h after measurement 3 (dotted), crosses – after another annealing in vacuum to 200°C.

the peak position is shifted to lower wavelength. These results are being confirmed and shall be published soon.

It is important to mention that the variation of conductivity comes from combined variation of free electron concentration plus formation of space charge layers with concomitant potential barrier at grain boundary [6]. Both effects are related to O^- species adsorption at grain

boundary and determine the observed conductivity. Photoconductivity of crystalline SnO_2 has been published [7] and presents two peaks, about 3.4 and 3.8 eV. In the results presented here the position of the second peak is light source dependent and, in Fig. 2, we see a step about 3.4 eV. We believe that oxygen photodesorption does not allow us to see a similar peak of crystalline SnO_2.

3 CONCLUSION

Variation of photoconductivity excitation with wavelength for SnO_2 points to oxygen participation in the electron and hole recombination. The peak position in the photoconductivity spectra depends on light source, which means that bandgap identification by means of photoconductivity spectrum is not a straightforward process, because it depends on electron and hole recombination with oxygen adsorbed species.

Acknowledgements

We acknowledge Brazilian financial agencies: CAPES, CNPq, FAPESP and PRONEX 402/96. Luis V.A. Scalvi specially thanks FAPESP for financial support of his participation at EURODIM98.

References

[1] Z.M. Jarzebski and J.P. Marton, *J. Electrochem. Society* **123**, 199C and 299C (1976).
[2] F. Prado, G. Meyer and J. Saura, *J. Phys.: Condens. Matter* **5**, A351 (1993).
[3] C. Terrier, J.P. Chatelon and J.A. Roger, *Thin Solid Films* **295**, 95 (1997).
[4] L.V.A. Scalvi, F.R. Messias, A.E. Souza, M. Siu Li, C.V. Santilli and S.H. Pulcinelli, *J. Sol-Gel Science and Technol.* (to be published).
[5] S.R. Morrison, *The Chem. Physics of Surfaces* (Plenum Press, New York, 1990) p. 341.
[6] J. Watson, K. Ihokura and G.S.V. Coles, *Meas. Sci. Technol.* **4**, 711 (1993).
[7] M. Nagasawa and S. Shionoya, *Jap. J. Appl. Phys.* **10**, 727 (1971).

Radiation Effects & Defects in Solids, Vol. 156, pp. 145–149
Reprints available directly from the publisher
Photocopying permitted by license only

© 2001 OPA (Overseas Publishers Association) N.V.
Published by license under
the Gordon and Breach Science Publishers imprint,
a member of the Taylor & Francis Group.

CONTRIBUTION OF OXYGEN RELATED DEFECTS TO THE ELECTRONIC TRANSPORT IN SnO_2 SOL-GEL FILMS

L. V. A. SCALVI[a,*], V. GERALDO[b], F. R. MESSIAS[b], M. S. LI[b], C. V. SANTILLI[c] and S. H. PULCINELLI[c]

[a]*Depto. Física - Fac. Ciências, UNESP, C.P. 473, 17033-360 Bauru SP, Brazil;* [b]*Instituto de Física de São Carlos - USP, C.P. 369, 13560-970 São Carlos SP Brazil;* [c]*I. Química de Araraquara - UNESP, C.P. 355, 14801-907 Araraquara SP, Brazil*

(Received 7 April 2000; In final form 7 October 2000)

SnO_2 deposited by sol-gel is a polycrystalline film with small grain size. Oxygen present at a less grain boundary traps electrons and then the depletion layer around the potential barrier of the grain boundary becomes wider, comparable to the grain size. We have modeled the conductivity taking into account the trapped charge at the depletion layer of the grain boundary and other scattering mechanisms such as ionized impurity and polar optical. Experimental data of photoconductivity of SnO_2 sol-gel films are simulated considering the dominant scattering at grain boundary and crystallite bulk. The fraction of trapped charge at the grain boundary depends on temperature and wavelength of irradiating light, being as high as 50% for illumination in the range 500–600 nm for SnO_2–2%Nb as grown sample annealed in air to 550°C. This fraction can be quite reduced depending on exposure to light and annealing under different oxygen partial pressure conditions.

Keywords: Tin dioxide; Photoconductivity; Oxygen; Sol-gel

1. INTRODUCTION

Tin dioxide has been widely used as gas sensors, transparent electrodes and other devices [1]. Confinement in SnO_2 nanocrystals makes this material very interesting for optoelectronic applications. The size and grain bound-

* Corresponding author. E-mail: scalvi@fc.unesp.br

ary of nanocrystals have great influence on their spectroscopic properties, mainly photoluminescence [2]. Deviation from stoichiometric composition and/or oxygen adsorption may cause insulating or *n*-type semiconducting behavior. SnO_2 deposited by sol-gel is a polycrystalline film with small grain size [3] (3–10 nm in this case) and the depletion layer can be comparable to the grain diameter [4], due to trapping of electrons by adsorbed oxygen. We have measured the photoconductivity spectrum using sources of light such as Deuterium or Xe [5, 6] and we have observed that the photoconductivity increases even for energies higher than the bandgap transition, which is related to previous annealing and oxygen partial pressure conditions inside the annealing chamber.

2 CALCULATION OF DEPLETION LAYER AT GRAIN BOUNDARY

Each crystallite presents an *n*-type conduction due to the presence of oxygen vacancies and doping. Oxygen can be adsorbed at grain boundaries in the range 200–400°C, mainly as O^- species [4]. The standard annealing temperature of our samples after deposition is 550°C. If N_d is the carrier concentration in the neutral region (proportional to the density of donor sites), the effective free carrier concentration N_a (which can be measured by Hall effect) is lower than N_d since some carriers can be trapped by oxygen intergrain states. The ratio of the width of the depleted region to the grain length is x. Conduction across the boundary layer occurs by thermionic emission [7] and Fermi-Dirac statistics must be considered. The actual resistivity becomes the weighted sum of two contributions, $\rho = (1 - x) \cdot \rho_{\text{bulk}} + x \cdot \rho_b$, where ρ_{bulk} characterizes the resistivity of the neutral region, and the contribution due to polar optical scattering and ionized impurity scattering are taken into account [8]; ρ_b is the resistivity due to grain boundaries. The adjusting parameter is the experimental resistivity and we obtain N_a and x for each temperature or wavelength of irradiation light.

We have used data of the resistivity as a function of temperature (which was reproduced in the inset of Fig. 1) and results are shown in Figure 1. As we can observe, N_a is slightly lower than N_d for all situations shown. In Figure 1 there is a tendency for the free electron concentration to decrease

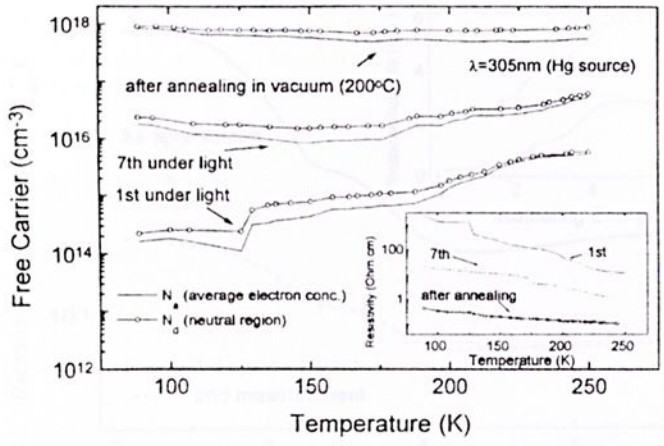


FIGURE 1 Calculated free carrier concentration, N_a, and carrier concentration in the neutral region, N_d, for Sb-doped (2at%) SnO_2 thin film. Inset – experimental data obtained under steady illumination with $\lambda = 305$ nm monochromatic light (1st and 7th cycle of consecutive resistivity measurement with decreasing temperature to 77 K, and after annealing in vacuum to 200°C).

until about 150°C, where it seems to saturate. Then the increase in resistivity (inset) would come from a decrease in mobility. Below 150°C, ionized impurities can not be neglected, and we must recall the high doping level (2at% Sb) and the possibility of oxygen vacancies inside the crystallite. Light excitation may actually ionize more defects at low temperature, a typical behavior of defect dominated semiconductor samples. The obtained fraction of trapped charge varies in the range 0.1 to 0.5, indicating that although the crystallites are quite small, they are not completely depleted

Figure 2 shows calculated values of the fraction of trapped charge at a grain boundary for the experimental results shown in the inset of Figure 2. After sample annealing in air to 200°C the photoconductivity is as shown by the full line (lower curve). Keeping the sample in vacuum, a new measurement is carried out 15 min after the first. The current magnitude increases since oxygen concentration is decreased by photodesorption in the first measurement [6]. Variation of conductivity comes from combined free carrier variation plus formation of space charge layers with concomitant potential barrier at the grain boundary [4]. In Figure 2 the higher the photoconductivity, the lower the amount of trapped carriers at the grain boundary, when the irradiating light goes from lower to higher energy. When the conductivity is increased the amount of trapped charge at the de-

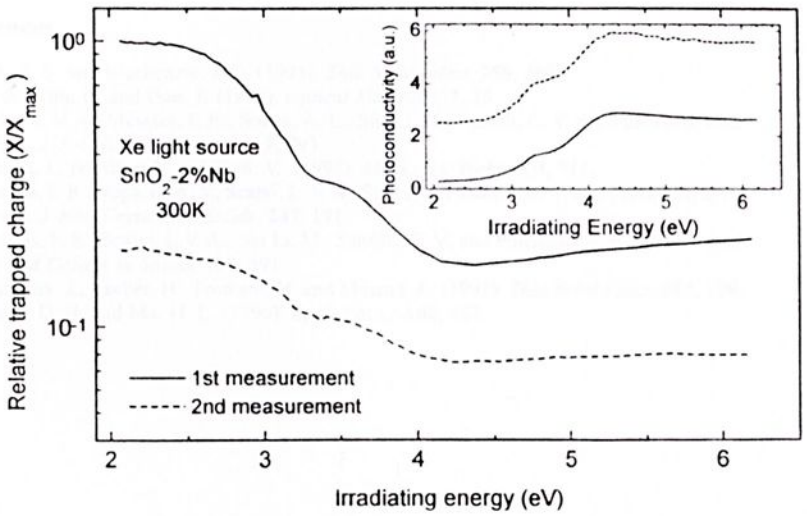


FIGURE 2 Relative fraction of trapped charge (x/x_{max}) for a SnO_2 2at%Nb film at 300 K, calculated from photoconductivity data, which are obtained after annealing in air to 200°C. 1st and 2nd measurement are separated by 15 min. Experimental data are shown in the inset.

T. 1362

pletion layer decreases. Although we use arbitrary units, our calculation always yields $X_{max} \cong 0.50$ which means a of wide depletion layer, but also that bulk scattering can not be neglected.

3. CONCLUSION

Temperature dependent and spectral photoconductivity lead us to conclude that the oxygen content of SnO_2 thin films determine their electric and electro-optical properties. We analyze the electron scattering in SnO_2 films where oxygen adsorption at grain boundary is the main mechanism. Some refinement is being done and the conclusion about oxygen participation will be published soon.

Acknowledgments

The authors would like to thank agencies: FAPESP, CNPq, CAPES and PRONEX.

References

[1] Park, S. S. and Mackenzie, J. D. (1995). *Thin Solid Films*, **258**, 268.
[2] Yu, B., Zhu, C. and Gan, F. (1997). *Optical Materials*, **7**, 15.
[3] Scalvi, L.V. A., Messias, F. R., Souza, A. E., Siu Li, M., Santilli, C. V. and Pulcinelli, S.H. (1998). *J. Sol-Gel Sci. Technol.*, **13**, 793.
[4] Watson, J., Ikomura, K.and G. S. V. (1993). *Meas. Sci. Technol*, **4**, 711.
[5] Messias, F. R., Vega, B. A. V., Scalvi, L. V. A., Siu Li, M., Santilli, C. V. and Pulcinelli, S. H. (1999). *J. Non Crystalline Solids*, **247**, 171.
[6] Messias, F. R., Scalvi, L.V. A., Siu Li, M., Santilli, C. V., and Pulcinelli, S. H. (1999). *Rad. Eff. and Defects in Solids*, **150**, 391.
[7] Bruneaux, J., Cachet, H., Froment, H. and Messad, A. (1991). *Thin Solid Films*, **197**, 129.
[8] Zhang, D. H. and Ma, H. L. (1996). *Appl. Phys.*, **A62**, 487.

Capítulo III

Pesquisas Atuais e a Proposta de Continuidade

O foco da atenção atual é o dióxido de estanho na forma de filmes finos depositados via- sol-gel. Estão sendo utilizados dois tipos de dopantes:

a) dopantes com intenção de melhorar a condutividade de SnO_2, principalmente Sb

b) dopantes terras-raras, principalmente Er e também temos utilizado codopagem com Yb, com objetivo de aumentar a eficiência da luminescência de Er. A meta aqui é combinar propriedades luminescentes dos íons terras-raras na matriz altamente transparente de SnO_2.

Em linhas gerais a proposta de investigação de SnO_2 é parte de um projeto financiado pela FAPESP e cujo plano consiste de 4 etapas:

1. Caracterização de filmes finos de SnO_2 com diferentes dopagens de Sb (ou Nb). Medidas de resistividade e corrente-voltagem em função da temperatura. Avaliação da influência de luz monocromática advindas de uma fonte de deutério e também de um laser de Nd:YAG acoplado com duplo cristal dobrador que possibilite e obtenção do quarto harmônico (266nm)
2. Investigação do comportamento eletro-ótico em função da temperatura. Medidas de fotocondutividade, absorção óptica e decaimento da condutividade fotoinduzida, principalmente na faixa 10-70K.

3. Cálculo dos mecanismos de espalhamento de elétrons e modelamento dos processos que determinam a condutividade eletrônica
4. Tratamento térmico dos filmes em diversas atmosferas (O_2, N_2, Ar) e diferentes pressões, e investigação do comportamento elétro-óptico a baixa temperatura.

Além disso possuo uma bolsa de Produtividade em Pesquisa do CNPq (nível IIB) em cujo plano de trabalho, além da pesquisa com SnO_2, está proposta também a investigação de GaAs dopado com terras-raras obtido por evaporação resistiva. Este trabalho ainda não deu resultados que mereçam destaque, talvez devido à dificuldade de se incorporar o terra-rara, Er particularmente, por este método de deposição, e também devido à volatilidade do As. Dois alunos de Iniciação Científica já foram envolvidos neste projeto. Um destes trabalhos está em andamento e no outro, já concluído e com bolsa financiada pela FAPESP, o aluno (Evandro A Morais) aproveitou a experiência adquiria com os terras-raras, e fez sua dissertação de mestrado sob o tema "SnO_2 dopado com Er", defendida e aprovada em 31/07/2002. Nossa motivação neste trabalho é de conseguir filmes de GaAs dopados com Er (e/ou Yb) por um método mais simples, ou seja, pela evaporação do semicondutor e do dopante terra-rara. Com a obtenção destas amostras de forma mais econômica, pode-se estudar a eficiência da luminescência das amostras produzidas desta forma, pela existência de bandas devido ao GaAs e às transições do Er (e/ou Yb) na matriz semicondutora, efetuando medidas de fotoluminescência. Além disso a proposta é investigar, através de medidas de fotocondutividade em diferentes temperaturas, como os níveis profundos baseados em complexos de Er (e/ou Yb) e aqueles advindos da matriz interferem nos processos de transporte e nas transições radiativas destas amostras.

Na sequência do texto, são dados maiores detalhes sobre o andamento do trabalho com SnO_2, que é a linha principal de pesquisa.

III.1 SnO_2 DOPADO COM Sb

A figura III.1 mostra a transmitância óptica no infravermelho de filmes preparados por dois procedimentos diferentes. Em ambos os casos os filmes possuem 30 depósitos, porém no caso do procedimento I (PI) após cada depósito, feito à temperatura ambiente, os

filmes são mantidos em ar por 20 minutos e então secados a 50°C por 30 minutos. Já no procedimento II (PII) entre cada depósito, o filme é calcinado a 400°C por 10 minutos. Nas duas situações, ao final dos 30 depósitos, o filme é submetido a um tratamento térmico a 500°C. A figura III.1 (principal) mostra a transmitância no infravermelho no intervalo 2,4-5,4 μm para amostras obtidas pelo procedimento PII, enquanto que o detalhe da figura III.1 mostra a transmitância no infravermelho no intervalo 1,8-5,4 μm para filmes PI. Nos dois casos a transmitância diminui conforme a concentração de Sb aumenta.

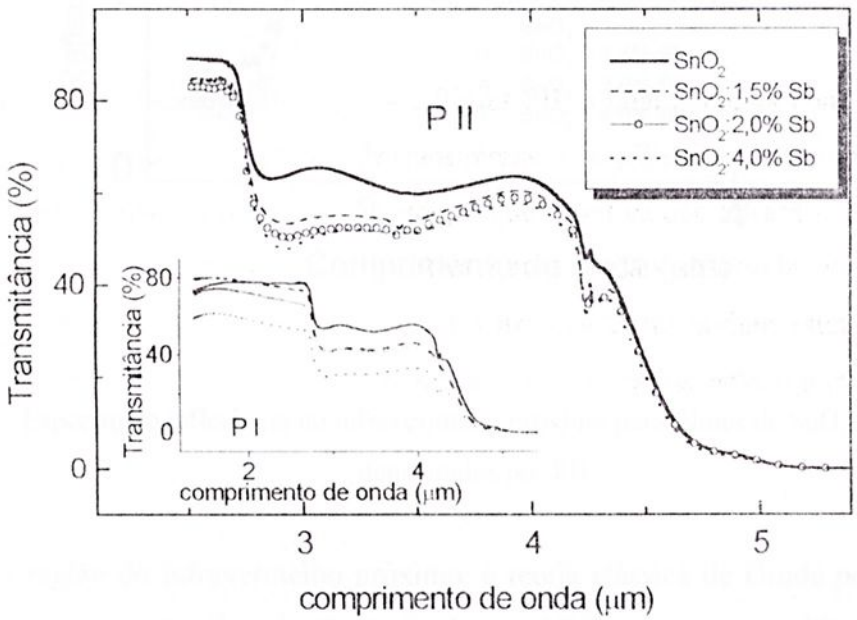


Fig. III.1 – Espectro de transmitância no infravermelho próximo de filmes finos de SnO_2 depositado por PII com várias composições do dopante Sb. Detalhe - Espectro de transmitância no infravermelho próximo de filmes depositados por PI.

A figura III.2 mostra reflexão para filmes PII, a qual aumenta com a concentração de Sb, em bom acordo com os dados de transmitância. Regiões de transmitância mais baixa coincidem com os máximos de refletividade, o que significa que a fração refletida do feixe incidente é provavelmente mais significativa que a fração absorvida no infravermelho. Pequenas bandas observadas em trono de 3,4 μm e 4,2 μm podem estar relacionadas a grupos hidroxila [11, 21] que não são completamente eliminados pelo tratamento térmico a

500°C. Grupos hidroxila começam a ser eliminados a 250°C mas não são completamente dessorvidos a 500°C [13].

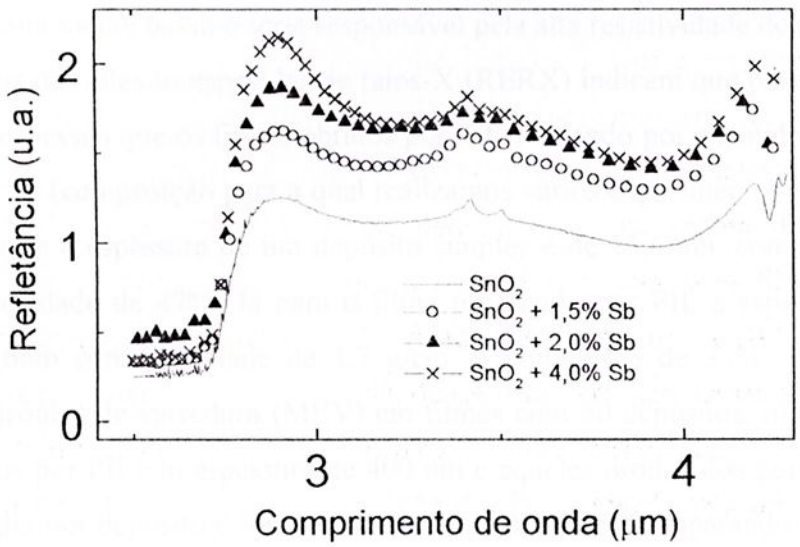


Fig. III.2 – Espectro de refletância no infravermelho próximo para filmes de SnO_2 dopados com Sb, depositados por PII

Na região do infravermelho próximo, a teoria clássica de Drude pode ser aplicada quando a concentração de portadores é alta o suficiente para permitir o fenômeno de ressonância de plasma. Então a reflexão na região do infravermelho aumentaria com a concentração de Sb. Para se descrever a reflexão na região do infravermelho usando a teoria de Drude, uma concentração de elétrons livres da ordem de 10^{20} cm^{-3} seria necessário[14,5]. Uma estimativa da freqüência de plasma para estes filmes mostra que o intervalo medido da transmitância e refletividade das figuras III.1 e III.2 estão acima deste valor, pois uma estimativa da concentração de elétrons livres em nossas amostras a partir de dados de resistividade forneceram valores de até $5x10^{18}$ cm^{-3}. A diminuição na transmitância com aumento da concentração de Sb observada nos filmes sugere que os filmes podem realmente ter uma alta concentração de elétrons livres na região neutra, mas possuem também um forte espalhamento no contorno de grão, o que implica numa baixa mobilidade. Os filmes usados nessas medidas possuem grão pequenos (3-10nm) e alta

resistividade. Então existe uma grande quantidade de cristalitos concomitante com barreiras de potencial no contorno de grão, que está relacionada a uma região larga de depleção no contorno de grão. Além disso a presença de poros deve ser levada em conta, pois diminui o livre caminho médio dos elétrons. Portanto a mobilidade dos elétrons, nestes filmes obtidos via sol-gel, é incomumente baixa e seria responsável pela alta resistividade dos filmes.

Resultados de reflexão especular de raios-X (RERX) indicam que os filmes obtidos por PI são mais espessos que os filmes obtidos por PII. Tomando por exemplo um filme de SnO_2 com 1,5% Sb (composição para a qual realizamos vários experimentos) resultados de RERX indicam que a espessura de um depósito simples é de 15,6 nm, com densidade de 3,6 g/cm^3 e porosidade de 47%. Já para o filme produzido por PII, a espessura de uma camada é de 6,6nm com densidade de 4,7 g/cm^3 e porosidade de 33%. Resultados de microscopia eletrônica de varredura (MEV) em filmes com 50 depósitos, mostram que os filmes produzidos por PII tem espessura de 400 nm e aqueles produzidos por PII, 300 nm. A espessura média por depósito é 8nm para PI e 6 nm para PII. Comparando resultados de RERX e MEV, observa-se uma melhor concordância para PII do que para PI, o que sugere que ao se usar o procedimento II, as características de uma monocamada são essencialmente preservadas após múltiplos depósitos. Por outro lado, a espessura de cada depósito sucessivo preparado por PI diminui conforme o número de imersões aumenta. Este efeito pode estar relacionado a uma maior porosidade obtida com PI, o que deve estar ligado à existência de mais espaço vazio, que poderia ser facilmente cheio com a solução precursora, ou de um filme de pior consistência que poderia ser parcialmente removido durante a aplicação do depósito adjacente superior. Como uma conseqüência, temos uma estrutura não homogênea e transmitância óptica inferior no visível.

A figura III.3 mostra resultados de resistividade em função da temperatura para filmes de SnO_2 dopados com Sb, com 30 depósitos. Pode ser claramente observado que a dopagem com Sb aumenta a condutividade do tipo n, embora a resistividade ainda seja alta. É interessante mencionar que quando filmes de SnO_2 são submetidos a tratamentos térmicos em vácuo sua resistividade diminui. Um filme similar àquele da figura III.3 com 4% de Sb, quando submetido a um tratamento térmico em vácuo a 500°C apresenta resistividade de $9x10^{-3}$ ohm.m à temperatura ambiente (contra os $3x10^{-2}$ ohm.m do filme da

cm 1 2 3 4 5 6 7 unesp 1 12 13 14 15 16 17 18

figura III.3). Porém este não é um resultado permanente e a exposição ao ar faz com que a resistividade aumente.

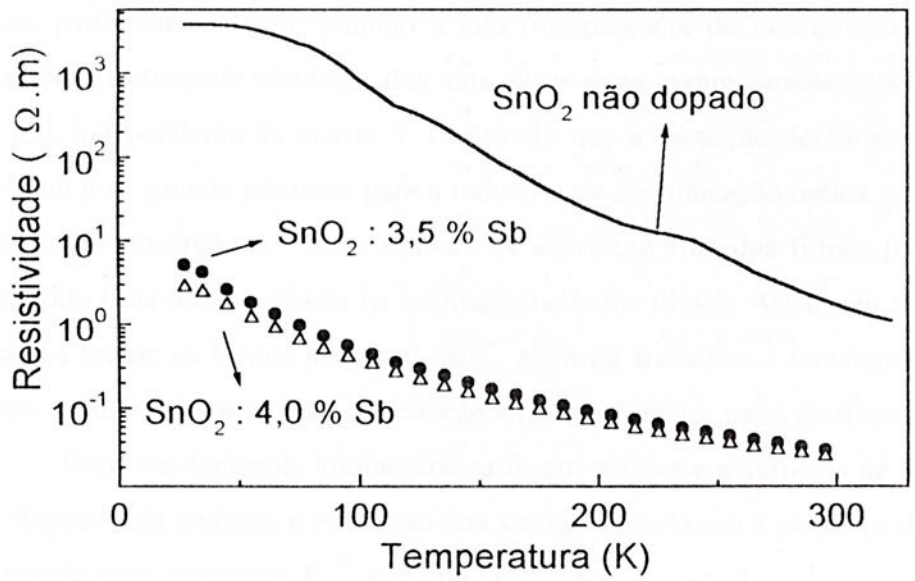


Fig. III.3 – Resistividade como função da temperatura para filmes finos de SnO_2 com 30 depósitos e diferentes composições de Sb.

Um gráfico de Arrhenius destas curvas fornece energias de ativação de 140 meV, 42 meV e 38 meV para o nível mais profundo (ionizado no intervalo de temperatura mais alto) de SnO_2 não dopado, dopado com 3,5%Sb e 4%Sb, respectivamente. Os valores mais baixos estão em boa concordância com o nível raso da dopagem com Sb e o mais profundo concorda com vacâncias de oxigênio [6]. No entanto neste nível tão alto de dopagem, o semicondutor deveria ser degenerado e nenhuma variação com a temperatura deveria ser observada, além de alta condutividade ser esperada. O comportamento observado sugere a existência de um outro nível de armadilhas, provavelmente relacionado à captura de elétrons no contorno de grão, que diminuiria a mobilidade e portanto, a condutividade. Os doadores. Sb que contribuem para a condutividade são localizados nos centros dos cristalitos, e seriam responsáveis pela reflexão no infravermelho, conforme já discutido.

III.2 – SnO_2 DOPADO COM Er

O objetivo principal aqui é a obtenção de filmes finos de SnO_2 dopado com terras-raras, particularmente Er, aliando a alta transparência da matriz semicondutora com as transições fortemente blindadas dos íons terras-raras, o que garante uma boa luminescência do íon, independente da matriz. É conhecido que a transição do Er em aproximadamente 1540nm é de grande interesse para a indústria de comunicação óptica, pois coincide com o mínimo de absorção de fibras ópticas. A espessura fina dos filmes produzidos não tem permitido uma boa eficiência na luminescência dos filmes. Assim um de nossos objetivos atuais é tornar os filmes mais espessos., além de trabalhar a montagem experimental de modo a conseguir que a luz de excitação atravesse a maior parte do filmes.

Bons resultados de luminescência foram obtidos em xerogéis de SnO_2 dopados com Er. Espetros de emissão e excitação nos xerogéis revelaram a presença de dois tipos de Er na matriz semicondutora: Er^{3+} substitucional a Sn^{4+} na estrutura do tipo cassiterita de SnO_2 e Er^{3+} segregado na superfície dos grãos. Medidas feitas em xerogéis codopados com Yb revelaram que o processo de transparência de energia de Yb^{3+} para Er^{3+} mostraram-se efetivos (ver cap. IV). Resultados de difração de raios-X nestes xerogéis mostraram que amostras com 4% de Er possuem menor tamanho de grão que amostras dopadas com 0,1% de Er, quando submetidas ao mesmo tratamento térmico. Isto indica que a presença de Er pode estar retardando o crescimento dos cristalitos no material [7].

Em filmes finos de SnO_2 dopados com Er, temos observado que a incorporação do terra-rara leva o filme a uma maior resistividade, o que aumenta com o aumento da concentração de Er. Isto pode ser uma evidência do caráter aceitador de Er e também da segregação para o contorno de grão, onde além de atuar como armadilha de elétrons, contribuiria também para um aumento na barreira de potencial e alargamento na região de depleção. Outra evidência do caráter aceitador do Er está nos resultados de decaimento da fotocondutividade, o que pode ser conferido na próxima seção.

III.3 – FOTOCONDUTIVIDADE PERSISTENTE EM SnO_2

Recentemente descobrimos um efeito que deve ser um dos temas centrais de investigação nos próximos meses: a existência de fotocondutividade persistente (PPC) a baixa temperatura. Apesar da origem do fenômeno ser totalmente diferente do que ocorre em $Al_xGa_{1-x}As$, os experimentos para se estudar os fenômenos de PPC nesta liga semicondutora foi o tema central de minha tese de doutorado, e então a descoberta do fenômeno em SnO_2 me chamou grande atenção.

A figura III.4 mostra o efeito de se iluminar um filme de SnO_2 não dopado com um laser de Nd:YAG pulsado, acoplado com 2 cristais dobradores (linha 266 nm), a baixa temperatura. A condutividade aumenta até 40 vezes sob esta excitação, até praticamente saturar. É interessante notar que quanto mais baixa a temperatura, maior o aumento na condutividade (diminuição da resistência). Isto está relacionado ao aumento da mobilidade devido ao espalhamento de elétrons no contorno de grão que é inversamente proporcional à temperatura. Quando a iluminação é removida, a condutividade permanece praticamente inalterada. A condutividade só volta a variar quando a temperatura é aumentada, porém só retorna ao seu valor original após algumas horas, se mantida à temperatura ambiente. Este retorno ao valor original de resistência descarta possíveis efeitos permanentes na estrutura, como aumento da cristalinidade devido ao aquecimento local pelo Laser. Para explicação deste efeito de PPC em SnO_2 temos que relembrar as equações II.1 a II.3 (ver capítulo II). Estas três equações acontecem simultaneamente, no entanto a reação II.2 tem probabilidade menor de ocorrer pois o sistema está imerso em vácuo (10^{-5} Torr) e a quantidade disponível de O_2 é diminuída. Como conseqüência geral, têm-se um aumento na quantidade de elétrons livres e então da condutividade do filme. Como o oxigênio liberado pela reação II.3 é continuamente eliminado pela bomba de vácuo, a remoção da iluminação não possibilita o retorno à condição inicial e então origina o fenômeno de PPC.

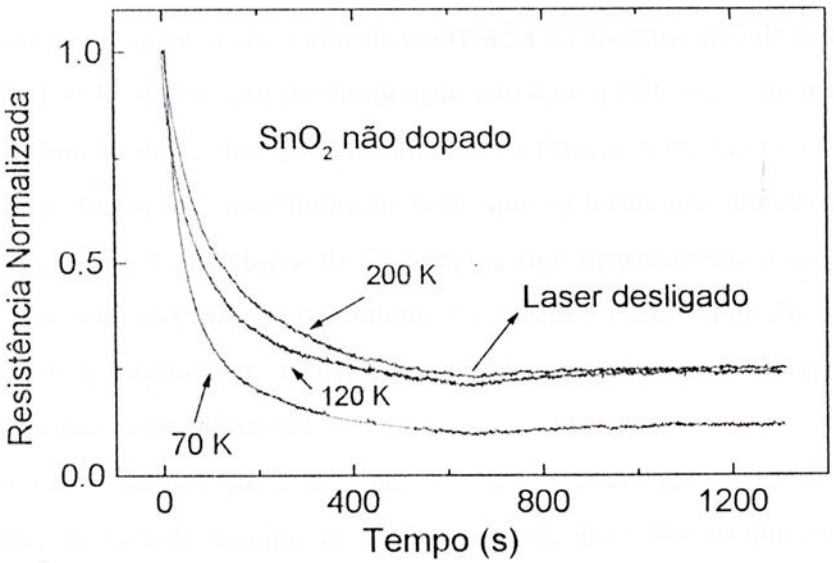


Fig. III.4 – Medida de resistência de uma amostra de SnO_2 não-dopada, excitada com o quarto harmônico de um laser de Nd:YAG , em diferentes temperaturas.

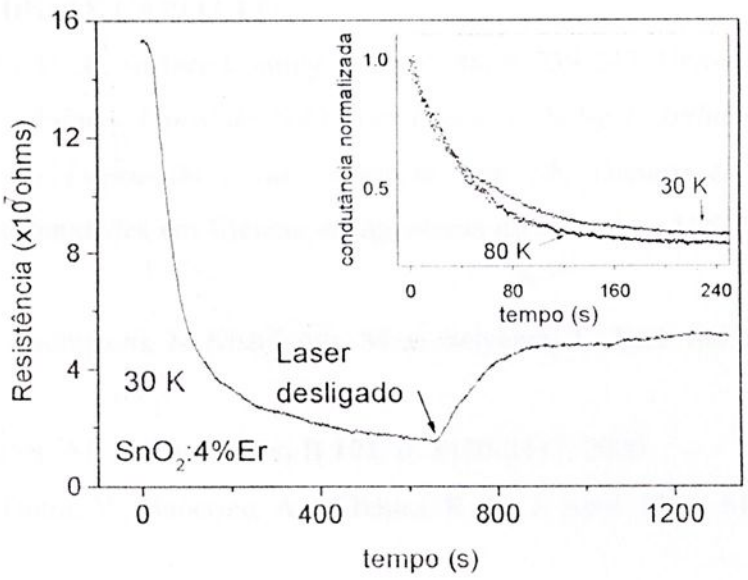


Fig. III.5 – Medida de resistência de uma amostra de SnO_2 dopada com 4% Er, excitada com o quarto harmônico de um laser de Nd:YAG, a 30 K. Detalhe – decaimento da condutividade fotoinduzida para duas temperaturas diferentes.

A figura III.5 mostra o mesmo tipo de experimento para uma amostra dopada com 4% de Er. É interessante notar o alto valor de resistência da amostra, devido à incorporação de Er. Abaixo de 100 K, a remoção da iluminação não leva a PPC mas sim a um aumento da resistência em função do tempo. Este decaimento da fotocondutividade é uma evidência do caráter aceitador do íon Er^{3+} nos filmes de SnO_2, que na forma não-dopada seria do tipo n, conforme já discutido. A introdução de Er aumenta significativamente a resistividade do filme, o que sugere uma alta taxa de recombinação. Assim a remoção da iluminação neste experimento induz à captura de elétrons. O detalhe da figura III.5 representa este decaimento em temperaturas diferentes.

Nos resultados obtidos até o presente, não foi possível identificar a dependência com a temperatura da taxa de decaimento da fotocondutividade. No detalhe da figura III.5, a mudança no comportamento da curva com a mudança de temperatura é muito pequeno. Continuamos a trabalhar nisso, pois estes resultados deverão fornecer informações importantes como a seção transversal de captura pelas armadilhas, com um procedimento similar ao realizado para $Al_xGa_{1-x}As$, no início da década de 90.

REFERÊNCIAS DESTE CAPÍTULO

[1] – Lin, Y.J. e Wu, C. S., Surface Coating Technol. **88**, p. 239-247, 1996

[2] – Geraldo, V., *Filmes Finos de SnO_2 via Processo Sol-gel: Influência de Alguns Parâmetros na Deposição e da Dopagem com Sb*, Dissertação de Mestrado, Programa Interunidades em Ciência e Engenharia de Materiais, U.S.P. – São Carlos, 2001

[3] - Yamazoe, N; Fuchigami, J.; Kishikawa, M. e Seiyama, T., Surf. Sci. **86**, p. 335-344, 1979

[4] – Nutz, T. e Haase, M. J. Phys. Chem B **104**, p. 8430-8437, 2000

[5] – Shanthi, E.; Dutta, V.; Banerjee, A e Chopra, K. L., J. Appl. Phys. **51 (12)**, p. 6243-6251, 1980

[6] – Jarzebski, J.M. e Marton, J. P., J. Electrochem. Soc. **123**, p. 299C-310C, 1976

[7] – Morais, E. A., *Incorporação de Er em SnO_2 obtido via Sol-gel: uma Análise de Xerogéis e Filmes Finos,* Dissertação de Mestrado, Programa Interunidades em Ciência e Engenharia de Materiais, U.S.P. – São Carlos, 2002

Capítulo IV

Outras Contribuições

Neste capítulo anexei algumas contribuições científicas que considero relevantes, produzidas a partir de 1993, e que estão relacionadas ao tema de investigação abordado neste trabalho. Porém não falam diretamente da investigação de defeitos em $Al_xGa_{1-x}As$, ou da caracterização de filmes finos de SnO_2 obtido via sol-gel.

IV.1 - ARTIGOS SELECIONADOS PUBLICADOS (anexados na sequência)

IV.1.1 – Degani, M. H e **Scalvi, L. V. A**, *Subbband Mixing Inducing Negative Resistance*, Solid State Comm. **86** (5), p. 301-304, 1993

IV.1.2 – **Scalvi, L.V. A.;** e Degani, M. H. *Substituitional Donor Related States and Au/Ge/Ni Contacts to $Al_xGa_{1-x}As$*, Phil. Magazine B **68** (5), p. 727-735, 1993

IV.1.3 – Scalvi, R. M. F.; Siu Li, M.; Ruggiero L. O e **Scalvi, L.V. A.,** *Light Induced Electric Dipole Relaxation in Synthetic and Natural Alexandrite*, Rad. Eff. & Def. Solids **156**, p. 295-299, 2001

IV.1.4 – Morais, E. A.; Ribeiro, S. J. L.; **Scalvi, L V A**; Santilli, C. V.; Ruggiero, L. O; Pulcinelli, S. H. e Messaddeq, Y., *Optical Characteristics of Er^{3+}-Yb^{3+} doped SnO_2 xerogels*, J. Alloys and Compounds (2002) (no prelo)

IV.1.5 – Gonçalves, R. R.; Ferrari, M.; Chiasera, A; Montagna, M.; Morais, E. A; **Scalvi, L. V. A;** Santilli, C. V.; Messaddeq, Y. e Ribeiro, S. J. L., *Planar Waveguides based on Nanocrystaliine and Er^{3+} doped SnO_2*, J. Metastable and Nanocrystalline Mater. **14**, p. 107-110, 2002

Solid State Communications, Vol. 86, No. 5, pp.301-304, 1993.
Printed in Great Britain.

0038-1098/93$6.00+.00
Pergamon Press Ltd

SUBBAND MIXING INDUCING NEGATIVE RESISTANCE

Marcos H. Degani
Instituto de Física e Química de São Carlos
Departamento de Física e Ciência dos Materiais
Universidade de São Paulo – Caixa Postal 369
13560 – São Carlos, S. P. Brazil
and
Luis V. A. Scalvi
Departamento de Física -UNESP, Bauru, C.P. 473,
17033 - Bauru, SP, Brazil.

(Received November 20, 1992)

(Received in revised form 20 January 1993 by C.E.T. Gonçalves da Silva)

ABSTRACT

A new double channel field–effect structure based on δ–doping technology is proposed. Resonant tunneling between the channels is employed to control the transport along the interface plane. A realistic simulation is performed for several temperatures. We solve the Schrödinger and Poisson equations self-consistently and have found that a large peak–to–valley ratio in the current-voltage characteristic occurs at the whole range of temperature investigated. This effect indicates the potential application of this phenomenon for switching devices, where the transversal conductivity can be controlled due to the coupling between states belonging to different channels.

In the last few years, the improvement in crystal growth techniques such MBE, MOCVD, LPE has made it possible to build interesting semiconductor nanostructures where unusual phenomena have been revealed. The quantum–mechanical nature present in these systems has been evidenced and several experiments have demonstrated the universal conductance fluctuations, localization, quantized Hall effect, the Aharonov–Bohm effect, etc.

On the one hand, these nanostructures offer us the possibility to investigate the physics in real low dimensional systems and, on the other hand, they are very important technologically, since very fast devices and switchers can be built.

Several devices have been proposed to achieve negative differential resistence (NDR). Ten years ago Sakaki[1] showed that NDR is achieved by velocity modulation in a quantum well. Kirchoefer et al.[2] have showed that in a quantum state device where tunneling of electrons takes place between localized states of distinct wells of high and low mobility, NDR can be present. Bigelow and Leburton[3] have proposed a modification of a modulation–doped heterostructure where the hybridization of the wave functions shows a new tunneling mechanism and they have proved the existence of NDR. Recently Palevski et al.[4] have demonstrated a new resistence resonance effect which is based on the quantum–mechanical delocalization of electrons in a symmetric–double–well potential.

We propose in this paper a new double channel field–effect structure which is based on δ–doping technology and exhibits negative resistance even at room temperature. Our results indicate the potential application of this new device as a fast switcher. The structure has aluminum gallium arsenide (AlGaAs) with a δ–doped layer grown on top of gallium arsenide (GaAs). This makes a double well confining potential as shown in Fig. 1. The electronic population of these two channels is controlled by the gate voltage (V_g). The channel which is localized in the AlGaAs layer is characterized by a low mobility and the other one localized at the GaAs–AlGaAs interface has high mobility. This mobility difference makes it possible, just by changing the gate voltage, to control the current between source and drain. When the energy separation between the first two levels is large the wave functions will remain localized to their wells of origin (see Fig. 1(a)). In this regime the ground state subband is not coupled to the first excited subband and the system behaves as two independent conducting channels and has a high effective mobility. However, just changing the value of V_g we can modify the confining potential such that the interaction between the two first levels becomes strong and a mixing of these two subbands occurs. As can be seen in Fig. 1(b), there is a well defined value of V_g where the subband mixing is maximum and consequently the effective mobility will be minimum. In this regime, both states are extended and belong to both channels. Using this effect, negative resistance is achieved even at room temperature.

The system we have simulated consists of 350Å of AlGaAs with 30% of aluminum grown on top of an unintentional *p* doped GaAs. A δ–doped layer is grown

unesp

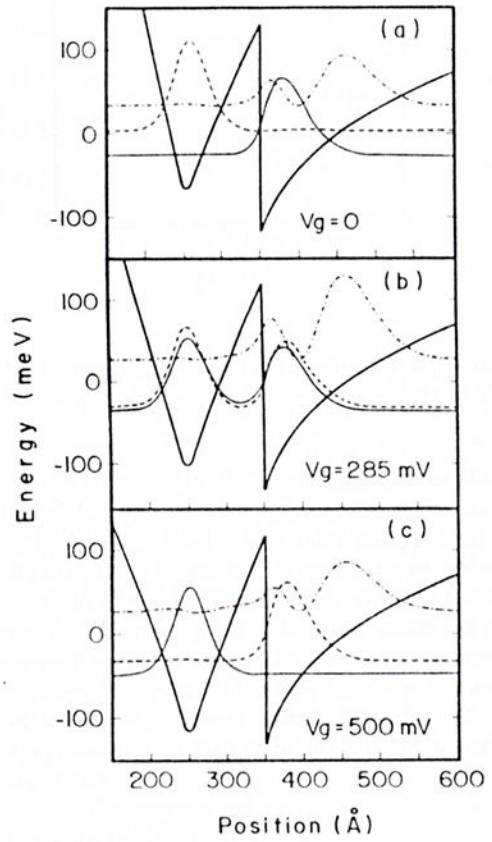


Figure 1 – Conduction–band–edge energy and probability density of the three lowest sublevels as a function of position for different values of the applied gate voltage V_g at room temperature. The wave functions are superimposed on the energies of the corresponding sublevels. Energy is referenced at zero for the Fermi energy.

inside AlGaAs 100Å from the GaAs interface. The donor concentration was kept constant and equal to $5x10^{12}$ cm^{-2} and the residual acceptor concentration in GaAs was taken equal to $5x10^{15}$ cm^{-3}. Since there is no ideal δ–doping monolayer due to diffusion of the donors, we have assumed that donors are uniformly distributed in a sheet 20Å wide. In this case, the ionized impurities are spatially separated from the two–dimensional electron gas at GaAs channel and thus, the electronic mobility of this channel is enhanced. In order to analyze the conduction–band–edge profile and the wave functions, the Schrödinger and Poisson equations were solved self–consistently employing a method which will be described elsewhere.[5-6] It is important to emphasize that the potential as well as the wave functions were discretized on a non–uniform grid points such that a large system could be simulated in order to appropriately describe the depletion layer.

Figure 1(a) shows the conduction–band–edge and the probability density of the lowest three sublevels for zero gate voltage and T=300K. For this value of V_g the ground state subband is totally localized inside GaAs and the first excited subband is localized inside AlGaAs. Because there is no mixing between these states the system behaves as two independently conducting channels and the current between source and drain is governed by the channel inside GaAs due to the mobility difference between both channels. The contribution of the third subband, which is totally localized inside the GaAs channel, to the current is practically insignificant because its population is low, but as we will see, it plays an important role at the resonance condition. At this moment, it is important to point out that the electric field applied between source and drain must be low in order to avoid heating effects and the appearence of the real space transfer mechanism as has been described by Bigelow and Leburton.[3]

When the gate voltage is equal to 285 mV at room temperature, the two lowest subbands reach the maximum mixing. This is shown in Fig. 1(b) where the conduction–band–edge and probability density of the lowest three sublevels are plotted as a function of the distance. Figure 1(c) shows the three lowest sublevels and the potential profile for V_g=500 mV. At this value of gate voltage the two lowest sublevels are not coupled. The comportment of the lowest three sublevels as a function of V_g is shown in Fig. 2. As it can be seen, initially for Vg=0 the two lowest subbands are very separated in energy and there is practically no interaction between these levels. The channels are independent for low values of V_g, however increasing its magnitude, these states become very close in energy so that a mixing takes place and the system behaves as a single channel because the main electronic density populates these two levels. For large values of V_g these two sublevels separate again. Also, we have plotted in Fig. 2 the probabilities of finding the ground state subband localized in the GaAs channel and the first excited state localized in the AlGaAs δ–doping channel. This plot shows that these probabilities are not complementary and this happens because the effective potential is not symmetric. From this figure it can be observed an inversion of the electronic population for values of V_g bigger than the critical value 285 mV where the maximum

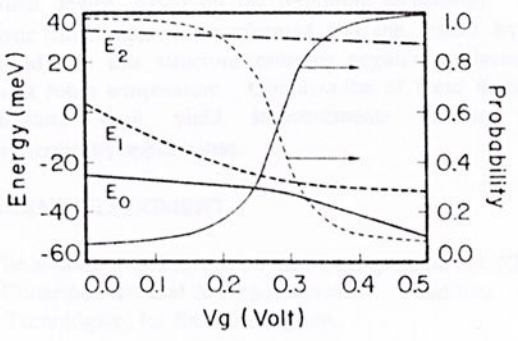


Figure 2 – Energy of the three lowest sublevels as a function of applied gate voltage V_g. (left side scale),and occupation probabilities of the two lowest sublevels at room temperature (right side scale).

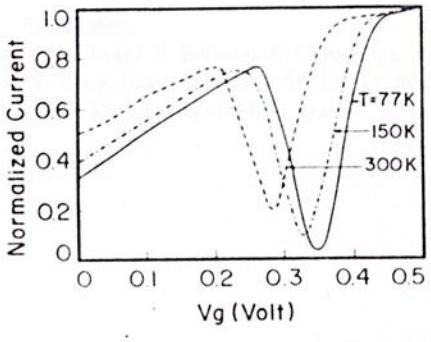


Figure 3 – Normalized source to drain current as a function of the applied gate voltage V_g for different values of the temperature.

mixing comes about. Now the ground–state is localized inside the AlGaAs channel and the first–excited state is localized in GaAs channel. The third energy level is practically insensitive to the variation of the gate voltage and remains localized inside the GaAs channel for the whole range of V_g investigated. The effect which has just been described above is not based on real space transfer of charge between the two wells but it is based on the wave nature of the electronic states which, depending of the value of V_g, extend into both wells probing the transport properties of both.

The longitudinal current in our model is derived from the following expression

$$J = e\,[(n_1\mu_1 + n_2\mu_2)(1 - \theta) + \theta(n_1 + n_2)\,\mu_{12} + n_3\mu_1]E, \quad (1)$$

where e is the electron charge, n_1, n_2, and n_3 are the electronic densities of the ground state, first and second excited states, respectively. μ_1 is the mobility of the GaAs channel and μ_2 the mobility of the AlGaAs channel. The effective mobility μ_{12} is given by

$$\mu_{12}^{-1} = \mu_1^{-1} + \mu_2^{-1}, \quad (2)$$

E is the longitudinal electric field, and θ is a function which describes the mixing amount of the two lowest sublevels and is defined as

$$\theta = 2\{1 + \exp[(|\Delta E| - E_{12})/\Gamma]\}^{-1} \quad (3)$$

where E_{12} is the energy difference between ground-state and first excited state at the resonance where the maximum mixing happens, ΔE is the energy difference between ground-state and first excited state. This function interpolates two different regimes. When electrons are localized in independent channels, θ tends to zero and the resistance can be determined using the classical rule for parallel configuration. On the contrary, the electrons are shared by both wells at resonance (θ = 1) and the effective mobility should approach that of the well with poor mobility. Γ is a parameter which was taken equal to 1 meV.

In order to substantiate the importance of this effect we have chosen μ_1=8000 cm²/V.s at room temperature, μ_1=40000 cm²/V.s at T=150K, and μ_1=180000 cm²/V.s at T=77K. μ_2 was kept constant and equal to 300 cm²/V.s at T=300K and 77K and taking equal to 430 cm²/V.s at 150K. These values were evaluated considering several scattering mechanisms in $Al_xGa_{1-x}As$ as given by Saxena and Mudares.[7] The longitudinal electric field used in this experiment must be small to prevent heating effects. In Fig. 3 we have plotted the normalized source-drain current as a function of the gate voltage for three different temperatures 300K, 150K and 77K. For low values of the gate voltage the current increases linearly as a function of V_g, in this range of V_g the two lowest sublevels are not coupled and the system responds as two parallel channels. Continuing the enhancement of V_g the current reaches a maximum and then drops abruptly indicating that the interaction between these sublevels has been significant. The current decreases as function of V_g until it reaches a minimum value exactly when the mixing between the ground state and the first excited state is maximum. At this point the contribution to the current due to the third sublevel becomes very important since the wave function of this level is completely localized at the high mobility channel. For higher values of V_g the two sublevels decouple and the system responds as two parallel channels again (see Fig. 1). This I-V characteristic presents a sharp transition in a short range of the gate voltage so that the peak to valley ratio is around 60% at room temperature. This effect is stronger at low temperatures. A peak to valley ratio of 75% can be reached at 77K. This feature can be used to design and model fast switchers. When the temperature is increased it is observed that the value of the gate voltage, where the minimum current turns out, has a lower value as well as the peak to valley ratio also decreases, but the effect remains very significant for the whole range of temperature.

In conclusion, we have found a quantum mechanical effect which can be used to design a new–three terminal device, based on the δ–doping technology. A realistic simulation was performed and the results have revealed that this structure presents negative resistance even at room temperature. Optimization of these device parameters shall yield improvements leading to high–frequency applications.

ACKNOWLEDGMENT

The authors would like to express their gratitute to CNPq (Conselho Nacional de Desenvolvimento Científico e Tecnológico) for financial support.

REFERENCES

1. H. Sakaki, Jpn. J. Appl. Phys. **21**, L381 (1982).
2. S. W. Kirchoefer, R. Magno & J. Comas, Appl. Phys. Lett. **44**, 1054 (1984).
3. J. M. Bigelow & J. P. Leburton, Appl. Phys. Lett. **57**,

795 (1990).
4. A. Palevski, F. Beltram, F. Capasso, L. N. Pfeiffer & K. W. West, Phys. Rev. Lett. **65**, 1929 (1990).
5. M. H. Degani, Appl. Phys. Lett.**59**, 57 (1991); Phys. Rev. B**44**, 5580 (1991).
6. M. H. Degani & L. V. A. Scalvi (unpublished).
7. A. K. Saxena & M. A. L. Mudares, J. Appl. Phys. **58**, 2795 (1985).

PHILOSOPHICAL MAGAZINE B, 1993, VOL. 68, NO. 5, 727–735

Substitutional donor related states and Au/Ge/Ni contacts to $Al_xGa_{1-x}As$

By LUIS V. A. SCALVI

Departamento de Física, UNESP – Bauru, C.P. 473, 17033 Bauru SP, Brazil

and MARCOS H. DEGANI

Departamento de Física e Ciência dos Materiais, Instituto de Física e Química de São Carlos-U.S.P.-Caixa Postal 369, 13560 São Carlos SP, Brazil

[*Received 26 January 1993 and accepted 1 July 1993*]

ABSTRACT

Current–voltage measurements performed on bulk $Al_xGa_{1-x}As$ equipped with Au/Ge/Ni contacts reveal surprising deviations from ohmic behaviour when the temperature is lowered to that of liquid nitrogen. Significant differences are observed between samples with $x=0{\cdot}3$ (direct band-gap material) and $x=0{\cdot}5$ (indirect band-gap material). The dominant states of the donor atoms Si (doping) or Ge are found to be responsible for such behaviour. Evidence for the existence of an effective-mass X-valley metastable state is also presented.

§1. INTRODUCTION

Recent years have seen rapid developing in semiconductor science and technology. Attempts to improve devices have required use of smaller and smaller dimensions. This has led to sophisticated proposals which invoke resonant tunnelling and multi-quantum-well interaction, just to name examples that have been employed to generate new mesoscopic devices. However, independent of scientific advances, there are technological issues which present barriers still to overcome. One of these is associated with the fabrication of reliable and reproducible contacts.

Au/Ge/Ni alloy has been widely used as an ohmic contact for n-type GaAs and $Al_xGa_{1-x}As$. Although there have been many recipes for obtaining ohmic contacts (Shih and Blum 1972, Kim and Chung 1981, Sharma 1981), the related physics is not fully understood. Furthermore, ohmic behaviour at room temperature does not assure that it will remain that way at low temperature. As the temperature decreases, the ohmic behaviour of the current–voltage curve often turns nonlinear which can affect experimental results. To explain the formation of ohmic contacts to GaAs it is generally accepted that a thin n^+ layer is produced near the interface (Popovic 1978, Yoder 1980), since Ge diffuses into the GaAs. Ge occupying a Ga site is a donor. The metallization is more efficient when Ge–Au is used in the eutectic composition (12 wt% Ge) (Kim and Chung 1981).

The metallurgy of the system Au/Ge/Ni on GaAs is very complex (Sharma 1981, Kuan, Batson, Jackson, Rupprecht and Wilkie 1983, Kim, Chung and Mahajan 1987a, b) and many workers have tried to relate the various compounds found in such an alloy, after annealing, with the ohmic behaviour. Although most papers believe in the Ge n^+ layer hypothesis, a decrease of barrier height to form the ohmic contact is a possibility which cannot be dismissed—see, for example, Waldrop and Grant (1987), who suggests the formation of a very thin metallic interfacial layer which is associated with a low barrier height.

0141-8637/93 $10·00 © 1993 Taylor & Francis Ltd.

Independently of how one explains ohmic contact formation, the compounds NiAs and Ni_2GeAs play a fundamental role as suggested by most papers. The solid-state reactions to form these compounds take place at about 220°C (Ball 1989). In the range of temperature normally employed for alloying (420–500°C), melting of the contact occurs, resulting in a lower specific contact resistance but also in poorer topography. Thus, the ideal ohmic contact should be obtained in an optimum time which balances the decreasing specific contact resistance with the quality of the topography. As described in this paper and elsewhere (Scalvi 1991), the longer the annealing time the lower the specific contact resistance. We believe that this is inconsistent with the hypothesis of barrier-height lowering and the results are interpreted on the basis of the formation of a Ge n^+ layer.

A few years ago, Chadi and Chang (1988, 1989) stated that every group IV substitutional donor in $Al_xGa_{1-x}As$ should become a *DX* centre capturing two electrons concomitant with a lattice distortion along a $\langle 111 \rangle$ direction and located at an interstitial site. Supposing that the Ge n^+ layer formation is indeed the correct hypothesis, one must be concerned about *DX* centre formation as the temperature is decreased. In the case of indirect-band-gap AlGaAs, besides the *DX* centre, the effective-mass *X*-valley state (Dmochowski, Dobaczewski, Langer and Jantsh 1989, Séguy, Zigone and Martinez 1992) can also trap electrons metastably and, depending on the range of temperature, may also play a fundamental role in electron recombination.

In this paper the supposed ohmic contact of the alloy Au/Ge/Ni to AlGaAs is discussed under the assumption of the existence of deep levels states in samples with direct and indirect bandgaps.

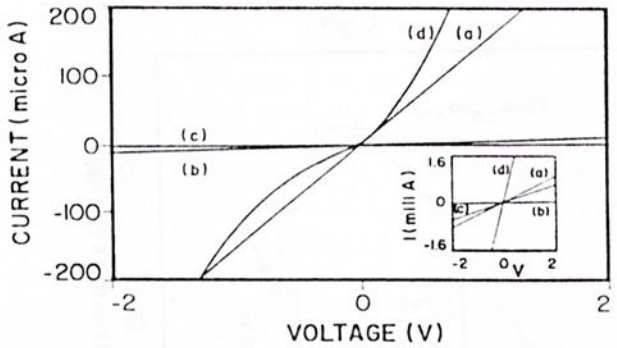
§2. Experimental

The samples used in this work were grown by molecular beam epitaxy on a semi-insulating GaAs substrate. The results reported here refer to Au/Ge/Ni contacts to a $Al_xGa_{1-x}As$ active layer. Care was taken to avoid the formation of a two-dimensional electron gas (2DEG) using the following structure: 0·25 μm of undoped Ga_xAs, 0·25 μm of a compositionally graded layer GaAs–$Al_xGa_{1-x}As$, an undoped 0·25 μm layer of Al_xGa_{1-x} and 1·75 μm of Si-doped $Al_xGa_{1-x}As$ (intentional doping with average value $\approx 8 \times 10^{17}$ cm^{-3}Si). Au and the eutectic Au–Ge (12 wt% Ge) were evaporated from Mo baskets and Ni from W baskets through a shadow mask in a VEECO evaporator under a pressure of 2×10^{-6} Torr. The final composition was 2·7 wt% Ni and 6·8 wt% Ge. Owing to difficulties in bonding a sample after each annealing, some samples were measured at room temperature and liquid-nitrogen temperature, whereas other samples were bonded using gold wires with the help of bonding pads (Ti, Au), and measured in the range 50–300 K using a closed-cycle helium Air Products cryostat. The current (*I*)–voltage (*V*) curves were measured with the help of a Hewlett Packard Semiconductor Parameter Analyser.

The reported results include a transient decay of persistent photoconductivity (TDPPC) measurement. TDPPC is a technique in which electrons trapped in impurity levels in the band-gap are excited to the conduction band by irradiating the sample with below band-gap light. The conductance increases until it reaches saturation. Then, the re-trapping of electrons by the mid-gap states is monitored by the decay of the conductance. More details concerning the TDPPC technique have been reported elsewhere (Dobson, Scalvi and Wager 1990).

cm 1 2 3 4 5 6 7 unesp 11 12 13 14 15 16 17 18

Fig. 1



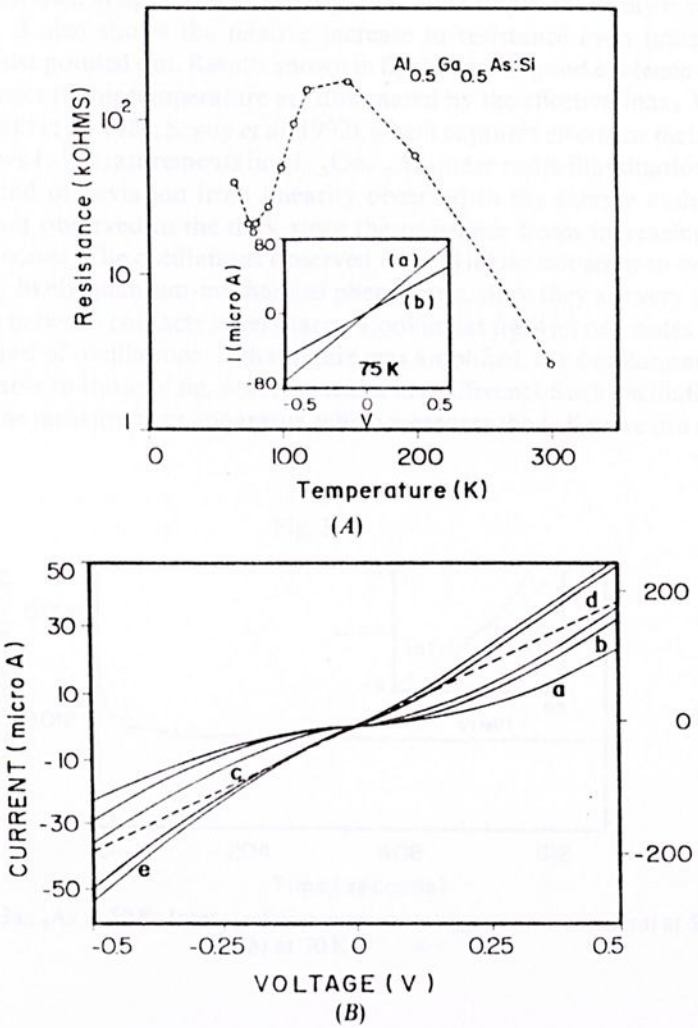
I–V curves for $Al_{0.3}Ga_{0.7}As$, annealing temperature 350 C; (*a*) room temperature; (*b*) 200 K; (*c*) 100 K; (*d*) 60 K. Inset: *I–V* curves for $Al_{0.3}Ga_{0.7}As$, annealing temperature 420°C; (*a*) room temperature; (*b*) 200 K; (*c*) 100 K; (*d*) 60 K.

§ 3. Current–voltage measurements

A sample of $Al_{0.3}Ga_{0.7}As$ was annealed at 350°C for 5 min and the current–voltage characteristics, measured under room illumination, are shown in fig. 1. The perfect straight curve at room temperature turns into a non-straight line when the temperature is lower than 100 K. When the same procedure is used for another sample of the same composition but with an annealing temperature of 420°C, the results are as shown in the inset in fig. 1. The line is perfectly straight over the whole range of temperature. At temperatures below ≈ 100 K the resistance becomes comparable with the resistance at room temperature. Lower temperatures lead to even lower resistances. The most probable hypothesis is that the structure first proposed by Chand *et al.* (1984), which was employed here to prevent 2DEG formation, is not as efficient as expected, and there may be an electron gas at some interface. In any case the deviation from the ideal ohmic behaviour (which is the issue treated in this paper) is not influenced by this problem. As can be seen from curve *d* of fig. 1, such a high conductance does not avoid the deviation from linearity.

Although the procedure does work fine for the sample with $x = 0{\cdot}3$, the same procedure does not lead to ohmic behaviour when it is employed on an indirect band-gap sample ($x = 0{\cdot}5$). Although a straight line is obtained at room temperature, when the temperature is low (in the range 70–100 K) the curve shape is similar to the one observed in curve *d* of fig. 1, the magnitude being one order lower than at room temperature, which shows that, at least in this case, the grown structure does avoid the 2DEG formation. Figure 2 (*A*) shows the variation in resistance of this sample under room illumination. When the temperature decreases, the resistance increases until it reaches a maximum at about 150 K; then it decreases to a minimum at about 78 K and increases again at lower temperature. The inset in fig 2 (*A*) represents an *I–V* plot for this sample at 75 K, when irradiated with a strong W light. The contact becomes perfectly ohmic and remains in that way 20 s after the illumination is removed. Shih and Blum (1972) obtained a minimum contact resistance for annealing temperatures within the range 480–540°C. Although their measurements were all realized at room temperature, the work suggests that it would be worth trying some annealing in this range of temperature for $Al_{0.5}Ga_{0.5}As$. Figure 2 (*B*) shows the evolution of the *I–V* plot at liquid-nitrogen temperature for a $Al_{0.5}Ga_{0.5}As$ sample after successive annealings at 480°C.

Fig. 2



(*A*) Resistance against temperature for $Al_{0.5}Ga_{0.5}As$ under room illumination. Inset: (*a*) the sample under strong illumination; (*b*) 20 s after the illumination is removed. (*B*) *I–V* curves at 77 K for $Al_{0.5}Ga_{0.5}As$ for successive annealing at 480°C; (*a*) 2 min; (*b*) 4 min; (*c*) 8 min; (*d*) 12 min; (*e*) 20 min. The broken line represents the room-temperature result and refers to the right-side scale.

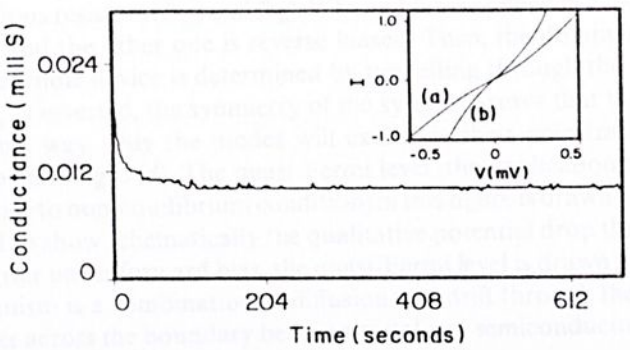
This temperature was chosen because it is within the range suggested by Shih and Blum (1972) and it is not too high to damage the sample surface. The sample was annealed for successive baking times of 2 min until a total of 8 min and then, for annealing times of 4 min, i.e. for a total time of 20 min. The *I–V* curve at room temperature remains unchanged (broken line in fig. 2(*B*)) and shows a fair improvement at liquid-nitrogen temperature, but it still remains not perfectly straight.

When a direct-band-gap sample is irradiated with light at 50 K, the conductance increases until it reaches saturation and remains in such a conductive state even after the illumination is removed. Although there is a decay in conductance, if the temperature is kept at 50 K, this decay is so slow that the return to the non-conductive

state will take an unmeasurably long time. TDPPC carried out for a $Al_{0.5}Ga_{0.5}As$ sample at 50 K is shown in fig. 3. Unlike the $Al_{0.3}Ga_{0.7}As$ sample, the decay is very fast. The inset in fig. 3 also shows the relative increase in resistance even under room illumination, as just pointed out. Results shown in fig. 3 provide good evidence that the transport properties in this temperature are dominated by the effective-mass X-valley state (Dmochowski *et al.* 1989, Séguy *et al.* 1992), which captures electrons metastably.

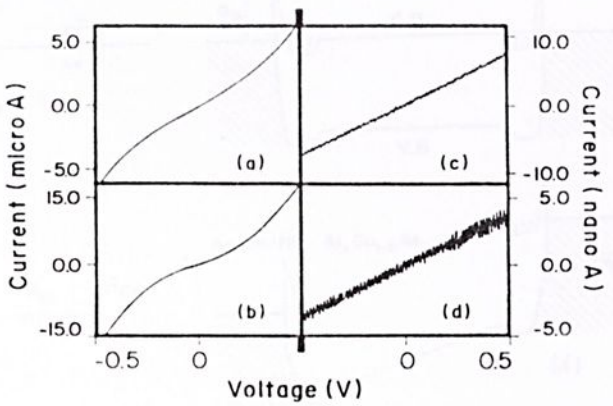
Figure 4 shows I–V measurements in $Al_{0.5}Ga_{0.5}As$ under room illumination and in the dark. The kind of deviation from linearity observed in the sample under room illumination is not observed in the dark since the resistance keeps increasing as the temperature decreases. The oscillations observed in fig. 4 (*d*) do not seem to be due to tunnelling or any likely quantum-mechanical phenomena, since they are very periodic and the distance between contacts is very large. Looking at fig. 4 (*c*) one notes that we have the same kind of oscillations. If that figure was amplified, the oscillations would become comparable to those of fig. 4 (*d*) (the scales are different). Such oscillations are associated with the measurement apparatus, which measures the I–V curve in a discrete

Fig. 3



TDPPC for $Al_{0.5}Ga_{0.5}As$ at 50 K. Inset—relative current–voltage measurement (*a*) at 50 K and (*b*) at 70 K.

Fig. 4



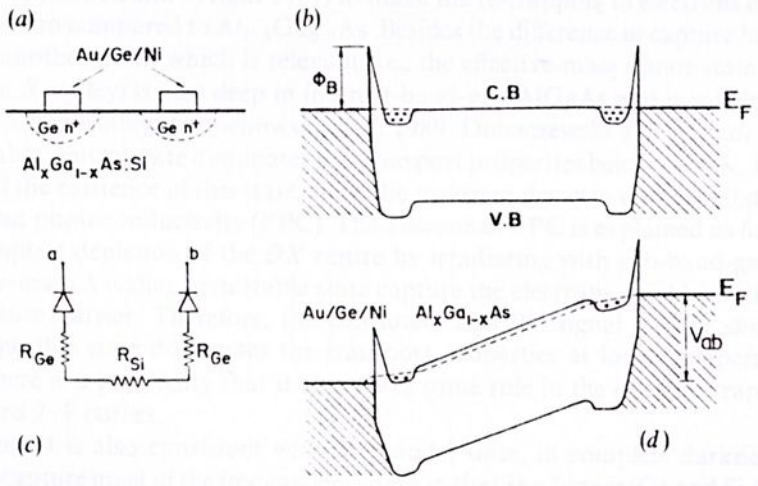
Current–voltage measurement for $Al_{0.5}Ga_{0.5}As$. (*a*) 110 K, room light; (*b*) 90 K, room light; (*c*) 110 K, dark; (*d*) 90 K, dark.

way, using steps of a few volts (the period seen in the figure). The resistance is about three orders of magnitude lower in the sample exposed to light than in the sample kept in the dark.

§4. A SIMPLE MODEL TO UNDERSTAND THE CURRENT–VOLTAGE CHARACTERISTICS

To explain why the I–V curve is no longer linear when the temperature is low, one should think of the symmetry of our problem. Figure 5 (*a*) shows a schematic diagram of the samples employed in this work. Supposing that the barrier height does not vary with annealing temperature and, thus, the formation of a thin Ge n^+ layer is actually the dominant mechanism, the metal–semiconductor interface can be drawn as in fig. 5 (*b*). The depletion region width is thin enough to allow electron tunnelling in both directions when a bias is applied across the device. When the temperature decreases, electrons are trapped by the substitutional donor states and the depletion region width becomes large enough to prevent tunnelling across the interface. In other words, in a simple way the system in open circuit can be represented by the schematic diagram shown in fig. 5 (*c*), where the two metal–semiconductor interfaces are bad diodes (due to the presence of room illumination) and the different regions of the semiconductor are represented as various resistors (R_{Ge} and R_{Si}). When a bias is applied in a a–b, one diode is forward biased and the other one is reverse biased. Then, the dominant transport process across the whole device is determined by tunnelling through the diode under reverse bias. If V_{ab} is inverted, the symmetry of the system assures that the device will behave in the same way, only the diodes will exchange their polarizations. This is schematically shown in fig. 5 (*d*). The quasi-Fermi level (the application of an electric field leads the device to non-equilibrium condition) in this figure is drawn only to assure its continuity and to show schematically the qualitative potential drop throughout the device. In the barrier under forward bias, the quasi-Fermi level is drawn assuming that the actual mechanism is a combination of diffusion and drift through the barrier plus the rate of transfer across the boundary between metal and semiconductor (Rhoderick

Fig. 5



Model to understand the I–V behaviour. (*a*) sample diagram, (*b*) energy diagram in real space with no applied bias, (*c*) simple electrical diagram for the device, (*d*) energy diagram with applied forward bias ($+V_{ab}$).

and Williams 1988). The actual shape of the quasi-Fermi level in the semiconductor under applied bias is not within the scope of this paper. In any case the quasi-Fermi level behaviour in the semiconductor does not lead to distinct conclusions according to our model, since the transport is dominated by the diode under reverse bias. If the diodes were ideal, there would be rectification on both directions, but the presence of light makes them bad (ideality factor different from unity (Tyagi 1984)) and then, curves like those shown in the previous § are observed, where the reverse characteristics of each diode is observed depending on the signal of the applied potential.

The fact that the increase in the annealing temperature improves the I–V characteristics as shown in fig. 1 is evidence that the amount of Ge accumulated in the n^+ layer is directly responsible for the observed behaviour. This is also in good agreement with the slow diffusion rate of Ge into GaAs as observed by Kavanagh and Magee (1987). A stronger evidence is seen in fig. 2, since annealing temperature and time are directly related to a fair improvement in the I–V curves. The decrease in the resistance with longer annealing times is also evidence that this arises from the contact itself, since the deterioration of the sample surface and the slight diffusion of Si doping to the next layer would increase the sample resistance.

It is well known that, as the temperature decreases, the DX centre concentration becomes higher in AlGaAs and there is carrier freeze-out. According to Chadi and Chang (1988, 1989) every group-IV substitutional donor in AlGaAs becomes a DX centre, trapping two electrons, concomitant with lattice distortion along a $\langle 111 \rangle$ direction, resulting in a negative effective-U interaction. If the measurement were to be carried out in the absence of light, it is expected that Ge and Si compete for the trapping of electrons, since at low temperatures and with no light on the sample, the DX centres are full of electrons whereas the conduction band is practically empty. However, the measurement is done under room illumination, which has a very wide spectrum of wavelengths. The photoionization energy has little dependence on alloy composition (Mooney 1990) and so this light should be able to excite electrons in the same way at any aluminium composition. However, the photoconductivity is a compromise between photoexcitation and thermal capture by the Ge and Si DX centres. In $Al_{0.5}Ga_{0.5}As$ the Si DX has the deepest depth in the forbidden gap, observed in AlGaAs alloys (Chand *et al.* 1984). Moreover the capture barrier is low enough (Mooney, Caswell and Wright 1987) to make the re-trapping of electrons easier in this composition compared to $Al_{0.3}Ga_{0.7}As$. Besides the difference in capture barrier, there is also another point which is relevant, i.e., the effective-mass donor state (associated with the X-valley) is also deep in indirect-band-gap AlGaAs and it is able to capture electrons metastably (Dmochowski *et al.* 1989, Dobaczewski and Kaczor 1991). This metastable neutral state dominates the transport properties below ≈ 60 K. Figure 3 is a proof of the existence of this state, since the transient decay is very fast and there is no persistent photoconductivity (PPC). The absence of PPC is explained as follows: after the complete depletion of the DX centre by irradiating with sub-band-gap light, the effective-mass X-valley metastable state capture the electrons quickly, as if there were no capture barrier. Therefore, the measured TDPPC signal is very short in time. Although this state dominates the transport properties at lower temperatures than 77 K, there is a possibility that it also plays some role in the electron trapping in the measured I–V curves.

Figure 4 is also consistent with this model since, in complete darkness, the DX centres capture most of the free carriers either in the Ge n^+ layer (Ge and Si DX centres) or in the bulk (Si DX centres). Then the 'active' layer behaves almost as an insulator,

decreasing drastically the conductance. Therefore the picture drawn in fig. 5 has to be abandoned, since a metal–highly doped semiconductor interface does not exist any more and, the whole device behaves as a highly resistive sample. In this case the specific contact resistance no longer matters.

§ 5. Conclusions

Supposing that the formation of a Ge n^+ layer is the actual mechanism which controls the contact in the system Au/Ge/Ni–$Al_xGa_{1-x}As$, we obtain clear evidence that the longer the annealing time the lower the specific contact resistance, since the sample resistance would never decrease in the range of annealing temperatures and times. A long annealing time only affects the sample surface quality, but does not deteriorate the contact quality.

By our data, it seems that the higher the aluminium fraction in the sample, the more difficult is the Ge diffusion. We believe that the alloying brings new types of difficulties to the Ge diffusion. These difficulties are unknown and will be the issue of a future work. The atomic size of the Al atom should not be a problem since it is comparable to the Ga atom.

A model to explain our data has been proposed and it is shown that either Ge from the n^+ layer, as well as the Si from the AlGaAs active layer, participate in the electron capture, as the temperature is lowered down and they become *DX* centres. Consequently the depletion layer width is varied and the contact behaves as a bad diode due to the presence of room illumination. Good evidence for the effective-mass *X*-valley metastable state proposed by other workers (Dmochowksi *et al.* 1989, Dobaczewski and Kaczor 1991, Séguy *et al.* 1992) has been found by TDPPC and *I–V* measurements at 50 K. Although such a state dominates the transport properties at lower temperatures, it may also play an important role in the capture at slightly higher temperatures (70–100 K). It could even act as an intermediate state for *DX* capture, which needs further investigation.

Acknowledgments

The sample growth and most of the measurements were carried out at the Advanced Materials Laboratory of Oregon State University. One of us (L. V. A. Scalvi) wishes to thank Professor John R. Arthur for his hospitality and for very useful discussions, and Leon Ungier for all the help with molecular beam epitaxy sample growth. We also acknowledge the Conselho Nacional de Desenvolvimento Cientifico e Tecnológico (CNPq) and Coordenadoria de Aperfeiçoamento de Pessoal de Ensino Superior (CAPES) for financial support.

References

Ball, R. K., 1989, *Thin Solid Films*, **176**, 55.
Chadi, D. J., and Chang, K. J., 1988, *Phys. Rev. Lett.*, **61**, 873; 1989, *Phys. Rev.* B, **39**, 10063.
Chand, N., Henderson, T., Klem, J., Ted Masselink, W., Fisher, R., Chang, Y. C., and Morkoç, H., 1984, *Phys. Rev.* B, **30**, 4481.
Dmochowski, P. M., Dodaczewski, L., Langer, J. M., and Jantsh, W., 1989, *Phys. Rev.* B, **40**, 9671.
Dobaczewski, L., and Kaczor, P., 1991, *Phys. Rev.* B, **44**, 8621.
Dobson, T. W., Scalvi, L. V. A., and Wager, J. F., 1990, *J. appl. Phys.*, **68**, 601.
Kavanagh, K. L., and Magee, C. W., 1987, *Can. J. Phys.*, **65**, 987.
Kim, T., and Chung, D. D. L., 1981, *Thin Solid Films*, **147**, 177.
Kim, T., Chung, D. D. L., and Mahajan, S., 1987a, *Mater. Soc. Symp. Proc.*, **77**, 369; 1987b, *Ibid.*, **77**, 749.

KUAN, T. S., BATSON, P. E., JACKSON, T. N., RUPPRECHT, H., and WILKIE, E. L., 1983, *J. appl. Phys.*, **54,** 6592.
MOONEY, P. M., 1990, *J. appl. Phys.*, **67,** R1.
MOONEY, P. M., CASWELL, N. S., and WRIGHT, S. L., 1987, *J. appl. Phys.*, **62,** 4786.
POPOVIC, R. S., 1978, *Solid-St. Electron.*, **21,** 1133.
RHODERICK, E. H., and WILLIAMS, R. W., 1988, *Metal–Semiconductor Contacts* (Oxford: Clarendon Press).
SCALVI, L. V. A., 1991, *Revista de Física Aplicada e Instrumentação* (Brazilian Society of Physics), **6,** 177.
SÉGUY, P., ZIGONE, M., and MARTINEZ, G., 1992, *Phys. Rev. Lett.*, **68,** 518.
SHARMA, B. L., 1981, *Semiconductors and Semimetals*, Vol. 15, chap. 1 edited by R. R. Willardson and A. C. Beer (New York: Academic Press).
SHIH, K. K., and BLUM, J. M., 1972, *Solid-St. Electron.*, **15,** 1177.
TYAGI, M. S., 1984, *Metal Semiconductors Schottky Barriers and Their Applications*, chap. 1, edited by B. L. Sharma (New York: Plenum Press).
WALDROP, J. R., and GRANT, R. W., 1987, *Appl. Phys. Lett.*, **50,** 250.
YODER, M. N., 1980, *Solid-St. Electron.*, **23,** 117.

Radiation Effects & Defects in Solids, Vol. 156, pp. 295–299
Reprints available directly from the publisher
Photocopying permitted by license only

© 2001 OPA (Overseas Publishers Association) N.V.
Published by license under
the Gordon and Breach Science Publishers imprint,
a member of the Taylor & Francis Group.

LIGHT-INDUCED ELECTRIC DIPOLE RELAXATION IN SYNTHETIC AND NATURAL ALEXANDRITE

R.M.F. SCALVI[a,b]*, M. SIU LI[b], L.O. RUGGIERO[a] and L.V.A. SCALVI[a]

[a]*Departamento de Física, Faculdade de Ciências, UNESP, C.P. 473, 17033-360 Bauru SP, Brazil;* [b]*Instituto de Física de São Carlos, USP, C.P. 369, 13560-970 São Carlos SP, Brazil*

(Received 7 April 2000)

We present results of thermally stimulated depolarization current (TSDC) measurements in synthetic and natural alexandrite, which show TSDC bands related to the presence of electric dipoles in both types of samples. Synthetic material shows a wide TSDC band with a peak at 179 K, which can be fitted by two distinct relaxing dipole distributions. For natural alexandrite the TSDC band has a maximum around 195 K and can be fitted by three different distributions. Both samples present one of the calculated curves with a peak about 179 K, with activation energy of 0.57 eV and constant relaxation time of 1×10^{-14} sec. Photo-induced TSDC shows that TSDC bands can also be generated by simultaneous application of light and an electric field at 77 K.

Keywords: Alexandrite, Dipole relaxation, Depolarization current, Electrical properties

1. INTRODUCTION

Alexandrite is a material with growing interest due to its important optical properties [1]. The major application of alexandrite is as a laser active medium, with better performance than other kinds of solid state lasers [2]. The alexandrite structure can be identified as a hexagonal close packed (hcp) arrangement of oxygen ions slightly distorted, with Al^{3+} and Be^{2+}

*Corresponding author. E-mail: nosama@fc.unesp.bn

ions located at octahedral and tetrahedral sites respectively. The distortion from a perfect hcp lattice of oxygen ions, which is shifted from the c axis, yields two octahedrally-coordinated sites: A_I, located at an inversion center, and A_{II}, located at a reflection plane. Interatomic distances in chrysoberyl structure are different for each Al^{3+} ion bonded to O^{2-} ions. The average distance between first neighbors are Al_I–O = 1.890 Å and Al_{II}–O = 1.934 Å [3].

In alexandrite, the presence of Cr^{3+} ions (ionic radii = 0.615 Å) in sites usually filled with Al^{3+} ions (0.535 Å) causes local distortion in the neighborhood structure, which may favor the formation of electric dipoles. Another possible dipole is related to oxygen vacancies, which may interact with close charged atoms. We investigate electric dipole relaxation phenomena, using the thermally stimulated depolarization current (TSDC) technique [4]. Electric dipoles are oriented according to a preferential direction, by the application of an electric field at room temperature and frozen in by dropping the temperature to 77 K. TSDC bands are generated during the increase of temperature. A modified TSDC procedure, where light is applied at 77 K, shifts TSDC band to lower temperature.

2. EXPERIMENTAL

Natural alexandrite samples from the state of Minas Gerais, Brazil and synthetic alexandrite grown by Allied Signal Inc, USA, were used, with similar thickness. The composition of these samples was obtained by microprobe analysis (WDX). In the natural sample we have detected about 0.13 at% of Fe and small amounts of other impurities such as Ti, K, Si, and Mg besides inclusions of quartz and mica. In the case of the synthetic sample only Cr was detected without any inclusions.

TSDC measurements were carried out in the range of 77 to 300 K using a bias of 7.0 kV/cm and heating rate of 0.08 K/sec. Photo-induced TSDC studies were also done under different initial conditions of pre-oriented and post-oriented dipole systems to probe the destruction/creation of dipole orientation. For this purpose a MLUV (337.5 nm, 350.7 nm and 356.4 nm) from a Kr^+ laser was used in order to observe the photo-induced effect.

3. RESULTS AND DISCUSSION

Results of TSDC in alexandrite reveals a typical behavior of distributive dipole relaxation in solids. These results are shown in Figure 1(a) for synthetic material and Figure 1(b) for the natural sample. Experimental data are fitted by Havriliak–Negami method [5], which takes into account

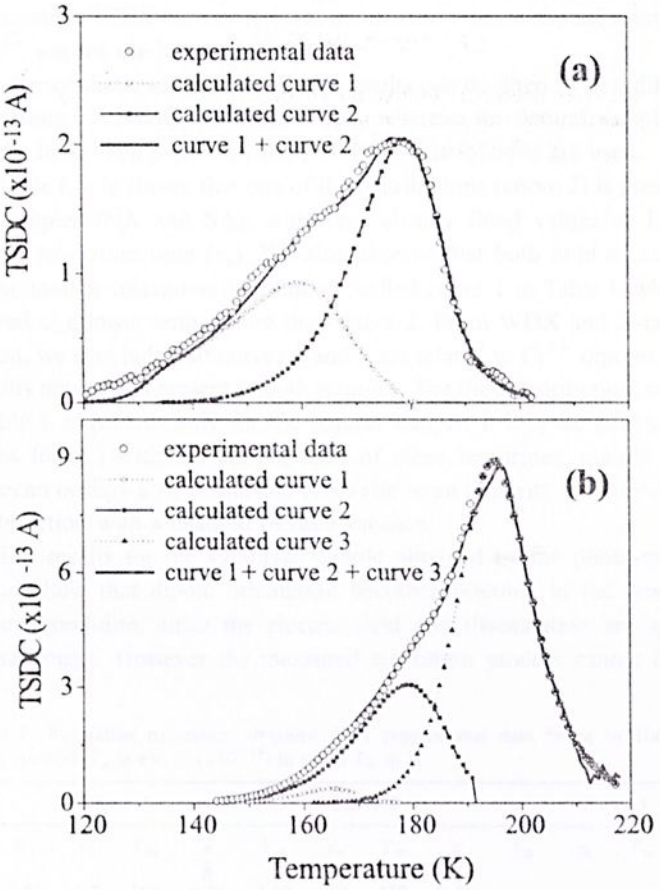


FIGURE 1 TSDC experimental data for (a) synthetic alexandrite (SA) and (b) natural alexandrite (NA). Curves are fitted by the Havriliak and Negami method, yielding two curves for SA and three curves for NA. Fitting parameters are as given in Table I.

continuous distribution of relaxation parameters involved in the thermal process, the activation energy (E_a) and relaxation time (τ).

TSDC results confirm that there is a mechanism of dipole relaxation in alexandrite either natural as well as synthetic. However the nature of these dipoles is still unknown and there are two strong possibilities: (i) oxygen vacancies, randomly distributed around the octahedrally coordinated Cr^{3+} ion as first neighbor, may generate dipoles of the impurity-vacancy type, which can interact with each other during the thermally activated process, that generates TSDC bands, (ii) local deformation due to the substitution of an Al^{3+} ion for the larger Cr^{3+} ion.

For the synthetic sample, the TSDC results can be fitted by two different distributions of Havriliak–Negami type, whereas for natural sample, the fitting is best when three Havriliak–Negami distributions are used.

In Table I, it is shown that one of the distributions (curve 2) is present in both samples (NA and SA), with very closely fitted values of E_a and constant relaxation time (τ_o). We also observe that both kind of samples present another relaxation distribution, called curve 1 in Table I, which is centered at a lower temperature than curve 2. From WDX and X-ray diffraction, we conclude that curves 1 and 2 are related to Cr^{3+} dipoles, since only this impurity is present in both samples. The third distribution, curve 3 in Table I, is present only for the natural sample. It may be attributed to dipoles formed with the participation of other impurities, mainly Fe^{3+}, which can occupy a Al^{3+} site and gives rise to an impurity vacancy dipole, by interaction with a charged oxygen vacancy.

TSDC results for the synthetic sample obtained by the photo-induced method show that dipole orientation becomes possible in the low temperature condition, since the electric field and illumination are applied simultaneously. However the measured relaxation process cannot be de-

TABLE I Relaxation parameters obtained from experimental data fitting by Havriliak–Negami method. E_a in eV; τ_0 ($\times 10^{-14}$) in s and T_m in K

	Curve 1				*Curve 2*				*Curve 3*			
	E_a	τ_0	T_m	α β	E_a	τ_0	T_m	α β	E_a	τ_0	T_m	α β
SA	0.51	1.7	159	0.30 0.37	0.57	1.0	179	0.20 0.69	–	–	–	–
NA	0.51	1.7	165	0.10 0.90	0.57	1.0	179	0.20 0.69	0.61	1.1	195	0.28 0.70

scribed by the same fitted parameters given in Table I, since the band is shifted to lower temperature. We believe that these dipoles have the participation of Cr^{3+} ions located in Al_{II} sites, which are responsible for the optical properties of alexandrite and then, more sensitive to light. In the case of natural samples, the results are not conclusive up to now, due to some peculiarities of these samples such as opacity and wrinkled lateral surfaces. Since sample illumination is done through the lateral surfaces, this causes pronounced light scattering.

4. CONCLUSION

In this paper we present evidence of electric dipole formation in natural and synthetic alexandrite. TSDC bands can be fitted by two continuous distributions, which are common to the TSDC bands obtained for both samples and can be associated with the Cr^{3+} ion. The exact type of dipole formed is still under investigation, since it can be an impurity-vacancy dipole or due to local deformation generated from substitution of Al^{3+} by Cr^{3+}. For the natural sample there is one more distribution probably related to the Fe^{3+} ion.

We also observe the orientation of existing dipoles in synthetic alexandrite by illumination with a Kr^{+} laser of wavelength in the range 337 nm to 356.5 nm, concomitant with electric bias at 77 K. The nature of these dipoles is also being analyzed.

Acknowledgements

The authors would like to thank Prof. Thomaz Catunda and H.P. Jenssen by the synthetic sample grown at Allied Signal Inc by R. Morris, USA. We also thank financial agencies: FAPESP, CAPES, FUNDUNESP and PRONEX.

References

[1] Powell, R.C. Xi, L. Gang, X. and Quarles, G.J. (1985) *Phys. Rev. B*, **32**, 2788.
[2] Fabeni, P. Pazzi, G.P. and Salvini, L. (1991) *J. Phys. Chem. Solids* **52**, 299.
[3] Rager, R. Bakhshandh-Khiri, A. and Schmetzer, K. (1998) *N. Jb. Miner. Mh*, **2**, 545.
[4] Bucci, C. and Fieschi, R. (1964) *Phys. Rev. Lett.* **12**, 16.
[5] Havriliak, S. and Negami, S. (1967) *Polymer* **8**, 161.

ARTICLE IN PRESS

ELSEVIER

Journal of Alloys and Compounds 1 (2002) 000–000

Journal of ALLOYS AND COMPOUNDS

www.elsevier.com/locate/jallcom

Optical characteristics of Er^{3+}–Yb^{3+} doped SnO_2 xerogels

E.A. Morais[a], S.J.L. Ribeiro[b], L.V.A. Scalvi[c,*], C.V. Santilli[b], L.O. Ruggiero[c], S.H. Pulcinelli[b], Y. Messaddeq[b]

[a]*Instituto de Física-USP, C.P. 369, 13560-970 São Carlos SP, Brazil*
[b]*Instituto de Química-UNESP, C.P. 355, 14801-970 Araraquara SP, Brazil*
[c]*Dipartmento Física, Faculdade de Ciências-UNESP, C.P. 473, 17033-360 Bauru SP, Brazil*

Abstract

Er^{3+} doped SnO_2 xerogels have been obtained from aqueous colloidal suspensions. Emission and excitation spectra were obtained and allowed the identification of two main families of sites for Er^{3+}. In the first one Er^{3+} substitutes for Sn^{4+} in the SnO_2 cassiterite structure. In the second Er^{3+} are found adsorbed at the SnO_2 particle surface. For the first family of sites the technological important infrared Er^{3+} emission about 1.5 μm is efficiently excited through absorption at the SnO_2 conduction band at 3.8 eV. On the other hand the emission due to adsorbed ions appears inhomogeneously broadened by the statistical distribution of sites available for Er^{3+} ions at the surface of the particles. Moreover it is not excited by the host. The emission of this second family of sites could be also excited by an energy transfer mechanism involving Yb^{3+} ions also adsorbed a posteriori at particles surface. Results are compared with spectra obtained for Eu^{3+} doped samples. © 2002 Published by Elsevier Science B.V.

Keywords: Tin dioxide; Rare earth doping; Xerogels; Sol–gel; Luminescence

1. Introduction

Tin dioxide is an wide bandgap material, (3.6 eV for crystalline SnO_2), used for many applications such as gas sensors, solar collectors, transparent conductors and others [1,2]. On the other hand, luminescent properties of tripositive rare-earth ions, such as Er^{3+} and Yb^{3+}, have contributed to development of a new technology, where they can be used as dopant for many kinds of semiconductor hosts, aiming the production of opto-electronic devices. Concerning SnO_2 some rare-earth doped samples have been prepared aiming at the preparation of phosphors for low energy electron (LEE) excitation [3–5].

In this work we present results on the preparation of SnO_2 xerogels with Er^{3+}. The solubility limit of tripositive rare-earth (RE) ions in SnO_2 is known to be around 0.05% and the excess ions are supposed to be segregated at grain boundaries probably as pyrochlore crystal phase $RE_2Sn_2O_7$ [5]. We present here emission and excitation spectra of these new Er^{3+} doped samples mainly focussing on the infrared emission and therefore on the possibility of preparing infrared light emitting diodes. Results are compared to those obtained by some of us for Eu^{3+} doped samples [6–8]

2. Experimental

Colloidal suspensions were prepared by sol–gel process [6], starting from a 0.2 M aqueous solution of $SnCl_4 \cdot 5H_2O$. $ErCl_3 \cdot 6H_2O$ was added to the solution in the desired concentration (0.1–4 mol%). The addition of an aqueous solution of ammonia leads to precipitation of tin oxi-hidroxide. The suspension was then dialyzed against distilled water in order to eliminate Cl^- and NH_4^+ ions. Clear sols were obtained after dialyze and xerogels were produced by drying the colloidal suspensions. A posteriori adsorption of Yb^{3+} was attained by adding the prepared SnO_2:Er powder to an aqueous solution of $YbCl_3 \cdot 6H_2O$. The powder was kept in contact with the solution for 24 h and after that it was decanted and washed with distilled water. All samples were fired at 1000 °C for 6 h.

Room temperature emission and excitation spectra were obtained using a 450 W Xenon lamp in an SPEX Fluorolog F212I spectrofluorimeter equipped with a North-Coast Ge detector.

*Corresponding author.

0925-8388/02/$ – see front matter © 2002 Published by Elsevier Science B.V.
PII: S0925-8388(02)00344-4

7914 DTD431 11-MAR-2002 16:47:33.87 v1.4.38

JALCOM7914

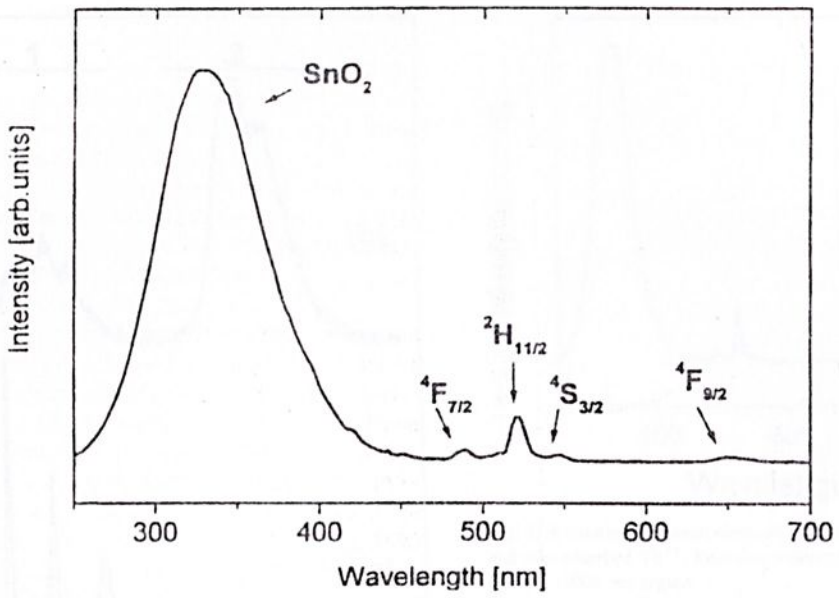


Fig. 1. Excitation spectrum obtained for the sample containing 0.1% mol Er^{3+}. Bandgap transition and also transitions from the Er^{3+} $^4I_{15/2}$ to the Er^{3+} excited states are indicated. Emission monitored at 1525 nm. Spectrum is corrected for lamp intensity and monochromator gratings and mirrors.

3. Results and discussion

Fig. 1 shows the excitation spectrum obtained for the sample containing 0.1 mol% Er^{3+} monitoring the infrared Er^{3+} $^4I_{13/2} \rightarrow {}^4I_{15/2}$ transition occurring on the 1525 nm region. A broad and strong band in observed in the UV peaking at 328 nm (≈3.78 eV) which corresponds to the SnO_2 bandgap energy. Weaker features are observed and that could be easily assigned to Er^{3+} intra f–f transitions from the fundamental $^4I_{15/2}$ manifolds to the Er^{3+} $^4F_{7/2}$, $^2H_{11/2}$, $^4S_{3/2}$ and $^4F_{9/2}$ excited states. Assignments are made in the figure. Comparing with results obtained before for Eu^{3+} [6,7] the observation of the strong intrinsic SnO_2 band suggests that Er^{3+} could substitute for Sn^{4+} in the SnO_2 cassiterite structure.

Emission spectra provided more information about the exact location of Er^{3+} ions in these materials. Fig. 2 shows emission spectrum obtained with different excitation wavelengths for the sample containing 0.1 mol% Er^{3+}. Upon excitation at 328 nm (SnO_2 bandgap) the spectrum displayed in the Fig. 2a presents maxima at 1512, 1525, 1543 1562 and 1578 nm. Small features are also observed in the lower wavelengths regions at 1447, 1462, 1478 and 1496 nm. A completely different spectrum is obtained upon excitation at 522 nm (Er^{3+} $^4I_{15/2} \rightarrow {}^2H_{11/2}$). The spectrum displayed in Fig. 2b is broadened, peaking at 1525 nm. Two weaker components are observed at 1536 and 1542 nm. Shoulders are also observed in the high (≈1560 nm) and low (≈1470 nm) wavelengths sides. The spectrum shown in Fig. 2c will be discussed hereafter.

To better understand this behavior we recall some results obtained before for Eu^{3+} doped SnO_2 [7]. Fig. 3

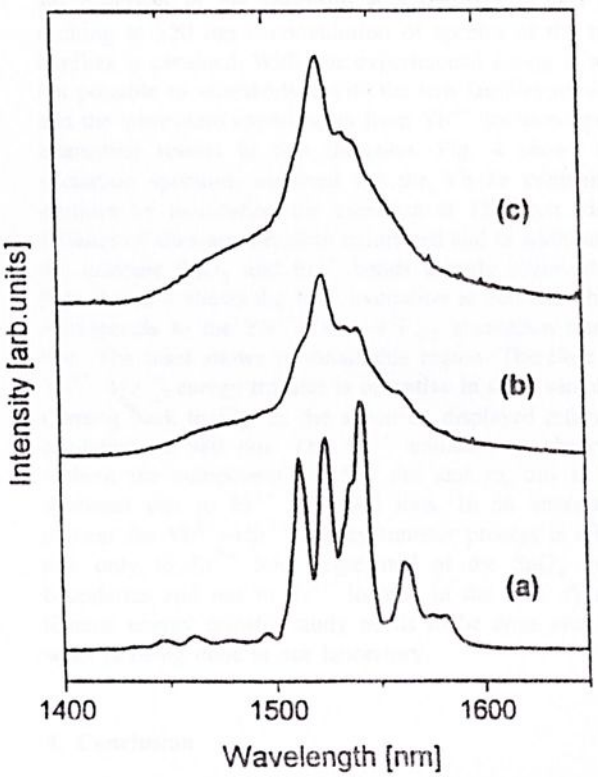


Fig. 2. Emission spectra obtained for the sample containing 0.1% Er^{3+} and also adsorbed Yb^{3+} ions. (a) Excitation at 328 nm; (b) excitation at 520 nm; and (c) excitations at 980 nm.

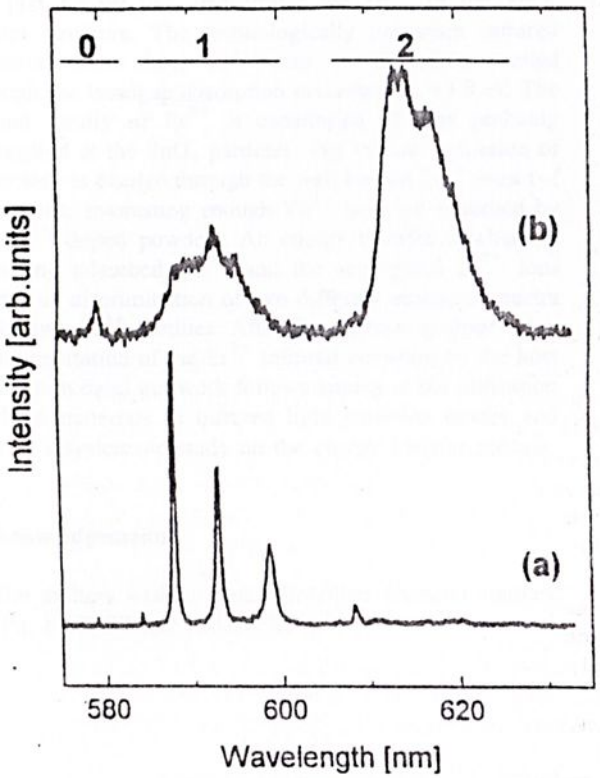


Fig. 3. Emission spectra obtained for a sample containing 2 mol% Eu^{3+}. (a) Excitation at 350 nm; (b) excitation at 394 nm (broadened bands assigned to the Eu^{3+} $^5D_0 \rightarrow {}^7F_{0,1,2}$ transitions).

shows the spectra obtained for a 2 mol% Eu^{3+} doped sample. Fig. 3a shows the spectrum obtained upon excitation with energy corresponding to the SnO_2 bandgap. A well defined spectrum with strong narrow bands peaking at 587.8, 592.8 and 598.6 nm is observed. Weaker peaks are also observed at 584.0 and 608.3 nm. The three main bands are easily assigned to the allowed magnetic dipolar Eu^{3+} $^5D_0 \rightarrow {}^7F_1$ transition. No electric dipolar transition is observed supporting the substitution of Eu^{3+} ions to the Sn^{4+} ions in the C_{2h} sites of the cassiterite structure (the small features in the emission spectrum could be assigned, from time resolution experiments, to transitions arising from the $^5D_1$ excited state) [7]. As cited before the solubility limit for rare earth ions in the SnO_2 is around 0.05 mol% and therefore for a 2 mol% sample the majority of Eu^{3+} ions is situated at the particles surface. When the excitation wavelength is fixed at 394 nm (Eu^{3+} $^7F_0 \rightarrow {}^5L_6$ transition) the emission spectrum (Fig. 3b) displays broadened bands assigned to the Eu^{3+} $^5D_0 \rightarrow {}^7F_{0,1,2}$ transitions (as named in the Fig. 3). Therefore the inhomogenously broadened bands could be attributed to Eu^{3+} ions segregated at the surface of particles in an amorphous structure.

The same reasoning could be used here to understand the different Er^{3+} spectra in Fig. 2. Therefore spectrum

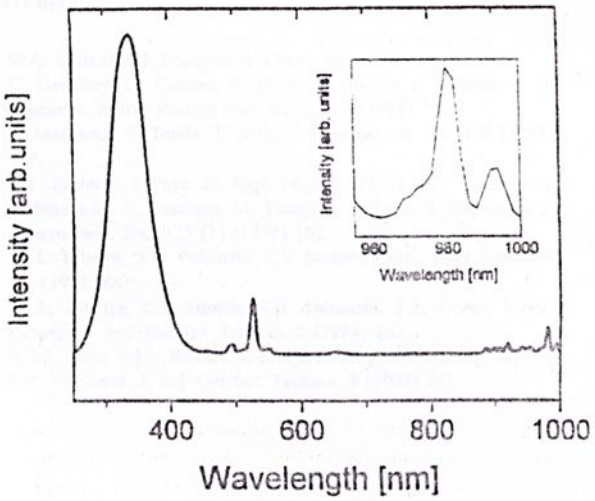


Fig. 4. Excitation spectrum obtained for the sample containing 0.1% Er^{3+} and also adsorbed Yb^{3+}. Emission monitored at 1525 nm. Inset: detail of the 950–1000 nm region.

displayed in Fig. 2a can be attributed to Er^{3+} located in the Sn^{4+} sites in the cassiterite structure. On the other hand the spectrum presented in Fig. 2b would refer to Er^{3+} segregated at the surface of particles. The component at 1543 nm observed in the spectrum suggests that in fact by exciting at 520 nm a convolution of spectra of the two families is obtained. With our experimental set-up it was not possible to selectively excite the two families of sites and the adsorption experiments from Yb^{3+} solutions gave interesting results in that direction. Fig. 4 shows the excitation spectrum obtained for the Yb–Er containing samples by monitoring the emission at 1525 nm. Both families of sites are therefore monitored and in addition to the intrinsic SnO_2 and Er^{3+} bands already observed in Figs. 1 and 4 shows the Er^{3+} excitation at 980 nm which corresponds to the Yb^{3+} $^2F_{7/2} \rightarrow {}^2F_{5/2}$ absorption transition. The inset shows in detail this region. Therefore an $Yb^{3+} \rightarrow Er^{3+}$ energy transfer is operative in these samples. Coming back to Fig. 2c the spectrum displayed refers to excitation at 980 nm. The Er^{3+} emission is observed without the component at 1543 nm and so, this is the spectrum due to Er^{3+} adsorbed ions. In an interesting manner the $Yb^{3+} \rightarrow Er^{3+}$ energy transfer process is effective only to Er^{3+} ions segregated at the SnO_2 grain boundaries and not to Er^{3+} located in the host. A systematic energy transfer study needs to be done and this work is being done at our laboratory.

4. Conclusion

The spectroscopic results suggest that by the experimental route employed here Er^{3+} doped SnO_2 materials with two main families of sites for Er^{3+} have been prepared. In

ARTICLE IN PRESS

the first family Er^{3+} substitutes for Sn^{4+} in the SnO_2 crystal structure. The technologically important infrared emission from these Er^{3+} ions is efficiently excited through the bandgap absorption occurring at ≈3.8 eV. The second family of Er^{3+} is constituted of ions probably segregated at the SnO_2 particles. The infrared emission of these ions is excited through the well known Er^{3+} intra f–f transitions. Interesting enough Yb^{3+} ions are adsorbed by the Er^{3+} doped powders. An energy transfer mechanism involving adsorbed Yb^{3+} and the segregated Er^{3+} ions allows us discrimination of two different emission spectra of the two Er^{3+} families. After the interesting observation of the excitation of the Er^{3+} infrared emission by the host conduction band our work follows aiming at the utilization of these materials as infrared light emission diodes and also to a systematic study on the energy transfer process.

Acknowledgements

The authors wish to thank Brazilian financial sources: CNPq, FAPESP and PRONEX.

References

[1] W.A. Badaway, J. Electroanal. Chem. 281 (1990) 85.
[2] C. Geoffroy, G. Campet, F. Menil, J. Portier, J. Salardenne, G. Couturier, Active Passive Elec. Comp. 14 (1991) 111.
[3] T. Matsuoka, T. Tohda, T. Nitta, J. Electrochem. Soc. 130 (1983) 417.
[4] D.F. Crabtree, J. Phys. D: Appl. Phys. 8 (1975) 107.
[5] T. Matsuoka, Y. Kasahara, M. Tsuchiya, T. Nitta, S. Hagakawa, J. Electrochem. Soc. 125 (1) (1978) 102.
[6] S.J.L. Ribeiro, S.H. Pulcinelli, C.V. Santilli, Chem. Phys. Lett. 190 (1) (1992) 64.
[7] S.J.L. Ribeiro, C.V. Santilli, S.H. Pulcinelli, F.L. Fortes, L.F.C. Oliveira, J. Sol–Gel Sci. Technol. 2 (1994) 263.
[8] G.E.S. Brito, S.J.L. Ribeiro, V. Briois, J. Dexpert-Ghys, C.V. Santilli, S.H. Pulcinelli, J. Sol–Gel Sci. Technol. 8 (1997) 261.

Materials Science Forum Vol. 403
Journal of Metastable and Nanocrystalline Materials Vol. 14 (2002) pp. 107-110
© 2002 Trans Tech Publications, Switzerland

Planar Waveguides based on Nanocrystalline and Er^{3+} doped SnO_2

R.R.Gonçalves[1], M.Ferrari[2], A.Chiasera[3], M.Montagna[3], E.A.Morais[4], L.V.A.Scalvi[5], C.V.Santilli[6], Y.Messaddeq[6] and S.J.L.Ribeiro[6]

[1]Dipartimento di Ingegneria dei Materiali, Università di Trento, I-38050 Mesiano, Trento, Italy
[2]Consiglio Nazionale delle Ricerche CeFSA, Centro Fisica Stati Aggregati, via Sommarive 14, I-38050 Povo, Trento, Italy
[3]Istituto Nazionale per la Fisica della Materia, Dipartimento di Fisica, Università di Trento, via Sommarive 14, I-38050 Povo, Trento, Italy.
[4]Instituto de Física- USP, CP 369, 13560-970, São Carlos-SP, Brazil
[5]Faculdade de Ciências- UNESP, P.O.Box 473, 17033-360 Bauru-SP, Brazil
[6]Institute of Chemistry- UNESP- P.O.Box 355, 14801-970 Araraquara-SP, Brazil

Keywords- planar waveguides, tin oxide, erbium

Abstract. Luminescent SnO_2: x%mol Er^{3+} (x=0.1-2.0) thin films have been spin coated on borosilicate and silica substrates from water colloidal suspensions that could be prepared containing up to 40% in weight SnO_2 nanocrystalline powders. High Resolution Transmission Electron Microscopy results show the well known SnO_2 cassiterite structure and nanocrystallites around 10 nm in diameter, corroborating results from X-ray diffraction. Mono and multi layers have been prepared from the stable colloidal suspensions and films thickness was observed to increase linearly, up to 200nm, with the colloidal suspensions nanoparticles amount. Excitation and emission spectra have been measured and Er^{3+} ions were found to be essentially incorporated into the cassiterite structure, substituting for Sn^{4+}, for doping concentration lower than 0.05 mol%. Er^{3+} ions also appear segregated at the grains surface for higher doping concentration. The optical parameters (refractive index, thickness and propagating modes) of a waveguide sample were measured at 632.8 and 543.4 nm by the prism coupling technique. A monomodal waveguide was obtained with attenuation loss of 3.5 dB/cm along a 2.5 cm optical path.

1- Introduction

SnO_2-based materials have potential application demonstrated in several different areas, as transparent electrode for solar cells and photochemical devices, gas sensors, membranes for special filtration, among others [1]. In addition rare earths doped SnO_2 are potentially interesting visible light emission phosphors for low energy electron (LEE) excitation [2]. In the preparation of these compounds the sol-gel process has been used before and the structural evolution of the system in the experimental route has been investigated by some of us [3-6].

This work aims at the investigation of the optical properties of SnO_2 films and their application in integrated optics, as planar waveguides. To our knowledge there is no report in the literature of such application for these nanocrystalline films despite of the good favorable optical properities such as high refractive index and low phonons energies which also allows interesting rare earth emission properties. Therefore we describe here the preparation and characterization of nanoscaled crystalline Er^{3+} doped SnO_2 planar waveguides spin coated on borosilicate and silica substrates.

2-Experimental

In a conventional synthesis, the intermediate particulate system minimizes its surface free energy by growing into larger particles which tend to agglomerate. These reactions can be avoided by adjusting the surface free energy of the particle by *in situ* surface modification during the precipitation and the controlled growth processes so that non agglomerate particles with a determined size can be prepared. A tin (IV) chloride solution in ethanol containing up to 2 mol % aqueous erbium chloride was added to an aqueous NH_4OH solution containing 10 wt.% 6-caprolatman, the surface modifying agent used here. The prepared suspensions were then refluxed at 90°C for 3h. The resulting powder was isolated by centrifugation, washed with water several times and then dried at 60°C. It was observed to be fully redispersed in water at pH>8 and colloidal suspensions were prepared with up 40 wt.% of nanoparticles. Thin films have been prepared on borosilicate and silica glass by spin coating. Crack free coatings were obtained by spinning at 2500 rpm. Thermal densification was carried out at 500°C for 60 min.

The films thickness were measured with a Tencor P10 surface profiler. The films were also characterized by high resolution transmission electron microscopy (HRTEM) and X-ray diffraction. Excitation and emission spectra were obtained at room temperature with a Spex Fluorolog F1211 fluorimeter with a 450W Xe lamp as excitation source.

The mode spectra of planar waveguides were measured by using an automatic prism coupler (Metricon Corp.). In order to measure propagation losses the light intensity scattered out of the waveguide plane, which is proportional to the guided intensity, was recorded by a optical fiber. The losses were evaluated by fitting the intensity to an exponential decay function. The measurements were performed by exciting a transverse electric (TE) waveguiding mode with a 632.8 nmHe-Ne laser.

3. Results

Homogenous and good optical quality films were obtained. Thickness increases with the concentration of the nanoparticles, varying from 65nm to 180nm for concentrations between 8 and 28 wt%. Figure 1(a) shows the linear behavior for the system doped with different amount of Er^{3+} ions. Films deposited from suspensions with the solid content higher than 30 wt% display cracks in the macro scale and also low transparency in the visible range. The optimized concentration in order to obtain films without cracks and with a maximal thickness was observed to be 26 wt.%. No significant thickness variation is observed for the different dopant amounts.

Figure 1b shows the thickness obtained for multi layer processes. Thin films up to 800nm thick could be easily prepared through the spin coating technique, without macro cracks.

Figure 2 shows TEM images of a 2 layers deposit. The porous, nanostructured film is composed of SnO_2 cassiterite nanocrystals with sizes in the range of 5-10nm.

Table 1 shows the results obtained by m-lines spectroscopy. A monomodal waveguide was observed using red and green laser lines (632.8 and 543.5 nm). The measured attenuation coefficient was 3.5 dB/cm at TE_0 over 2.5 cm.

Figure 3 shows Er^{3+} luminescence results. At the right one excitation spectrum obtained for the sample containing 0.1mol% Er^{3+} monitoring the infrared Er^{3+} $^4I_{13/2} \rightarrow {}^4I_{15/2}$ occurring in the 1525nm region. A broad and strong band in observed in the UV peaking at 328 nm (≈3.78eV) which corresponds to the SnO_2 band gap energy. Weaker features are observed in the visible part due to Er^{3+} intra-ff transitions from the fundamental $^4I_{15/2}$ manifolds to the Er^{3+} $^4F_{7/2}$, $^2H_{11/2}$, $^4S_{3/2}$ and $^4F_{9/2}$ excited states. Comparing with results obtained before for Eu^{3+} [6-7] the observation of the strong intrinsic SnO_2 band suggests that Er^{3+} could substitute for Sn^{4+} in the SnO_2 cassiterite structure. Emission

spectra shown at the left provided more information about the exact location of Er^{3+} ions in these materials. Upon excitation at 328nm (SnO_2 band gap) the spectrum displayed in the figure 3(a) presents maxima at 1512, 1525, 1543 1562 and 1578 nm. Small features are also observed in the lower

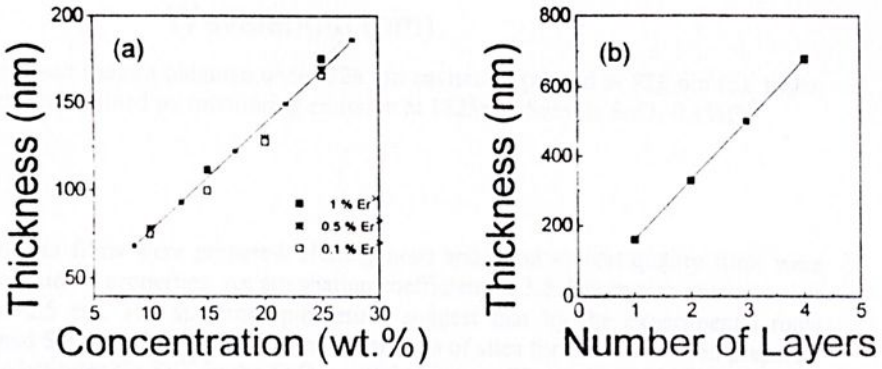


Figure 1- (a) Thickness of the Er^{3+} doped SnO_2 films as a function of the nanoparticles concentration (wt%). (b) Thickness of the Er^{3+} doped SnO_2 films in function of the number of the layers

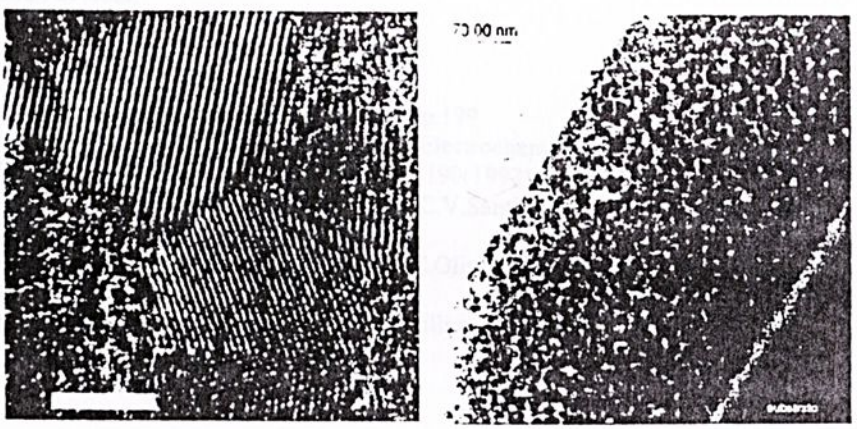


Figure 2- TEM images for a two layers SnO_2 deposits. Bar=5nm

Table1- Optical properties obtained from the prism coupling technique

Properties	632.8nm	543.5nm
Refractive index of film η_f	1.6906	1.7058
η_{eff}	TE$_0$ 1.5790	TE$_0$ 1.6057
Thickness (μm)	0.3	0.3

wavelenghts regions at 1447, 1462, 1478 and 1496 nm. This spectrum is assigned to Er^{3+} substituting for Sn^{4+} ions in the cassiterite structure. A completely different spectrum is obtained upon excitation at 522 nm (Er^{3+} $^4I_{15/2} \rightarrow {}^2H_{11/2}$). The spectrum displayed in figure 3(b) is broadened, peaking at 1525nm. Two weaker components are observed at 1536 and 1542 nm. Shoulders are also observed in the high (≈1560nm) and low (≈1470nm) wavelengths sides. This spectrum is assigned here to excess Er^{3+} ions that could not enter the cassiterite strucuture due to solubility limits. Er^{3+} ions segregated at the grain boundaries display a spectrum typical of Er^{3+} in glasses denoting the amorphous nature of these sites.

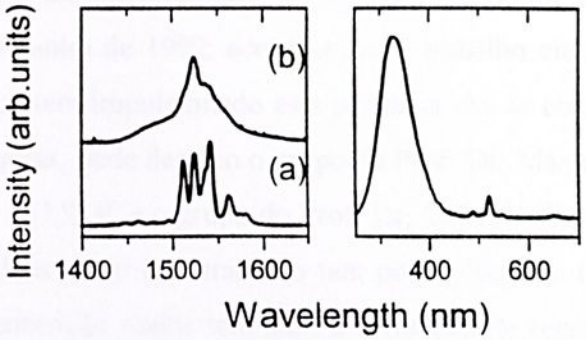


Figure 3- Left- Er^{3+} emission spectra obtained under 328 nm excitation (a) and at 522 nm (b). Right- excitation spectrum obtained by monitoring emission at 1525nm. Sample SnO_2:0.1%Er^{3+}.

4- Conclusions

Er^{3+} doped SnO_2 thin films were prepared. Homogenous and good optical quality films were obtained displaying waveguiding properties. An attenuation coefficient of 3.5 dB/cm was obtained over a propagation lenght of 2.5 cm. The spectroscopic results suggest that by the experimental route employed here Er^{3+} doped SnO_2 materials with two main families of sites for Er^{3+} have been prepared. In the first family Er^{3+} substitutes for Sn^{4+} in the SnO_2 crystal structure. The technologically important infrared emission from these Er^{3+} ions is efficiently excited through the band gap absorption occuring at ≈3.8eV. The second family of Er^{3+} is constituted of ions probably segregated at the SnO_2 grain boundaries. The results presented here suggest that these materials could found potential application in Integrated optics amplification devices.

5-References

[1]-Z.M.Jarzebski and J.P.Marton, J.Electrochem.Soc. 123 (1976), p.199
[2]-T.Matsuoka, Y.Kasahara, M.Tsuchiya, T.Nitta, S.Hagakawa, J.Electrochem. Soc. 125 (1978), p.102
[3]-S.J.L. Ribeiro, S.H.Pulcinelli and C.V.Santilli. Chem.Phys.Lett 190(1992), p.64
[4]-S.J.L.Ribeiro, R.S.Hiratsuka, A.M.G.Massabni, M.R.Davolos, C.V.Santilli and S.H.Pulcinelli, J. of Non-Crystalline Sol. 147/148 (1992), p.162
[5]-S.J.L.Ribeiro, C.V.Santilli, S.H.Pulcinelli, F.L.Fortes and L.F.C.Oliveira, J. of Sol-Gel Science and Technology 2 (1994), p.263
[6]-G.E.S.Brito, S.J.L.Ribeiro, V.Briois, J.Dexpert-Ghys, C.V.Santilli and S.H.Pulcinelli, J. of Sol-Gel Science and Technology 8 (1997), p.261

CONCLUSÃO

O presente trabalho ilustra a pesquisa que venho desenvolvendo nestes anos. Apesar das dificuldades da infraestrutura no campus de Bauru quando de meu ingresso nesta instituição, em junho de 1992, acredito que o trabalho científico tem sido desenvolvido a contento. O que tem impulsionado esta pesquisa são as colaborações mantidas com outros grupos de pesquisa, onde destaco o grupo do Prof. Dr. Máximo Siu Li do Instituto de Física de São Carlos – U.S. P. e o grupo do Prof. Dr. Celso V. Santilli do Instituto de Química de Araraquara. Além disso este trabalho tem possibilitado a implantação de laboratórios em Bauru. A contribuição maior tem sido a formação de recursos humanos. Diversos alunos dos cursos de graduação da UNESP – Bauru (Licenciatura em Física, Engenharia Elétrica e Ciência da Computação) já realizaram trabalhos de Iniciação Científica sob minha orientação, e alguns deles já fizeram até suas dissertações de Mestrado trabalhando em nossos laboratórios. Acredito que, dentro das limitações que me são impostas pelo local de trabalho e de minhas próprias limitações, tenho dado minha contribuição científica ao desenvolvimento da UNESP e do país.

0810001362